ÖAW
Austrian Academy
of Sciences

IBn
INSTITUTE OF BIOPHYSICS AND
NANOSYSTEMS RESEARCH

ANNUAL REPORT 2008

Think...

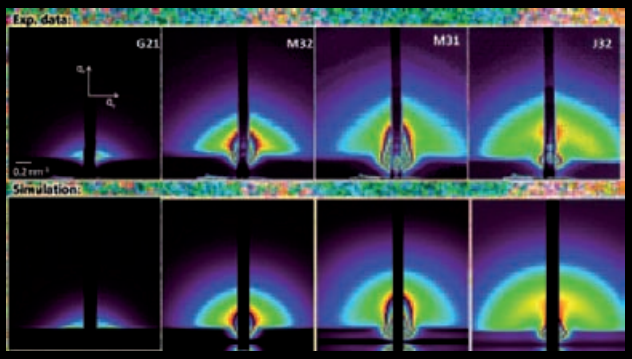

AUSTRIAN SAXS BEAMLINE AT elettra

Austrian
Small Angle X-ray Scattering
(SAXS) Beamline
at ELETTRA

Annual Report 2008

Compiled by the SAXS-Group:

- for IBN: B. Sartori, M. Rappolt & H. Amenitsch
- for ELETTRA: S. Bernstorff

Table of Contents

Preface

Peter Laggner
Director
Institute of Biophysics and Nanosystems Research
Austrian Academy of Sciences

It is good to look back to 2008 as another successful year for the Austrian SAXS station at Elettra. Several important achievements have been made: First, of course, the new booster full-energy injector for the storage ring has indeed been a major step forward towards ever increased beam quality and the average usable flux for the users. This does not seem too exciting at first sight, but is of very high practical value for SAXS, where typically the changeover between different beamline and optimal sample environment settings takes a substantial part of the time, and hence the constant availability of near-perfect beam conditions is a major quality factor. The second major improvement has been afforded by the upgrade of the beamline itself, where the experimental hutch was enlarged, so that the effective optical length could be substantially increased providing higher flexibility, higher SAXS resolution, and microfocus potential.

With these improvements in place, the powerful potential for experimentation at the SAXS beamline has been proven by a number of innovative studies. Time-resolved studies on dynamic systems, the classical core-competence of the SAXS beamline, have explored new frontiers, as demonstrated e.g. by new techniques of rapid mixing (p.45) or by stopped-flow experiments on gelation processes (p. 100). Increasingly, SAXS or SWAXS methods are not just being used in isolation, but combined with other techniques *in-situ*, such as ellipsometry (p.97) or with infrared spectroscopy (p.113), as has been first demonstrated already in 2006. Not only *in-situ*, but also '*off-situ*' combinations are gaining importance. Here, in particular the integration with X-ray lithography needs to be mentioned, whereby SAXS can be used to combine the top-down and the bottom-up approaches to study self-aggregating mesostructures on solid sub-micrometer support patterns (p.108).

In a climate of budget squeezes everywhere, it is reassuring that such innovations could be realized. We believe, that it is just in these times, when new ideas and initiatives have to be explored in order to stay in the game. One of these is being formulated within the NFFA-Project (http://nffa.tasc.infm.it/). This EC feasibility study, 'Nanofoundries and Fine Analysis', aims at defining a scheme for the integration of various fine-analysis techniques existing at large research infrastructures with micro- and nanofabrication facilities. There are intimate links between nanosciences, such as nanomaterials and nanobiology, and large scale scientific research facilities. By co-locating nanoscience foundries with the large-scale facilities, an integrated research environment can be created in a cluster of globally

competitive nanoscience centers distributed throughout the European research area. We are very pleased to be part of this initiative.

As always, I want to thank our partners and users most cordially for their efforts that contributed so valuably to this success.

Peter Laggner
Graz, November 2009

Alfonso Franciosi
Director, ELETTRA Laboratory
Chief Executive Officer, Sincrotrone Trieste S.C.p.A.

We are pleased to welcome publication of the 2008 Annual Report of the SAXS Beamline of the Austrian Academy of Sciences. The notable scientific production and constantly high demand by the user community continue to make the SAXS Beamline one of the most successful scientific enterprises at Elettra.

Many achievements, challenges and opportunities emerged in 2008 for Elettra and its Partners as several major upgrade projects were gradually implemented while user operation continued. The new booster full-energy injector, inaugurated by the President of the Republic of Italy, Giorgio Napolitano, on 28th March 2008, has brought on a major decrease in injection time and overall improvements in the reliability of the storage ring.

The ensuing Elettra and booster machine physics activities concentrated on the top-up tests, in other words, on the system that will be capable of selectively filling with electrons the single electron bunches circulating in Elettra, thus maintaining the current constant without interrupting the operation of the beamlines. The possibility of top-up operation was conclusively demonstrated at both 2.4 and 2.0 GeV, and top-up operation for users is scheduled to begin by the end of 2009.

In 2008 we also initiated a program to strengthen the services and research in structural biology, in cooperation with other research centers in this field. A major upgrade of the XRD1 beamline is nearing completion, with the installation of a new robot and related management software developed at Elettra. The optical design of the second protein diffraction beamline has been completed and procurement of the optical components has begun. A new state-of-the-art facility for the expression, the purification and the crystallization of proteins was designed and built on the Elettra site in close cooperation with SISSA and staffed with newly hired senior researchers of international repute.

In 2008, both the construction and civil engineering works related to the FERMI@Elettra seeded Free Electron Laser (FEL) source have taken off, as well as the acquisition of technical components for the FEL. A new industrial spin-off company, Kyma S.r.l. was established for the construction and commercialization of undulators and magnetic measurements equipment.

Through collaboration with the MAX-lab Laboratory in Lund (Sweden), which started in the framework of the actual construction of the European Consortium EuroFEL (formerly, IRUVX), the FERMI photoinjector was tested in Lund while the civil construction was being completed in Trieste. The photoinjector was eventually installed in Trieste, and at 6:44 p.m. on August 19, 2009, the first electron beam was extracted from the copper photocathode and accelerated to 5 MeV in the linac tunnel of FERMI@Elettra. This was a step of capital importance in the commissioning of this new seeded FEL source, which is scheduled to produce gigawatt pulses of 20-100 femtosecond duration at 10 nm by the end of 2010 and at

3-4 nm by the end of 2011. Initially, three beamlines will be devoted to time-dependent imaging, diffraction, spectroscopy, and scattering experiments, with the initial involvement of over 30 partner institutions worldwide.
The new strategic directions opening up for Elettra and its Partners are illustrated by the two workshops that took place as part of the XVI Elettra Users' Meeting: "Time-resolved Studies with Synchrotron and FEL Radiation" and "Emerging Applications of Synchrotron Radiation in the Life Sciences". The SAXS beamline had a prominent role in the second event, addressing the emerging applications of synchrotron radiation in the life sciences, a highly strategic field for our Laboratory.

We take this opportunity to thank our Partners of the Austrian Academy of Sciences for their enthusiasm and dedication over the years. We at Elettra look forward to expanding the scope and depth of our collaboration and exploring together the frontiers that the new upgraded Elettra and FERMI will open for all of us.

Alfonso Franciosi
Chief Executive Officer
Sincrotrone Trieste S.C.p.A.

The SAXS Group

HEAD OF PROJECT: Peter Laggner [1)]

e-mail: peter.laggner@oeaw.ac.at

SCIENTISTS: Heinz Amenitsch [1), 3)]

e-mail: amenitsch@elettra.trieste.it

Sigrid Bernstorff [2])

e-mail: bernstorff@elettra.trieste.it

Michael Rappolt [1), 3)]

e-mail: michael.rappolt@elettra.trieste.it

POST DOCS: Fernando Cacho [1), 3)]

e-mail: fernando.cacho@elettra.trieste.it

Shyjumon Ibrahimkutty [1, 3)]

e-mail: shyju.ibrahimkutty@elettra.trieste.it

Benedetta Marmiroli [1, 3)]

e-mail: benedetta.marmiroli@elettra.trieste.it

PhD-STUDENT: Fabian Schmid [1), 3)] (until August 2008)

e-mail: fabian.schmid@elettra.trieste.it

SCIENTIFIC ASSISTANT: Barbara Sartori [1, 3)]

e-mail: barbara.sartori@elettra.trieste.it

TECHNICIAN: Christian Morello [2)]

e-mail: christian.morello@elettra.trieste.it

1) Institute for Biophysics and Nanosystems Research, Austrian Academy of Sciences, Schmiedlstraße 6, 8042 Graz, Austria.
Tel 0043-316-4120 302
Fax 0043-316-4120 390

2) Sincrotrone Trieste, Strada Statale 14, km 163.5, 34012 Basovizza (TS), Italy.
Tel 0039-040-375 81
Fax 0039-040-938 0902

3) Institute for Biophysics and Nanosystems Research, Austrian Academy of Sciences
c/o Sincrotrone Trieste

The SAXS-Beamline in General

Small Angle X-ray Scattering has become a well known standard method to study the structure of various objects in the spatial range from 1 to 1000 Å, and therefore instruments capable to perform such experiments are installed at most of the synchrotron research centers. The high-flux SAXS beamline at ELETTRA is mainly intended for time-resolved studies on fast structural transitions in the sub-millisecond time region in solutions and partly ordered systems with a SAXS-resolution of 10 to 1400 Å in real-space.
The photon source is the 57-pole wiggler whose beam is shared and used simultaneously with a Macromolecular Crystallography beamline. The wiggler delivers a very intense radiation between 4 and 25 keV of which the SAXS-Beamline accepts 3 discrete energies, namely 5.4, 8 and 16 keV. The beamline optics consists of a flat double crystal monochromator and a double focusing toroidal mirror.
A versatile SAXS experimental station has been set-up, and an additional wide-angle X-ray scattering (WAXS) detector monitors simultaneously diffraction patterns in the range from 1 to 9 Å. The sample station is mounted move-able onto an optical table for optimising the sample detector distance with respect to SAXS resolution and sample size.
Besides the foreseen sample surrounding the users have the possibility to install their own specialised sample equipment. In the design phase, besides technical boundary conditions, user friendliness and reliability have been considered as important criteria.
The optimisation of the beamline with respect to high-flux and consequently high flux density, allows to perform the following experiments:

- Low Contrast Solution Scattering
- Grazing Incidence Surface Diffraction
- Micro-Spot Scanning
- X-ray Fluorescence Analysis
- Time-Resolved Studies ≥ 11 μs
- Simultaneously Performed Small- and Wide-Angle Measurements (SWAXS) on:
    - Gels
    - Liquid Crystals
    - (Bio) Polymers
    - Amorphous Materials
    - Muscles

Furthermore, using 5.4 and 16 keV energies, the beamline is widely applicable also to very thin, e.g. single muscle fibers, and optically thick (high Z) specimen, as often used in e.g., material science and solid state physics.

THE INSERTION DEVICE

The wiggler for the SAXS beamline consists of three 1.5 m long segments, each having 19 poles. The device can work with a minimum gap of 20 mm, which corresponds to K=20 at 2 GeV. The main parameters of the wiggler are:

- Critical Energy 4.1 keV
- Radiation Power 8.6 kW
- Flux 3.5×10^{14} ph/s/mrad/0.1%BW (at 400 mA)

The wiggler radiation cone has a horizontal width of 9 mrad. From this the SAXS-beamline accepts vertically 0.3 mrad, and horizontally +/-0.5 mrad at a 1.25 mrad off-axis position. The resulting source size for 8 keV photons is 3.9 x 0.26 mm^2 (horiz. x vert.).

THE OPTICS

The optics common with the diffraction beamline consists of:

- C-Filter and Beryllium window assembly to reduce the power load on the first optical elements by a factor of 2 and to separate the beamline vacuum from the storage ring.
- Beam defining slit chamber which allows to define the SAXS beam on three sides before the monochromator in order to reduce the straylight in the downstream beamline sections.

The SAXS beamline optics consists of:

- A double-crystal monochromator consisting of four individual chambers, in which three interchangeable asymmetric Si(111) crystal pairs are used to select one of three fixed energies. Each of the crystal pairs is optimised for the corresponding energy to accomplish a grazing angle of 2°. The energy resolution $\Delta E/E$ of the monochromator is in the range of 0.7 - 2.5 10^{-3}.
- A baffle chamber after the monochromator is used as an adjustable straylight fenditure.
- A segmented toroidal mirror focuses the light in horizontal and vertical direction with a 1/2.5 magnification onto the SAXS-detector.
- An aperture slit reduces the straylight after the monochromator and the toroidal mirror.
- A guard slit defines the illuminated region around the focal spot. The spot size on the detector is 1.6 mm horizontally and 0.6 mm vertically. The calculated flux at the sample is in the order of 10^{13} ph/s at 400 mA. For a maximum sample size of 5.4 x 1.8 mm^2 correspondingly a flux density of 10^{12} ph/s/mm^2 has been calculated.

SAMPLE STAGE

The multipurpose sample stage allows to perform fast time-resolved relaxation studies based on temperature- or pressure-jumps as well as stopped flow experiments. Shear jump relaxation experiments are planned. Specifically, T-jumps can be induced by an infra-red light pulse (2 ms) from an Erbium-Glass laser, raising the temperature about 20 °C in an aqueous sample volume of 10 µl. A hydrostatic pressure cell with a maximal accessible angular range of 30° for simultaneous SAXS and WAXS measurements is available. P-jumps are realised by switching fast valves between a low and a high pressure reservoir, increasing or decreasing the hydrostatic pressure in the range from 1 bar to 2.5 kbar within a few ms. A Differential Scanning Calorimeter (DSC) allows for DSC-scans simultaneously to SWAXS measurements. In an overview, the following sample manipulations are possible (further details, see page 30-34):

- Temperature Manipulations: Ramps, Jumps and Gradient Scans
- Pressure Manipulation: Scan and Jumps
- Stopped Flow Experiments
- SWAXS Measurements Applying Mechanical Stress
- Calorimetric measurements

Scientific Applications

Low Contrast Solution Scattering, Grazing Incidence Surface Diffraction, Micro-Spot Scanning, X-ray Fluorescence Analysis, Time-Resolved Studies ≥ 11 μs and Simultaneously Performed Small- and Wide-Angle Measurements (SWAXS) on:

Gels
Liquid Crystals
(Bio) Polymers
Amorphous Materials
Muscles

Source characteristics

Wiggler (NdFeB Hybrid):

Period	140 mm
No. full poles	57
Gap	20 mm
B_{max}	1.607 T
Critical Energy ε_c	4.27 keV
Power (9 mrad)	8.6 kW
Effective source size FWHM	3.9 x 0.26 mm^2(HxV)

Optics

Optical elements:	*Double crystal monochromator*:	*Mirror*:
	Si (111) asym. cut, water cooled.	two–segment,toroidal, Pt coated.
Distance from source:	18.4 m	26.5 m

Acceptance	1 mrad/0.3 mrad (HxV)
Energy (3 selectable)	5.4, 8, 16 keV (0.77, 1.54, 2.3 Å)
Energy resolution $\Delta E/E$	0.7-2.5 x 10^{-3}
Focal spot size FWHM	1.2 x 0.6 mm^2 (HxV)
Spot at Sample FWHM	5.4 x 1.8 mm^2(HxV)
Flux at sample	5 x 10^{12} ph s^{-1}(2 GeV, 200 mA, 8 keV)

Experimental apparatus

Resolution in real space: 10-1400 Å (small-angle), 1- 9 Å (wide-angle)

Sample stage: temperature manipulations: ramps, jumps and gradient scans, pressure manipulation: scan and jumps, stop flow experiments, SWAXS measurements applying mechanical stress, SWAXS measurements applying magnetic fields. In-line calorimetric measurements simultaneously with SWAXS.

Detectors: 1D gas-filled detectors for simultaneous small- and wide-angle (Gabriel type), 2D CCD-detector for small-angle, Vantec-1 detector (Bruker AXS).

Experiment control

Beamline control: Program-units written in LabView for Windows
1 D detector control: PC-card and software from Hecus X-ray Systems GmbH, Graz.
2 D detector control: Software from Photonic Science, Oxford.

CURRENT STATUS

The beamline has been built by the Institute for Biophysics and Nanosystems Research (IBN), Austrian Academy of Science in collaboration with staff members from Sincrotrone Trieste, and is in user operation since September 1996. The set-up of the beamline started at the beginning of January 1995 with the installation of the support structure. Until the end of 1995, the 8 keV single energy system had been realised. The upgrade to the full three energy system was finished in spring 1998. Time resolved experiments require fast X-ray detectors and data acquisition hard- and software. Depending on the desired resolution in time and in reciprocal space, on isotropic or anisotropic scattering of the sample, one-dimensional position sensitive (delay-line type) or two-dimensional CCD detectors are employed.

In August 2002 our new chemistry and X-ray laboratory went into operation. The chemistry unit serves mainly for sample preparation and analysis for both, in house research and external user groups, whereas the X-ray laboratory allows on-site testing of samples before moving on to the SR beamline (see page 29).

In May 2008 we extended about 3 m also our experimental hutch. It is now possible to increase the sample to detector distance and therefore improve our minimum SAXS resolution or maximise the flux density at sample position for certain experiments.

In conclusion, due to wide versatility of the beamline and the highly flexible sample stage, there are nearly no limits for the realisation of an experiment, and you are welcome by our team to propose any interesting and highlighting investigation for the benefit of material and life sciences.

Application for Beamtime at ELETTRA

1. Beamtime Policy at SAXS beamline

According to the agreement from March 2001 regarding the co-operation between the Austrian Academy of Sciences and Sincrotrone Trieste, at the Austrian SAXS-beamline the available beamtime of about 5000 hours/year is distributed as follows:

- 35% for Austrian Users, type: "CRG" (Collaborating Research Group)
- 35% for Users of Sincrotrone Trieste (General Users (GU))
- 30% is reserved for beamline maintenance and in-house research

In both user beamtime contingents also any industrial, proprietary and confidential research can be performed according to the "General User Policy" of Sincrotrone Trieste.

To apply for CRG and GU user beamtime proposals must be submitted according to the rules of Sincrotrone Trieste. The international review committee at ELETTRA will rank the proposals according to their scientific merit assessment. Based on this decision beamtime will be allocated according to the specific quotes for the beamtimes (CRG/GU) either for the following semester ("normal application") or for the next two years ("long term application"). However, at the moment no more than a maximum of 10% of the beamtime will be assigned to "long term" projects.

2. How to apply for beamtime

There are two deadlines each year for proposals, namely August 31st and February 28th. Accepted proposals will receive beamtime either in the then following first or second half year period, respectively. The Application Form must be completed on-line according to the following instructions.

ELETTRA USERS OFFICE
Strada Statale 14 - km 163.5
34012 Basovizza (Trieste), ITALY
Tel: +39 040 375 8628 - fax: + 39 040 375 8565
e-mail: useroffice@elettra.trieste.it

INSTRUCTIONS GIVEN BY THE USERS OFFICE
(see also http://www.elettra.trieste.it/UserOffice/)

1. Read carefully the General Guidelines.

2. Connect to the Virtual Unified Office: https://vuo.elettra.trieste.it/pls/vuo/guest.startup using your favorite browser with JavaScript enabled.

3. Select the Virtual Unified Office link.

4. When prompted, insert your ID and password. If you are a new user fill in the registration form with your data and choose your institution with the search button; in case your institution does not appear in the list, please contact useroffice@elettra.trieste.it giving all the details about it. When registered, you will receive an acknowledgment with your ID and password. You can change your password, if you wish. In case you forget your password, please don't register again but contact useroffice@elettra.trieste.it. At any moment you can select the help button and view more detailed instructions. By inserting your ID and password you will be able to continue.

5. Select the proposals button in the User functions group.

6. Select add and fill in on-line the proposal form. Please, type your proposal in English. Repeat this procedure for each proposal you intend to submit.

7. In case of continuation proposal: a) attach the experimental report of previous measurements; b) give your previous proposal number.

8. When finished, submit the proposal electronically, selecting the save button.

9. Print the proposal form together with each related safety form.

10. Sign the safety form(s).

11. Mail all signed safety form(s) as printed copy to the Users Office.

NOTE:

For technical questions related to proposals submission or other practical issues contact useroffice@elettra.trieste.it

For scientific questions related to the possibility of performing a given experiment contact bernstorff@elettra.trieste.it or amenitsch@elettra.trieste.it

List of Users and Institutes 2008

Australia

Bragg Institute, Australian Nuclear Science and Technology Organisation (ANSTO), Menai

DUFF Anthony
GARVEY Chris J.

University of Sydney, School of Molecular and Microbial Biosciences

KUCHEL P.
LARKIN Timothy

RMIT University, Applied Physics, Melbourne

BRYANT G.

La Trobe University, Department of Biochemistry, Victoria

ANDERS R.

Walter and Eliza Hall Institute of Medical Research, Structural Biology Division, Parkville, Victoria

NORTON R.

Austria

Austrian Academy of Science, Institute of Biophysics and Nanosystems Research, Graz

AMENITSCH Heinz
BOULGAROPOULOS Beate
CACHO-NERIN Fernando
GANDER Edgar
HODZIC Aden
HOEGER Birgit
IBRAHIMKUTTY Shyjumon
KRIECHBAUM Manfred
LAGGNER Peter
MANAVBASI Yasemin
MARMIROLI Benedetta
PABST Georg
RAPPOLT Michael
SARTORI Barbara
SCHMID Fabian
SHAMSUDEEN Shamna

Hecus Braun, Graz

BODNER Sabine

Institute of Nanostructured Materials and Photonics, Weiz, Austria

HAASE A.
JAKOPIC G.

LKT-TGM, Laboratorium für Kunststofftechnik G.m.b.H, Wien
WILHELM Harald

Technical University, Inst. for Chem. and Technology of Organic Materials, Graz
BOHNEMANN Kathrin
RATH Thomas
TRIMMEL Gregor

University of Technology, Institute of Biomechanics, Graz
HOLZAPFEL Gerhard A.

University of Vienna, Research Group Physics of Nanostructured Materials, Faculty of Physics
KERBER Michael
SCHAFLER Erhard
SPIECKERMANN Florian
ZEHETBAUER Michael J.

Croatia

Faculty of Sciences, Zagreb
TONEJC Antun

Institute of Physics, Zagreb
SALAMON Kresimir

"Rudjer Boskovic" Institute, Zagreb
BOGDANOVIC-RADOVIC I.
BULJAN Maya
CAPAN Ivana
DESNICA-FRANKOVIC Ida-Dunja
DESNICA Uroš
DUBČEK Pavo
ETLINGER Božidar
GAJOVIĆ Andreja
GRACIN, Davor
IVANDA Mile
JERČINOVIĆ Marko
JURAIC' Krunoslav
LONCARIC Martin
MUSIĆ Svetozar
PAVLOVIC Mladen
PIVAC Branko
RADIĆ Nikola
RAKIC Mario
RISTIĆ Mira
SANCHO-PARRAMON J.
SIKETIC Z.
TURKOVIC Aleksandra
ZORC Hrvoje
ZORIC Nedeljko

University of Split, Faculty of Chemical Technology, Split
LUCIC LAVCEVIC Magdy
SREDER Aljoska

University of Split, FESB, Split
BETTI Tihomir
ZULIM Ivan

Czech Republic

University of Pardubice, Department of Physics, Pardubice, and Academy of Sciences of the Czech Republic, Institute of Macro-molecular Chemistry, Prague
STEINHART Milos

Denmark

University of Copenhagen, Faculty of Pharmaceutical Sciences, Department of Pharmaceutics and Analytical Chemistry, Copenhagen
YAGHMUR Anan

Finland

University of Helsinki, Viikki Drug Discovery and Development Technology Center (DDTC)
SUBRIZI Astrid
PAASONEN Lauri
URTTI A.
YLIPERTTULA Marjo

France

SOPRA SA, Bois-Colombes
EVRARD Patrick

Université de Haut Alsace, Laboratoire de Matériaux à Porosité Contrôlée, Ecole Nationale Supérieure de Chimie, Mulhouse
YORDANOV Ivan

Université de Paris-sud XI, Faculté de Pharmacie, Chatênay- Malabry
BARBARA Pili
BOURGAUX Claudie
OLLIVON Michel
PERRINE Pivette

Université de Paris-sud, Laboratoire de Physico-Chimie des Systèmes Polyphasés, Chatênay-Malabry
FAIVRE Vincent
OUATTARA M.

Université Pierre et Marie Curie, Chimie de la Matière Condensée, Paris

BASS John D.
BOISSIÉRE Cédric
GROSSO David
NICOLE Lionel
SANCHEZ Clément

Germany

Forschungszentrum Borstel, Borstel

BRANDENBURG Klaus
GUTSMANN T.
HOWE Joerg

Universität Erlangen-Nürnberg, Inst. für Kristallographie und Strukturphysik, Erlangen

VOSS Nicole
WALZ Marco

University of Munich, Department of Chemistry and Biochemistry and Center for NanoScience (CeNS)

BEIN T.
KEILBACH Andreas
KOEHN Ralf
SCHUSTER Joerg
ZUERNER Andreas

Greece

National Centre for Scientific Research "Demokritos", Aghia Paraskevi

CORDOYIANNIS G.

Hungary

Eötvös University, Department of General Physics, Budapest

RIBARIK Gabor

India

Indian Association for the Cultivation of Science, Department of Materials Science, Jadavpur, Kolkata

BAHADUR SRIVASTAVA Bhupendra

Indian Institute of Science, Solid State and Structural Chemistry Unit, Bangalore

NAG Angshuman
SANTRA Pralay
SARMA Dipankar Das

Italy

Associazione CIVEN, Nano Fabrication Facility, Venice
FALCARO Paolo

CNR di Pozzuoli, Istituto di Chimica e Tecnologia dei Polimeri (ICTP)
DURACCIO Donatella

INFM - CNR Laboratorio TASC, Trieste
BUSINARO Luca
FERRARI Enrico
GRENCI Gianluca

Sincrotrone Trieste, Trieste
BERNSTORFF Sigrid
MORELLO Christian

Università Ca' Foscari, Dipartimento di Chimica, Venezia
CARTA Davide
VASCOTTO Veronica

Università di Cagliari, Dipartimento di Scienze Chimiche and INSTM, Cagliari
MASILI A.
CORRIAS A.
CASULA M. F.

Università di Cagliari, Dip. di Scienze Chimiche, Monserrato
MONDUZZI Maura
MURGIA Sergio

University of Camerino, Dep. of Molecular Cellular and Animal Biology, Genetic Immunization Laboratory
AMICI A.
MARCHINI C.
MONTANI M.

Università Politecnica delle Marche, Dipartimento di Scienze Applicate ai Sistemi Complessi, sez. Scienze Matematiche Fisiche e Naturali, Ancona
MARIANI Paolo

University of Pisa, Dep. of Chemistry
LISI Fabio

University of Rome “La Sapienza”, Department of Chemistry
CAMINITI Ruggero
CARACCIOLO Giulio
POZZI Daniela

University of Rome “La Sapienza”, Dipartimento di Chimica e Tecnologie del Farmaco, Faculty of Pharmacy
MARIANECCI C.

Università di Sassari, Dipartimento di Architettura e Pianificazione, Laboratorio di Scienza dei Materiali e Nanotecnologie, Alghero/ Sasseri

COSTACURTA Stefano
INNOCENZI Plinio
MALFATTI Luca
SANNA Vanna

Pakistan

National Centre of Nanotechnology (NCN), Pakistan Institute of Engineering and Applied Sciences (PIEAS), Islamabad

MEHMOOD Mazhar
MIRZA Jamil Ahmad
WAHEED Abdul

Portugal

Universidade do Minho, Centro de Física, Braga

GOMES M.J.M.
KHODOROV Anatoli
LEVICHEV Sergey
PINTO Sara R. C.
ROLO A. G.

Slovenia

Josef Stefan Institute, Ljubljana

KANCLER Aljosa
OVCAR Silvester
ZIDANSEK Alexander

Jozef Stefan International Postgraduate School, Ljubljana

KUTNJAK Z.
LAHAJNAR G.

University of Maribor, Faculty of Natural Sciences and Mathematics, Maribor

JESENEK D.
KRALJ Samo

Sweden

Mid Eka Chemicals - Chemical Analysis, Bohus

CAMERANI Caterina
CAMERANI Cesare
JANSSON Inger
PETERSEN Catarina

University of Lund, Institute for Physical Chemistry 1

DAHLENBORG Hanna

Life Science and Chemical Industries Section YKI, Ytkemiska Institutet AB (YKI, Institute for Surface Chemistry), Stockholm,
KALNIN Daniel

Switzerland

ETH-Zurich, Department of Materials, Laboratory for Polymer Chemistry, Zurich
SCHLÜTER A. Dieter
ZHANG Afang

Néstlé Research Center and CNR, Lausanne
MEZZENGA Raffaele

University of Fribourg, Department of Physics and Fribourg Center for Nanomaterials, Fribourg
HAMMOND Matthew
LI Chaoxu
MEZZENGA Raffaele

United Kingdom

ISIS Facility, Rutherford Appleton Lab., Didcot Oxon.
TERRY Ann

University of Kent, School of Physical Sciences, Canterbury
BENFIELD Robert

University of Manchester, School of Materials, Nanostructured Materials Research Group, Manchester
BANGERT U.
KASHTIBAN R.J.

University of Reading, Dept of Chemistry, Reading Berkshire
CASTELLETTO Valeria
HAMLEY Ian
O'DRISCOLL Ben M.

University of Reading, Dept of Physics, Reading Berkshire
MITCHELL Geoffrey
OLLEY Robert H

List of Performed Experiments

2008 (first half year)

Proposal	Proposer	Institution	Country	Title	Research Area
2007424	KEILBACH Andreas	University of Munich, Dept. of Chemistry and Biochemistry	Germany	In-situ GiSAXS measurements of PMO materials formation within anodic alumina membranes	Chemistry
2007504	CAMERANI Caterina	Eka Chemicals - Chemical Analysis, Bohus	Sweden	The kinetics of aggregation and gelation in silica dispersions	Chemistry
2007517	MEZZENGA Raffaele	University of Fribourg, Dept. of Physics	Switzerland	Stimuli responsive hierarchical structures based on ionic supramolecular complexation of surfactants and dendronized block copolymers	Chemistry
2007529	SCHAFLER Erhard	Research Group Physics of Nanostructured Materials, Faculty of Physics, University of Vienna	Austria	Investigation of stacking faults in severely plastically deformed (SPD) metals by in-Situ Synchrotron WAXS, Part II: Body Centered Cubic (bcc) and Hexagonal (hcp) Metals	Materials Science
2007532	GROSSO David	Université Paris 6, Chimie de la Matiere Condensee	France	In situ Ellipsometry/SAXS/WAXS analyses of mesoporous TiO2 films crystallisation	Chemistry
2007585	MONDUZZI Maura	University of Cagliari, Dep. of Chemical Sciences	Italy	Characterization of the Internal Structure of Lipidic Nanoparticles by Synchrotron SAXS	Life Sciences
2007647	YAGHMUR Anan	Austrian Academy of Sciences (AAS), Inst. of Biophysics and Nanosystem Research (IBN), Graz	Austria	In Situ Monitoring of Mg+2 and Sr+2 Induced Lamellar to Non-Lamellar Phase Transitions: Combination of SAXS and Rapid Mixing	Life Sciences
2007765	SARMA Dipankar Das	Indian Institute of Science, Bangalore	India	In-situ investigation of novel size-focusing effects in the growth of semiconductor nanoparticles	Chemistry
2007822	IBRAHIMKUTTY Shyjumon	AAS, IBN, Graz	Austria	In situ analysis of the mesostructuring of silica by SAXS	Materials Science
2007832	GARVEY Chris	Bragg Institute, Australian Nuclear Science and Technology Organisation (ANSTO), Menai	Australia	Characterization of different conformational forms of Malarial antigen	Life Sciences

2007835	CACHO NERIN Fernando	AAS, IBN, Graz	Austria	Intra-subject changes in the structure and mechanical properties of the arteries	Life Sciences
2007836	MARMIROLI Benedetta	AAS, IBN, Graz	Austria	Ultrafast Nucleation and Growth Study of Zinc Sulfide by SAXS	Materials Science
Inhouse research	AMENITSCH Heinz & CARACCIOLO Giulio	AAS, IBN, Graz & University of Rome "La Sapienza", Dep. of Chemistry	Austria & Italy	Interaction between lipid/DNA complexes and anionic liposomes intended as model systems of cellular membranes	Life Sciences
Inhouse research	BERNSTORFF Sigrid & PIVAC Branko	Sincrotrone Trieste & Ruder Bošković Insitute, Zagreb	Italy & Croatia	Nano Si Superlattices for the next generation solar cells	Materials Science
Inhouse research	AMENITSCH Heinz & INNOCENZI Plinio	AAS, IBN, Graz & University of Sassari	Austria & Italy	Patterning of mesostructured transition metal-oxide films	Chemistry
Inhouse research	BERNSTORFF Sigrid & GRACIN Davor	Sincrotrone Trieste & Ruder Bošković Insitute, Zagreb	Italy & Croatia	Si nanocrystals in amorphous silicon matrix	Materials Science
Inhouse research	AMENITSCH Heinz & BOULGAROPOULOS Beate	AAS, IBN, Graz	Austria	Structure and Dynamics of Apoptotic Model Membranes	Life Sciences
Inhouse research	BERNSTORFF Sigrid & PAVLOVIC Mladen	Sincrotrone Trieste & Ruder Bošković Insitute, Zagreb	Italy & Croatia	GISAXS study of silver metal islands films on glass substrates	Materials Science

2008 (second half year)

Proposal	Proposer	Institution	Country	Title	Research Area
2008026	ZIDANSEK Aleksander	Jozef Stefan Institute, Ljubljana	Slovenia	Smectic ordering in ferrofluid doped liquid crystals	Chemistry
2008078	DESNICA Uros	Ruder Bošković Insitute, Zagreb	Croatia	Growth of three-dimensional superlattices from Ge quantum dots	Materials Science
2008106	MITCHELL Geoffrey	University of Reading, Dept. of Physics	United Kingdom	Control of Polymer Morphology through Additives	Materials Science
2008213	BOULGAROPOULOS Beate	AAS, IBN, Graz	Austria	Effect of Sphingomyelinase on Sphingomyelin containing Lipid Model Membranes	Life Sciences

2008227	BARBARA Pili	Univ .Paris-sud XI, Faculty of Pharmacy, Châtenay-Malabry	France	New PEGylated nanoparticles of gemcitabine-squalene anti-cancer drug	Life Sciences
2008248	PIVAC Branko	Ruder Bošković Insitute, Zagreb	Croatia	Si quantum dots production in SiO2/SiO multilayers: a search for better morphology and self organization in 3D	Materials Science
2008276	MEHMOOD Mazhar	National Centre of Nanotechnology, Pakistan Institute of Engineering and Applied Sciences, Islamabad	Pakistan	SAXS Structural Investigation of Organised Nanomaterials: Mesoporous Alumina Membranes containing Cobalt Nanowires	Materials Science
2008278	YAGHMUR Anan	AAS, IBN, Graz	Austria	Structural elucidation of light activated liposomes	Life Sciences
2008294	VOSS Nicole	University of Erlangen-Nürnberg, Dep. of Crystallography and Structure-Physics	Germany	Dependance of micellar form factor on temperature and salt concentration.	Life Sciences
2008300	IBRAHIMKUTTY Shyjumon	AAS, IBN, Graz	Austria	In situ analysis in gas phase to reveal the self assembly of silica mesostructure by SAXS	Materials Science
2008338	MARMIROLI Benedetta	AAS, IBN, Graz	Austria	Investigation of Ultrafast Nucleation and Growth of Zinc Sulfate by SAXS	Materials Science
2008345	GOMES Maria	Physics Center, University of Minho, Braga	Portugal	Characterization of SixGe1-x nanocrystals embedded in SiO2 and Al2O3 thin films	Materials Science
2008356	HAMLEY Ian	Dept of Chemistry, University of Reading	United Kingdom	Gel phase behaviour of mixed nonionic block copolymers and anionic surfactants	Life Sciences
2008393	KRIECHBAUM Manfred	AAS, IBN, Graz	Austria	Ternary lipid/oil/water nanostructure behavior under hydrostatic pressure	Life Sciences
2008407	PAVLOVIC Mladen	Ruder Bošković Insitute, Zagreb	Croatia	Morphology study of metal nanocluster films via simultaneous GISAXS, GIWAXD and GIXR techniques	Materials Science
2008417	SCHAFLER Erhard	Research Group Physics of Nanostructured Materials, Faculty of Physics, University of Vienna	Austria	Investigation of the existence and of the kinetics of dislocation generation in biodegradable semicrystalline poly(3-hydroxybutyrate) (PHB) by in-situ WAXS and SAXS deformation.	Materials Science

2008418	INNOCENZI Plinio	Lab. of Materials Science and Nanotechnology, University of Sassari, Alghero	Italy	Confined growth of iron cobalt nanocrystals in mesoporous silica thin films: FeCo–SiO2 nanocomposites	Chemistry
2008430	CACHO NERIN Fernando	AAS, IBN, Graz	Austria	Assessment of nonaffine kinematics and network effects in arterial collagen	Life Sciences
2008531	FAIVRE Vincent	Lab. de Physico-Chimie des Systèmes Polyphasés, University Paris-Sud, Châtenay-Malabry	France	Triacylglycerol Tempering in Emulsion: Model and Pharmaceutical Emulsion Requirements (TAG-TEMPER)	Life Sciences
2008548	LUCIC LAVCEVIC Magdy	Faculty of Chemical Technology, University of Split	Croatia	Analysis of nanostructures in metal oxide thin films by simultaneous application of the GISAXS and GIXRD techniques	Materials Science
Inhouse Research	BERNSTORFF Sigrid & TURKOVIC Aleksandra	Sincrotrone Trieste & Ruder Bošković Insitute, Zagreb	Italy & Croatia	GISAXS Measurements of Nanostructured Titanium Dioxide Thin Films	Materials Science
Inhouse Research	RAPPOLT Michael & BRANDENBURG Klaus	AAS, IBN, Graz & Research Center Borstel, Biophysics, Borstel	Austria & Germany	Conformational studies on bacterial virulence factors and interaction with binding proteins and antimicrobial peptides	Life Sciences
Inhouse Research	BERNSTORFF Sigrid & GRACIN Davor	Sincrotrone Trieste & Ruder Bošković Insitute, Zagreb	Italy & Croatia	Si nanocrystals in amorphous silicon matrix	Materials Science
Inhouse Research	BERNSTORFF Sigrid & RADIC Nikola	Sincrotrone Trieste & Ruder Bošković Insitute, Zagreb	Italy & Croatia	Surface layer morphology of Tungsten-Carbon thin films	Materials Science
Inhouse Research	AMENITSCH Heinz & TRIMMEL Gregor	AAS, IBN, Graz & Institute for Chemistry and Technology of Materials, Graz University of Technology, Graz	Austria	Thermal formation of thin nanocomposite layers - a time resolved X-Ray scattering study	Chemistry
Inhouse Research	BERNSTORFF Sigrid & DUBCEK Pavo, PIVAC Branco	Sincrotrone Trieste & Ruder Bošković Insitute, Zagreb	Italy & Croatia	Nano Si Superlattices for the next generation solar cells	Materials Science

User Statistics

1. Number of submitted proposals and assigned shifts from 1995 until June 2010

The Austrian SAXS-beamline at ELETTRA opened to users in September 1996. Since then many experiments have been performed related to the fields of life science, materials science, physics, biophysics, chemistry, medical science, technology and instrumentation.

The assignment of beamtime at this beamline is done separately for the group of "General Users" (GU) and the "Collaborating Research Group" (CRG), i.e., the Austrian users. Beamtime was assigned to the proposals of each group in the order of the rating received by the Scientific Committee, and up to the maximum number of shifts available to each group according to the contract between "The Austrian Academy of Sciences" and the "Sincrotrone Trieste". Until December 1997 up to 30 % of the beamtime was given to CRG, up to 55 % to GU, and 15% was reserved for maintenance purposes. From January 98 to June 2001 the quota for beamtime was up to 35 % for CRG, up to 50 % for GU, and again 15% reserved for maintenance purposes. From July 2001 on the two contingents for user proposals from CRG and GU receive up to 35% of the beamtime each. The remaining 30 % of beamtime are used for inhouse research projects as well as for maintenance purposes.

Figure 1 gives an overview of the numbers of received proposals, the numbers of requested and assigned shifts, as well as the percentage between assigned and requested shifts during the last years. As can be seen in Fig.1, the request for beamtime at the SAXS-beamline increased strongly until the first half year of 1999. Then, probably due to the high rejection rates, the number of submitted proposals decreased somewhat during 2001, which resulted in a better ratio of accepted / rejected proposals. This oscillating behaviour of beamtime request can also be seen for the period 2002 – 2009 where after higher numbers of submitted proposals slightly reduced request periods follow. The numbers for the second semester of 2007 and first of 2008 reflect also that, due to the long shut-down from 1.10.2007 to 3.03.2008 (for the booster installation) less proposals were submitted, and less beamtime was available.

In 2008, in total 68 proposals (12 from CRG, and 56 from GU) were submitted. From these 18 proposals (0 from CRG and 18 from GU) were submitted by "new" usergroups, i.e. groups which so far had never beamtime at the SAXS beamline. From these, 6 GU proposals were accepted by the review committee.

Figure 1 (Next page). The statistical information about the beamtime periods since March 1997 are given for the groups "CRG", and "GU" separately, as well as for both together ("Total"). Shown are, for all beamtime periods (from top to bottom):
● Number of received proposals, ● Number of requested shifts,
● Number of assigned shifts, and ● Relation between assigned and requested shifts

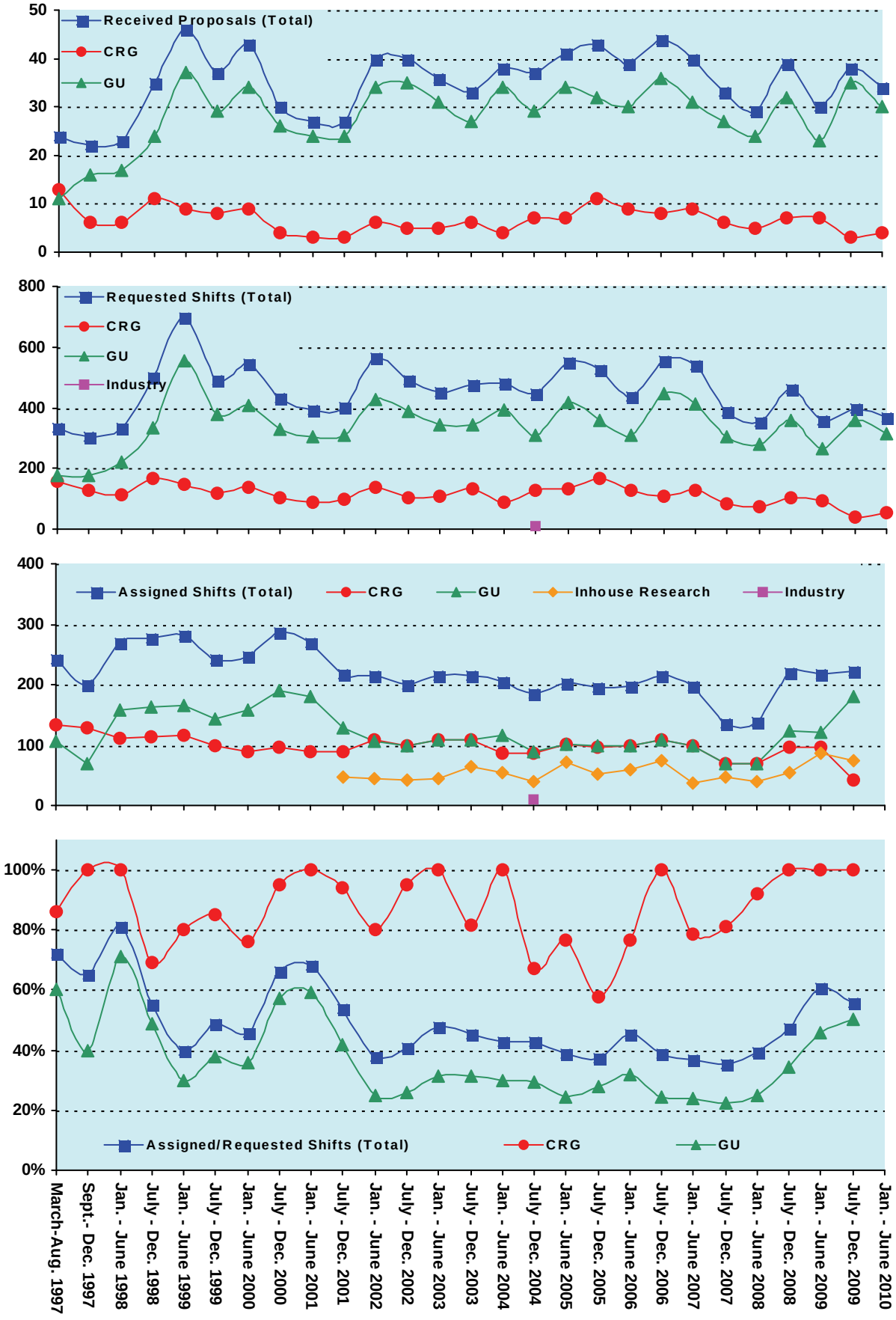
Received Proposals (Total)
CRG
GU
Requested Shifts (Total)
CRG
GU
Industry
Assigned Shifts (Total)
CRG
GU
Inhouse Research
Industry
Assigned/Requested Shifts (Total)
CRG
GU
March-Aug. 1997
Sept.- Dec. 1997
Jan. - June 1998
July - Dec. 1998
Jan. - June 1999
July - Dec. 1999
Jan. - June 2000
July - Dec. 2000
Jan. - June 2001
July - Dec. 2001
Jan. - June 2002
July - Dec. 2002
Jan. - June 2003
July - Dec. 2003
Jan. - June 2004
July - Dec. 2004
Jan. - June 2005
July - Dec. 2005
Jan. - June 2006
July - Dec. 2006
Jan. - June 2007
July - Dec. 2007
Jan. - June 2008
July - Dec. 2008
Jan. - June 2009
July - Dec. 2009
Jan. - June 2010

2. Provenience of users

During 2008, 158 users from 65 institutes in 18 countries have performed experiments at the SAXS beamline. In Fig. 2 are shown both the provenience of these users, and of their respective institutes. Each user or institute was counted only once, even though many users performed experiments in both beamtime periods of 2008.

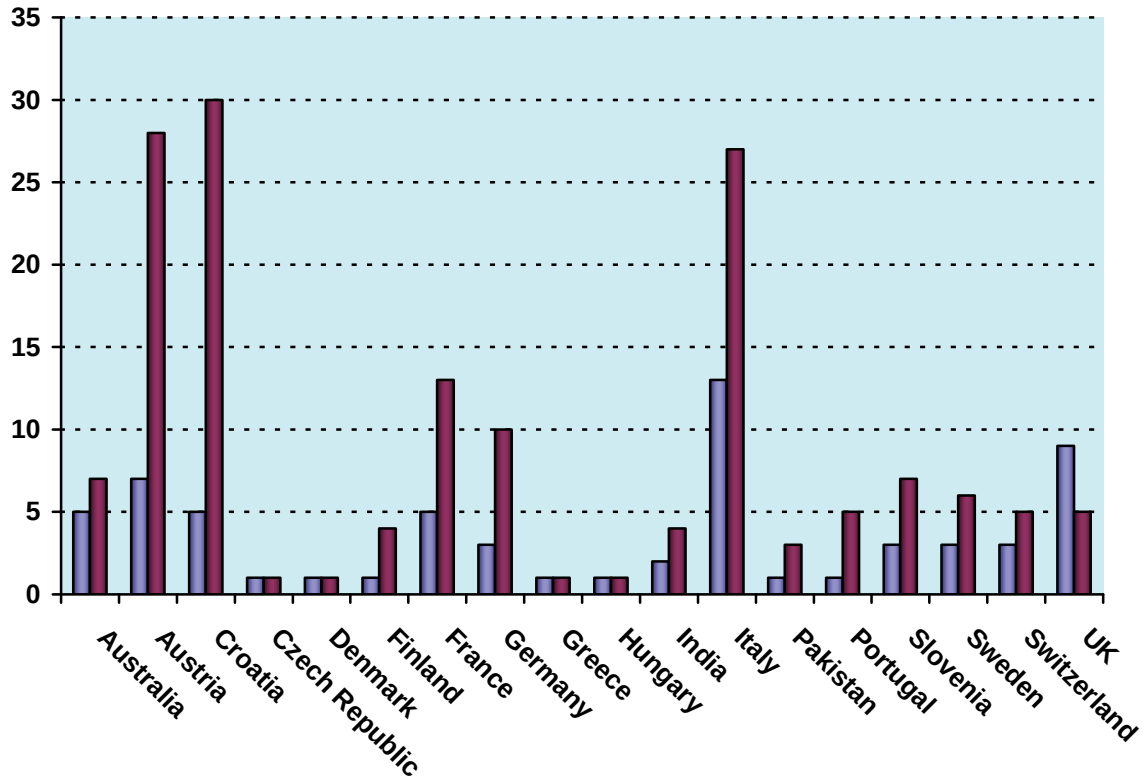

Figure 2. Provenience of users (red) and of their corresponding institutes (blue).

3. Documentation of experimental results

As could be expected, with the start of user-operation at the SAXS-beamline the number of contributions to conferences started to increase strongly. With a delay of one year - the average time needed for paper publications - also the number of publications increased accordingly, as can be seen in Fig. 3.

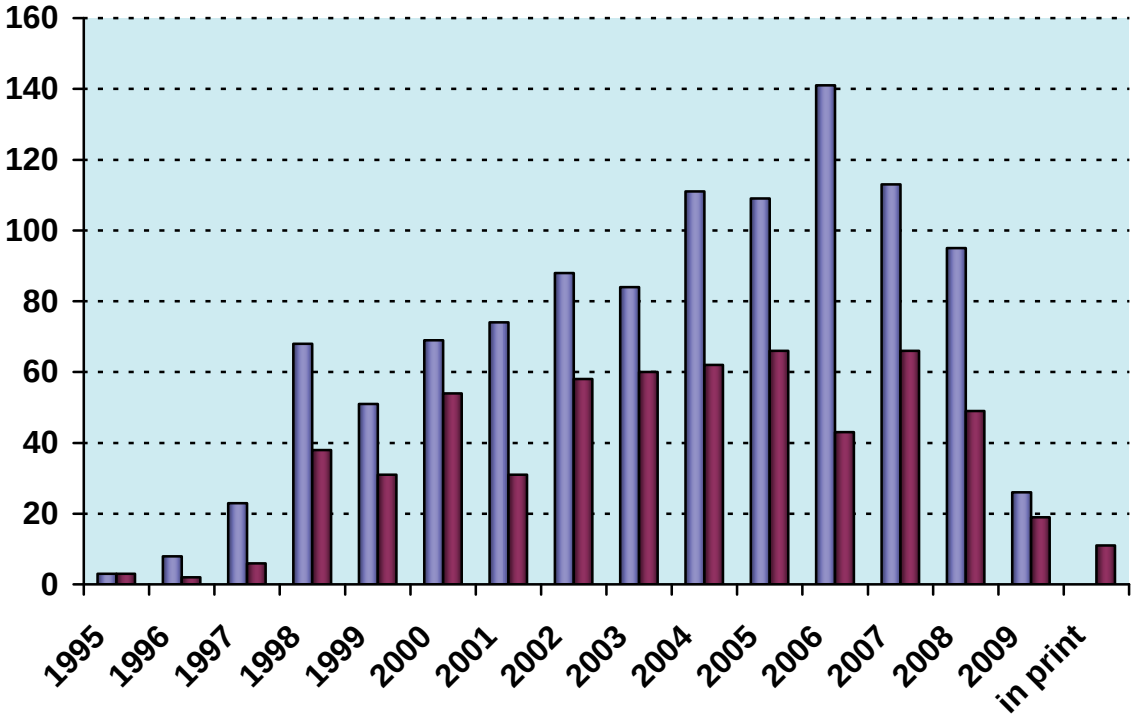

Figure 3. Number of conference contributions (blue) and of refereed paper publications (red) for the years 1995-2008. Also contributions, which have been published until June 2009 as well as those in print at that time are included.

In addition, from 1995 until June 2009, the following documentations based on instrumentation of the SAXS-beamline, or on data taken with it, have been produced.

Unrefereed publications:
Technical Reports on Instrumentation: 5
Contributions to Elettra Newsletters: 15
Contributions to Elettra Highlights: 29
Habil Thesis: 4
PhD Thesis: 69
Master Thesis : 29

Experimental Possibilities at the SAXS-beamline

1. LATEST DEVELOPMENTS

Larger experimental hutch

As our neighbour beamline (HXD) has moved downstream their experimental set-up, in May 2008 we took the opportunity and extended about 3 m also our experimental hutch. The beamline has reached now an overall length according to our initial plans in 1993. Immediately this allows e.g. the permanent installation of a diffractometer (roll on/roll off) or temporarily of an optimized micro focus set-up, which delivers focal spot sizes down to 10 μm and will allow for micro spot scanning SWAXS experiments with a new X-Y scanning stage. On the other hand we can increase the sample to detector distance and therefore improve our minimum SAXS resolution or maximise the flux density at sample position for certain experiments. Nevertheless this prolongation of the experimental hutch will ensure the sustainable development of the beamline also in the future by giving us the opportunity to realize new optical concepts, e.g. new mirrors, Fresnel or refractive lenses.

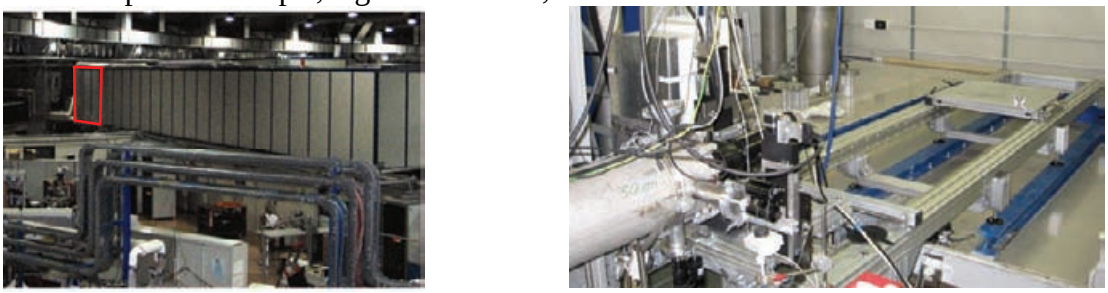

Figure 1: The expanded experimental hutch: external (left - new part highlighted in red); inside with extended optical table (right)

Upgraded and improved computing infrastructure

In order to improve steadily the user friendliness and performance of the beamline, the following improvements have been made to the computing and data acquisition infrastructure:
High-speed private network: A private gigabit network has been deployed at the beamline. This makes it possible to save data from one (or several) instruments (e.g. SWAXS with the gas detectors and the CCD) and simultaneously inspect and/or process it on a different computer.
Larger network storage: the network disk previously available for users to store their data during their experiments at the SAXS beamline has been expanded, and now offers ~700GB of safe, redundant storage. Note that the policy that users MUST take their data with them when they finish their experiments still applies!
New users-dedicated workstation: a new workstation has been acquired and dedicated to users of the beamline. This computer is connected to the internal network and its intended use is to perform on-line data inspection and processing, in addition to providing users with backup facilities and network access.
Hardware upgrade of Image Plate computer: late in 2007 the group acquired a Mar300 Image Plate detector. In 2008 a new computer has been deployed to drive this detector, substituting the older one.
Operating system upgrade for the CCD: the operating system of the computer that controls the Photonic Science CCD camera has been upgraded, enabling it to use a larger amount of memory efficiently. This has resulted in a more stable configuration, and the possibility to capture long series of frames (over 200) at high speed (4 frames per second).

2. ACCESSIBLE SAXS AND WAXS RANGES

Simultaneous SAXS- and WAXS-measurements can be performed using a linear sensitive gas detector (Gabriel type, windows size 8 x 100 mm, active length 86.1 mm with a resolution of 0.135 mm/channel) for the WAXS-range, and either a second linear Gabriel type detector (windows size 10 x 150 mm, active length 134 mm with a resolution of 0.159 mm/channel), or the 2D CCD-system for the SAXS-range. A specially designed vacuum chamber (SWAXS-nose, see Annual Report of 1996/97, p. 32) allows to use both scattering areas below (for SAXS) and above (for WAXS) the direct beam, respectively.

Depending on the photon energy maximum SAXS resolutions of 2000 Å (5.4 keV), 1400 Å (8 keV) or 630 Å (16 keV) are available. The available possible WAXS-ranges are summarised in Table 1. The overall length of the SWAXS-nose in the horizontal direction, measured from the sample position, is 512 mm and the fixed sample to WAXS-detector distance is 324 mm. At the shortest SAXS camera-length an overlap in the d-spacings covered by the SAXS- and WAXS-detectors, respectively, is possible: then, the common regime lies around 9 Å.

Range	2θ [deg]	d-spacing (Å)		
		8 keV	5.4 keV	16 keV
1	9.4	*9.40*	14.03	4.27
	27.6	*3.23*	4.82	1.47
2	27.4	3.25	4.86	1.48
	45.6	1.99	2.97	0.90
3	45.4	2.00	2.98	0.91
	63.6	1.46	2.18	0.66
4	63.4	1.47	2.19	0.67
	81.6	1.18	1.76	0.54

Table 1. Possible d-spacing ranges in the WAXS-regime at the SAXS-beamline at ELETTRA. Since the WAXS-detector can be mounted at four different fixed positions on the SWAXS-nose (range 1-4), with the three possible energy choices (5.4, 8 and 16 keV) this results in 12 different d-spacing regimes. In italic the most common choice (8 keV, range 1) is highlighted. This range is suited for experiments, e.g., on lipid-systems and (bio)polymers.

3. CALIBRATION OF THE S-AXIS AND FLAT FIELD CORRECTION

At the SAXS beamline various standards are used for the angular (s-scale) calibration of the different detectors:

- Rat tail tendon for the SAXS detector - high resolution (rtt*.dat)
- Silver behenate for the SAXS detector – medium and low resolution (agbeh*.dat)
- Para-bromo benzoic acid for the WAXS detector – WAXS range 1 and 2 (pbromo*.dat)
- Combination of Cu, Al foils and Si powder for the WAXS detector – WAXS range 2 and higher

In Figure 2 a typical diffraction pattern of rat tail tendon is shown, depicting the diffraction orders (from the first to the 14th order) measured with a "high" resolution set-up (2.3 m) and the delay-line gas detector. The d-spacing is assumed to be 650 Å, but this value can vary depending on humidity up to 3%. Thus, the rat tail tendon is often used only to determine the position of the direct beam (zero order), while the absolute calibration is performed using the diffraction pattern of Silver behenate powder. Fig. 3 depicts a diffraction pattern of Silver behenate measured with "medium" resolution set-up (1.0 m) from the first to the 4th order (repeat spacing 58.4 Å) [1].

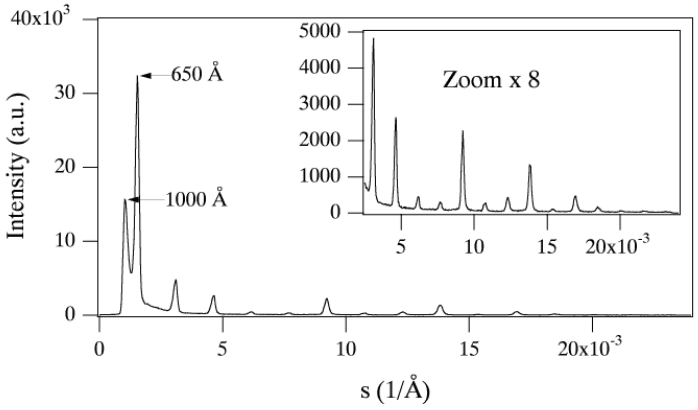

Figure 2. SAXS diffraction pattern of the collagen structure of rat tail tendon fibre at a distance of 2.3 m.

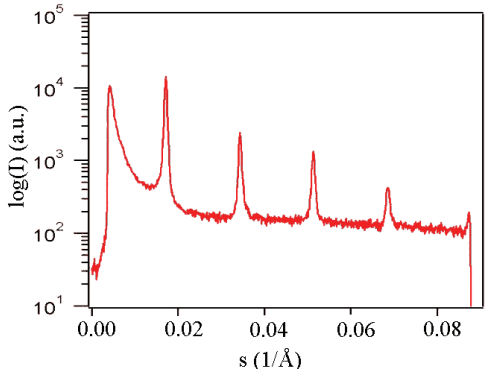

Figure 3. SAXS diffraction pattern of Ag behenate powder at a distance of 1.0 m

In Figure 4 a typical WAXS pattern of p-bromo benzoic acid is shown. The diffraction peaks are indexed according to the values given in Table 2, taken from [2].

d-spacing / Å	rel. intensity	d-spacing / Å	rel. intensity
14.72	18000	4.25	490
7.36	1200	3.96	2380
6.02	330	3.84	10300
5.67	980	3.74	26530
5.21	6550	3.68	1740
4.72	26000	3.47	760

Table 2. d-spacings and relative intensities of p-bromo benzoic acid according to [2].

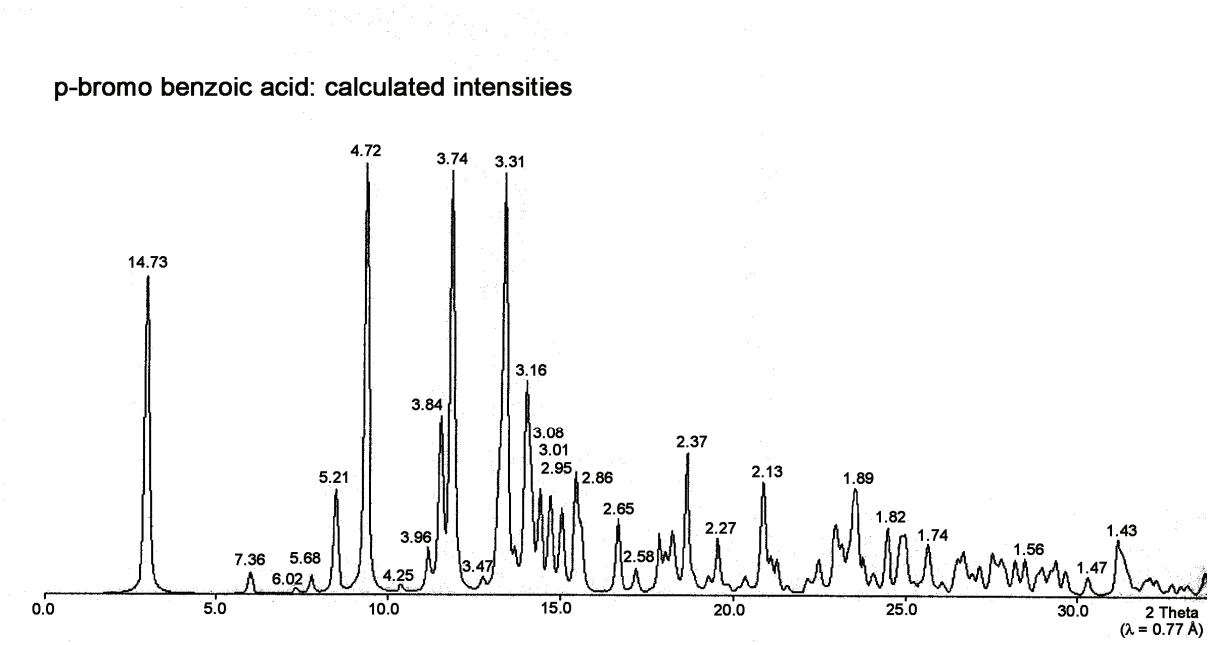

Figure 4. Calculated diffraction pattern of p-bromo benzoic acid. d-spacings are given in Å.

The s-scale for both, the SAXS and the WAXS range, can be obtained by linear regression, i.e., the linear relation between the kown s-values of the calibrant versus the measured peak positions has to be found.

A further correction is regarding the flat field response (efficiency) of the detectors. For this correction, the fluorescence light of various foils are used to illuminate the detectors rather homogeneously:

At 8 keV: iron foil (100 μm thick), fluorescence energy: 6.4 keV K_α, 7.1 keV K_β (effic*.dat)
At 16 keV: copper foil (> 100 μm thick), fluorescence energy: 8.028 keV $K_{\alpha 2}$, 8.048 keV $K_{\alpha 1}$, 8.905 keV K_β (effic*.dat)

The measured scattering pattern are corrected for the detector efficiency simply by dividing them by the fluorescence pattern. Note: The average of the detector efficiency data should be set to unity and a small threshold should be applied to avoid any division by zero.

[1] T.N. Blanton et. al., Powder Diffraction 10, (1995), 91
[2] K. Ohura, S. Kashino, M. Haisa, J. Bull. Chem. Soc. Jpn. 45, (1972), 2651

4. SITE LABORATORIES

In August 2002 our new chemistry and X-ray laboratory went into operation. The 70 m^2 big laboratory is divided in two parts, in which the bigger share of 43 m^2 is occupied by the chemistry lab. This unit serves mainly for sample preparation and analysis for both, in house research and external SAXS user groups. In the X-ray laboratory the set-up of a SWAX camera for simultaneous small and wide angle scattering has been completed (Hecus X-ray Systems, Graz, Austria: www.hecus.at), which allows on-site testing of samples before moving on to the SR beamline. The chemistry lab is meanwhile equipped with:

- micro centrifuge (max. 13200 rpm; model 5415D from Eppendorf , Hamburg, Germany)
- Chemical fume hood, equipped with a carbon filter for general organic solvents (model GS8000 from Strola, Italy)
- vacuum drying oven (min. pressure 1 mbar; max. T: 200 °C, precision +/- 0.4°C; Binder WTB, Tuttlingen. Germany)
- balance (min.-max.: 0.001 - 220g; model 770 from Kern & Sohn, Balingen, Germany)
- Magnetic stirrer with heating plate and thermometer, temp max 260°C
- vortex for microtubes (model MR 3001 and REAX; both from Heidolph, Schwabach, Germany)
- two water baths :
  - Unistat CC, freely programmable in the range from -30 to 100°C (Huber, Offenburg, Germany);
  - Lauda M3, available for heating only (Lauda-Könighofen, Germany)
- ultrasonic bath with water heater (VWR International, Milano, Italy)
- Ultrasonic processor equipped with a 3 mm probe (Sonics VCX130, SY-LAB Geräte GmbH, Germany)
- HPLC pump, Pharmacia LKB; working range, 0,01-9,99 ml/min, 0,1-40MPa
- HPLC pump, Gilson 307; working range, 0,010- 5 ml/min, 0,1-60MPa
- three syringe pumps, low pressure; flow rate range, 1µl/hr – 2120 ml/hr
- three syringe pumps, high pressure: P max ~ 60 bar
- three high pressure infusion modules: P max ~ 690 bar

Further, four working benches (one with a water sink), two fridges (+ 4°C) and a separate freezer (- 20 °C), standard glassware, syringes and needles of different sizes, µ-pipettes (10 - 50 - 200 - 1000), as well as some standard chemical reagents (e.g., chloroform, ethanol, methanol); deionized water (milli-RO and ultrapure milli-Q water) is available.

Figure 6.
Typical lab activity: Barbara Sartori loads the centrifuge.

5. AVAILABLE SAMPLE MANIPULATIONS STAGES

1. General

Usually the sample is mounted onto the sample alignment stage which allows the user to place the sample into the beam with a precision of 5µm (resolution: 1µm). In Fig. 7 the ranges for vertical and horizontal alignment as well as the maximum dimensions of the sample holders are given. The maximum weight on the sample stage is limited to 10 kg. In case the envelope dimensions of a sophisticated sample station provided by the users are slightly larger than those given in Fig. 7, the user can ask the beamline responsible for a check up of his space requirements. If it does not fit at all to these specifications, user equipment can also be mounted directly onto the optical table, which allows much larger spatial dimensions.

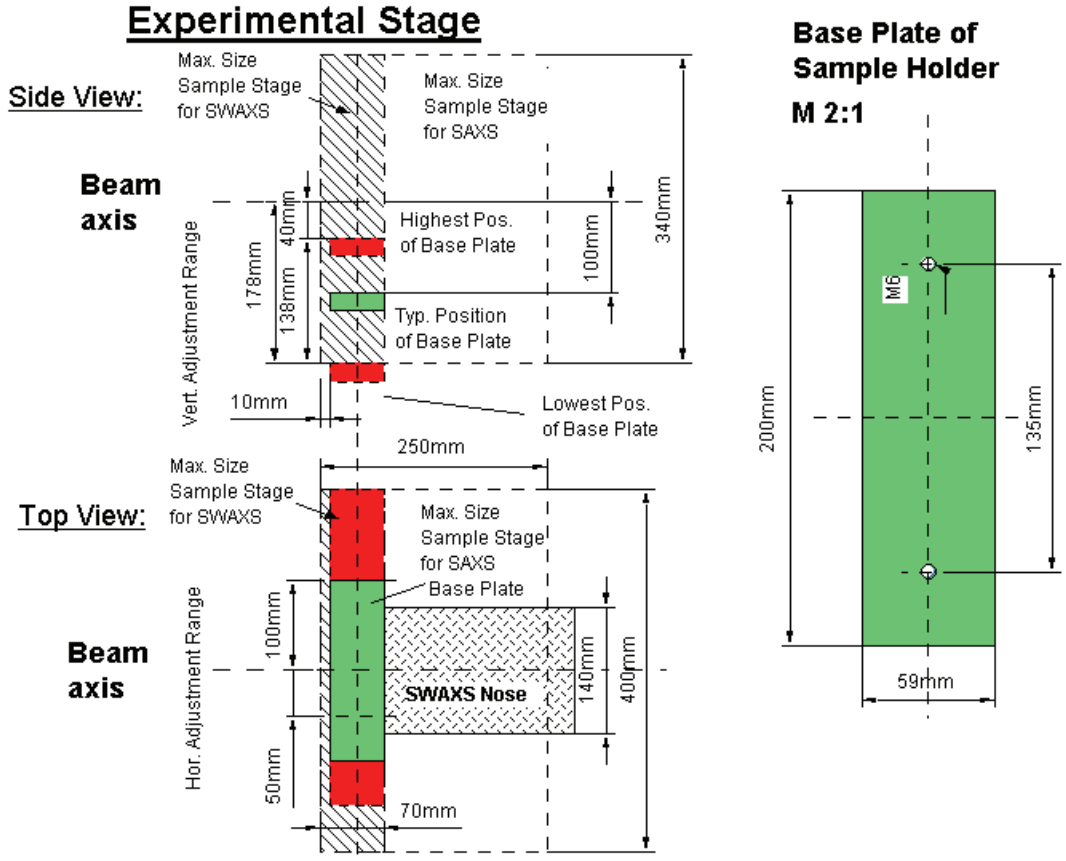

Figure 7. Maximum dimensions and alignment range of the sample holder to be mounted via a base-plate onto the standard alignment stage (left), and dimensions of the base-plate (right).

2. Sample Holders

As standard equipment for liquid samples Paar capillaries (diameter: 1 and 2 mm) are used thermostated with the KPR (Peltier heating/cooling) sample holders (Anton Paar, Graz, Austria). For use in these sample holders flow through capillaries and Gel holders are standard equipment. Temperature scans can be performed with KPR (-30-70 °C). Typically the precision and the stability of this systems is 0.1 °C. Additionally thermostats for temperature control or cooling proposes can be used at the beamline (-40 - 200 °C). Helium and Nitrogen gas bottles are available at the beamline, for other gases please contact the beamline responsible.

Multiple-sample holders can be mounted onto the standard sample manipulator. At present holders are available for measuring in automatic mode up to 30 solid samples at ambient temperature or up to 4 liquid or gel samples in the temperature range 0 – 95 °C.

3. Online Exhaust System

At the experimental station is available a custom-built fume cover and chemical exhaust system for toxic gases. Thus it is possible to e.g. study in-situ chemical reactions, during which toxic gases might develop.

4. Stopped Flow Apparatus

A commercial stopped flow apparatus (manufactured by Bio-Logic, Paris, France), especially designed for Synchrotron Radiation SAXS investigations of conformation changes of proteins, nucleic acids and macromolecules, is available. The instrument consists of a 4 syringe cell with 3 mixer modules manufactured by Bio-Logic. Each syringe is driven independently from the others by an individual stepping-motor, which allows a high versatility of the mixing sequence (flow-rate, flow duration, sequential mixing). For example, injection sequences using one or up to 4 syringes, unequal filling of syringes, variable mixing ratio, reaction intermediate ageing in three- or four-syringe mode etc.. The solution flow can be entirely software-controlled via stepping motors, and can stop in a fraction of a millisecond.

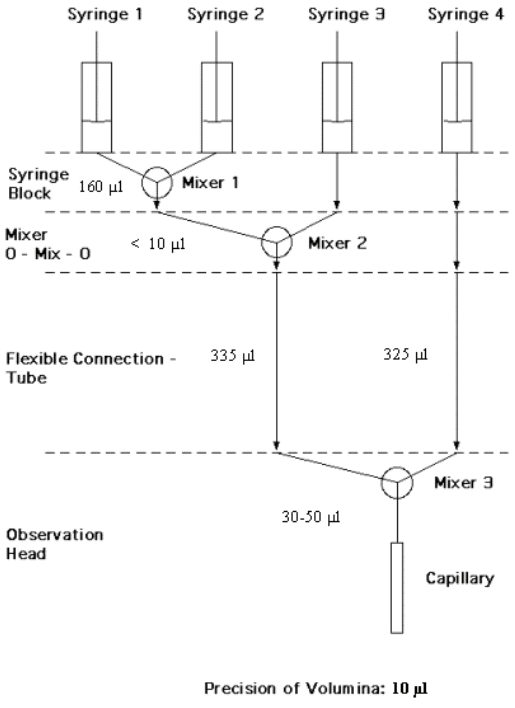

Figure 8. Sketch of the stop flow system.

The software allows the set-up of the shot volumes of each of the 4 syringes in a certain time interval. Up to 20 mixing protocols can be programmed. Additionally macros for the repeated execution of individual frames can be defined. Furthermore, the input and output trigger accessible for user operation can be programmed. In the usual operation modus the start of rapid mixing sequence is triggered from our X-ray data-acquisition system (input trigger).

After the liquids have been rapidly mixed, they are filled within few ms into a 1 mm quartz capillary - situated in the X-ray beam- , which is thermostated with a water bath. Depending on the diffraction power of the sample time resolutions of up to 10 ms can be obtained.

The main parameter of the system are:

- Thermostated quartz capillary (1 mm)
- Temperature stability 0.1 °C
- Total sample used per mixing cycle (shot volume): 100 µl
- Maximum 2θ angle of 45°
- Total Volume 8 ml
- Dead volume 550 µl
- Speed: 0.045 – 6 ml/s
- Duration of flow 1 ms to 9999 ms/Phase
- Dead time: 1 ms
- Reservoir volume: 10 ml each

Further information can be found at the webpage: http://www.bio-logic.fr/

5. Grazing Incidence Small Angle X-ray Scattering

Grazing incidence studies on solid samples, thin film samples or Langmuir-Blodget-films can be performed using a specially designed sample holder, which can be rotated around 2 axes transversal to the beam. Furthermore the sample can be aligned by translating it in both directions transversal to the beam. The precisions are 0.001 deg for the rotations and 5 µm for the translations. Usually the system is set to reflect the beam in the vertical direction. According to the required protocol and the actual assembly of the rotation stages ω, θ, 2θ and φ scans can be performed.

6. Temperature Gradient Cell

A temperature gradient cell for X-ray scattering investigations on the thermal behaviour of soft matter manybody-systems, such as in gels, dispersions and solutions, has been developed. Depending on the adjustment of the temperature gradient in the sample, on the focus size of the X-ray beam and on the translational scanning precision an averaged thermal resolution of a few thousands of a degree can be achieved.

7. Flow-through Cell

The flow through cell works in a simple manner: Special quartz capillaries (Glas Technik & Konstruktion, Schönwalde/Berlin) of 1.5 mm diameter and wide openings of about 3 mm at each end, can be inserted into the standard Anton Paar sample holder, which allows various temperature treatments (T-range 25-300 or –30-70 °C, respectively). Thin tubes are connected directly to the capillary ends and a constanst flow is achieved by a peristaltic pump.

8. IR-Laser T-Jump System for Time-Resolved X-ray Scattering on Aqueous Solutions and Dispersions

The Erbium-Glass Laser available at the SAXS-beamline (Dr. Rapp Optoelektronik, Hamburg, Germany) delivers a maximum of 4 J per 2ms pulse with a wavelength of 1.54 μm onto the sample. The laser-beam is guided by one prism onto the sample, which is filled in a glass capillary (1 or 2 mm in diameter) and Peltier or electronically thermostated in a metal sample holder (A. Paar, Graz, Austria). With a laser spotsize of maximal 7 mm in diameter a sample-volume of maximal 5.5 μl or 22 μl, respectively, is exposed to the laser-radiation. In a water-solutions/dispersions with an absorption coefficient of A = 6.5 cm^{-1} T-jumps up to 20°C are possible.

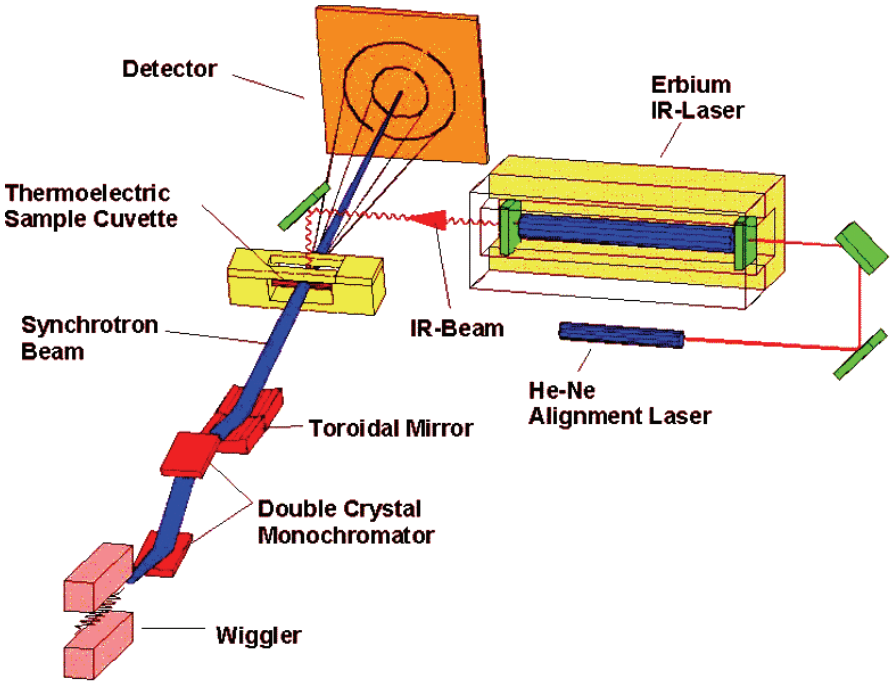

Figure 9. Sketch of the T-jump set-up.

9. High Pressure Cell System

SWAXS measurements of samples under pressure can be performed from 1 to 2500 bar, from 0 to 80 °C in the scattering angle region up to 30 degrees, both in the static or time-resolved mode, e.g. p-jump or p-scan, with a time-resolution down to the ms range. Precise pressure scans of any speed within a broad range (e.g. ca. 1.0 bar/s - 50 bar/s in the case of water as pressurising medium, and a typical sample volume) can be performed. Alternatively, dynamic processes can be studied in pressure-jump relaxation experiments with jump amplitudes up to 2.5 kbar/10ms in both directions (pressurising and depressurising jumps).
In most applications diamond windows of 0.75 mm thickness (each) are used. The transmission of one pair (entrance and exit window) is 0.1 at 8 keV, i.e. lower than 0.3, the value for the originally used 1.5 mm thick Be-windows. However the loss in intensity is more than compensated for by the considerably lower background scattering of diamond thus leading to higher q-resolution in the experiments.
The sample thickness can be 0.6-4.0 mm, with a volume of approximately 0.5-3 mm^3 completely irradiated by pin-hole collimated (< 1.0 mm diameter) X-rays.
The pressure cell system is flexible and can be built according to the needs of the particular experiment. Normally, a liquid (water, ethanol or octanol) is used as pressurising medium.

But in principle, also gaseous media can be employed as well. N_2 has been successfully tested, and measurements in supercritical CO_2 became frequent.
Beside bulk measurements on samples in transmission set-up, also grazing incidence experiments using silicon wafer with highly aligned samples on its surface inserted in the high-pressure cell have been carried out successfully.

10. Oxford Cryostream Cooler

The Cryostream cooler creates a cold environment only a few millimeters from the nozzle position. The temperature and the flow of the nitrogen gas stream is controlled and regulated by a Programmable Temperatur Controller based on an 'in stream' heater and a thermo-sensor before it passes out over the sample.

The system has been especially developed for X-ray crystallography to perform diffraction experiments on e.g. shock frozen bio-crystals. However, the programmable temperature controller allows further implication for SAXS-experiments, e.g., rapid temperature drops in solvents. The design of the Cryostream Cooler facilitates:

- Nitrogen stream temperatures from -190 to 100 °C
- Stability of 0.1 °C,
- Refill without any disturbance of the temperature at the sample
- Temperature ramps can easily be carried out remotely controlled with scan rates up 6 °C/min
- Individual temperature protocols can be cycled
- T-jumps in both directions can be performed by rapid transfer of the sample in a pre-cooled or -heated capillary using an fast syringe driver reaching a minimum temperature of -80 °C. Here, typical scan rates are about 15 °C/sec with a total process time in the order of 10 sec.

Further information can be found at the webpage: http://www.oxfordcryosystems.co.uk/

11. In-line Differential Scanning Calorimeter (DSC)

The in-line micro-calorimeter built by the group of Michel Ollivon (CNRS, Paris, France) allows to take simultaneously time-resolved synchrotron X-ray Diffraction as a function of the Temperature (XRDT) and high sensitivity DSC from the same same sample.
The microcalorimetry and XRDT scans can be performed at any heating rate comprised between 0.1 and 10 °C/min with a 0.01 °C temperature resolution in the range -30/+130 °C. However, maximum cooling rates are T dependent and 10°C/min rates cannot be sustained below 30°C since cooling efficiency is a temperature dependent process. Microcalorimetry scans can be recorded independently, and also simultaniously, of X-ray patterns. The microcalorimeter head can also be used as a temperature controlled sample-holder for X-ray measurements while not recording a microcalorimetry signal. Isothermal microcalorimetry is also possible when a time dependent thermal event such as meta-stable state relaxation or self-evolving reaction, is expected. The sample capillaries have a diameter of 1.5 mm and are filled over a length of 10 mm.

12. 2D Detectors: Image Plate & CCD-Camera System

The Mar300 Image Plate detector with a circular active area of 300mm in diameter is the largest-area detector available to users of the beamline, with a spatial resolution (pixel size) of 150μm. This detector has two modes of operation (180mm or 300mm), depending on the desired active area, which result in image sizes of 1200x1200 and 2000x2000, respectively. They are stored in the mar image format (16 bit for compactness, with higher precision extensions for values out of range), and can be processed and converted using the Fit2D program [1]. Typical applications are those that need a large Q-range with high dynamic range (typical values of 10^5), i.e. solution scattering from proteins and nanoparticles, temperature-step scans, slow processes like nanoparticle formation, mesophase formation, etc. The exposure time for the Image Plate is given in seconds, with typical values between 1 and 60. Readout time depends on the chosen active area (for 180mm mode, about 130 seconds; for 300mm mode, about 210 seconds), and therefore it is not suitable for samples where high time resolution is needed. Exposure information, number of images in the series and other information is automatically written to a summary file after each image.
So far the detector cannot be triggered by an external trigger input. Controlling an additional (external) device or experiment can only be done by hardware wiring of the TTL shutter signal.

The CCD has a 115 mm diameter input phosphor screen coupled by means of a fiber optic to the image intensifier, which itself is coupled with an additional taper to the CCD (charged coupled device). The spatial resolution of a pixel is 79 μm. The number of pixels is 1024 x 1024 and they can be pinned down to 2 x 2 and 4 x 4. The dynamic range of the CCD is 12 bit. The dark current of the CCD is in the order of 100 ADU (off-set) and the readout noise (read out speed: 10 MHz) is in the order of 6 ADU. (The CCD is cooled by multistage Peltier element for reducing the dark noise.) The intensifier gain is adjustable between 200 and 20000 photons full dynamic range. Typical readout times and exposure times are 150 ms and 100 ms, respectively. The readout times can be reduced down to 100 ms by using the pinning mode of the CCD. Between the frames additional wait times can be programmed e.g. for reducing the radiation damage in the sample or to extend the time for measuring long time processes. For the external control a TTL trigger signal is provided (active low, when the CCD is accumulating an image), which is used to control the electromagnetic fast shutter of the beamline on one hand. On the other hand this signal can be used also to trigger processes as requested by the user.
The CCD is controlled by Image Pro+, which also includes some simple data treatment capabilities:

- flat fielding/background corrections
- enhanced filters and FFT
- calibration utilities (spatial and intensity)
- segmentation and thresholding
- arithmetic logic operations
- various measurements, like surface, intensity, counts, profiles
- advanced macro management

The data are stored in 12 bit – TIFF format and can be directly processed with FIT2D [1]

[1] A.P. Hammersley, "Fit2D: an introduction and overview", ESRF Internal Report, ESRF97HA02T, 1997
[2] http://www.esrf.eu/computing/scientific/FIT2D/

13. Vantec Detector

The one-dimensional high count rate capable Vantec-1 Detector from BrukerAXS Inc. has an active area of 50 x 16 mm and reaches a spatial resolution of about 50 µm, which is smaller than the resolution obtained by the presently used Gabriel Type Gas detectors. Moreover its new gas amplification principle based on the Microgap technology [1] allows much higher count rates compared to the old system. Now the main limitation is the data acquisition system with its maximum integral count rate of about 1 MHz. In the present data acquisition system HCI (Hecus X-ray Systems, Graz, Austria) the detector has the following performance:

- Minimal time resolution: 11 µs
- Maximum No. of frames: 512 (depending on the no. of channels)
- Maximum integral count rate: 1 MHz

14. Tension Cell

Together with the external user group Schulze-Bauer/Holzapfel the research team constructed a general-purpose tension cell. This particular cell was designed for *in-situ* tensile testing with the particular feature that the sample could be completely immersed in a solvent (e.g. physiological solution), which is of particular interest for the blood vessel or collagen fiber testing. The sample container can be attached to a thermal bath to control the temperature in the range from 5 to 95 ºC. A screw with an appropriate opening for the passage of the X-ray beam can adjust the optical thickness of the sample container continuously and optimize the set-up for different sample geometries.
The fully remote controlled system allows to control not only the fiber extension from 0 to 50 mm, but also it records simultaneously the force signal in the range from 0 to 25 N and as an option the optically determined Video extensometer signal to measure the transversal contraction of the sample.

Users Contributions

Material Science

GROWTH OF 3-D SUPERLATTICES FROM Ge QUANTUM DOTS

U.V. Desnica[1], M. Buljan[1], P. Dubcek[1], N. Radic[1], K. Salamon[2], I.D. Desnica-Frankovic[1], Z. Siketic[1], I. Bogdanovic-Radovic[1], M. Ivanda[1] and S. Bernstorff[3]

1.) R. Boskovic Institute, Physics Department, Bijenicka 54, HR-10000 Zagreb, Croatia
2.) Institute of Physics, Bijenicka 56, HR-10000 Zagreb, Croatia
3.) Sincrotrone Trieste, SS 14 km 163.5, 34012 Basovizza (TS) Italy

Semiconductor materials in the form of Quantum Dots (QDs) display a significant dependence of electronic, optical and other properties on the size of nanoparticles, which opens a large number of potential applications in semiconductor and other industries [1-2]. Specifically, physical properties of nano-Ge material are of particular interest since its bandgap is particularly strongly dependent on the Ge QD size [3]. If QDs can be produced to be ordered in 3D dimension (the superlattice, i.e. QDs ordered analogously to atoms in a crystal lattice), new very exciting possibilities for designing new materials are obtained via combination of versatile geometrical arrangements and QDs superlative properties [4,5].
The samples are prepared by deposition of 20 alternating ($Ge+SiO_2$) and SiO_2 bi-layers in a multisource magnetron sputtering KJLC CMS-18 system. The molar ratio of Ge: SiO_2 was 40:60 in the mixed layers, while the SiO_2 layers served as spacers. This report presents a few examples of the most interesting results obtained by the Grazing Incidence Small Angle X-ray Scattering (GISAXS) technique in studying the synthesis of Ge GDs, their properties as well as the comparison of observed self-organization of Ge QDs in SiO_2 after co-deposition at various deposition temperature, Td, followed by thermal treatment at Ta = 800 ^{o}C.

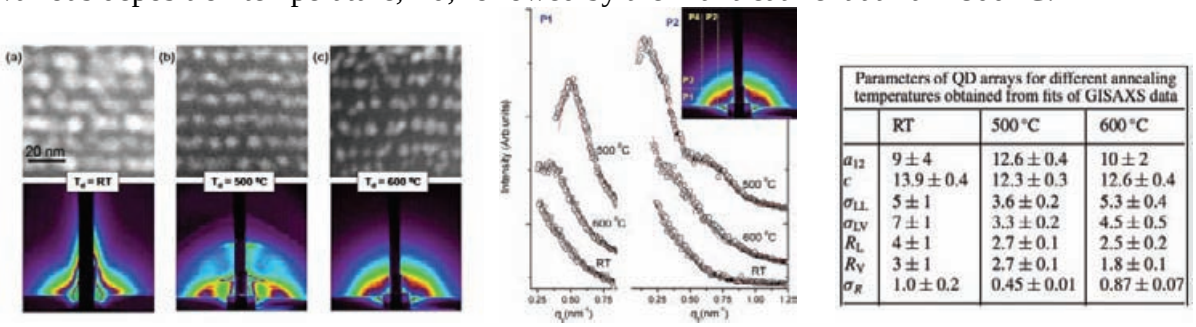

Parameters of QD arrays for different annealing temperatures obtained from fits of GISAXS data			
	RT	500 °C	600 °C
a_{12}	9 ± 4	12.6 ± 0.4	10 ± 2
c	13.9 ± 0.4	12.3 ± 0.3	12.6 ± 0.4
σ_{LL}	5 ± 1	3.6 ± 0.2	5.3 ± 0.4
σ_{LV}	7 ± 1	3.3 ± 0.2	4.5 ± 0.5
R_L	4 ± 1	2.7 ± 0.1	2.5 ± 0.2
R_V	3 ± 1	2.7 ± 0.1	1.8 ± 0.1
σ_R	1.0 ± 0.2	0.45 ± 0.01	0.87 ± 0.07

Figure 1. Left: (a)–(c) HAAFD/STEM images and corresponding 2D GISAXS spectra of samples deposited at different temperatures (indicated) and subsequently annealed at 800°C. **Middle:** Numerical analysis of the experimentally measured GISAXS spectra of annealed samples. 1D intensity profiles P1 and P2 for different deposition temperatures, showing the experimentally measured data (circles) and their theoretical fits (lines). The fitting procedure is performed simultaneously on four 1D profiles P1–P4 extracted from the 2D spectra. The 1D profiles were taken along the lines indicated in the inset. The best-fit parameters are given in the Table **(Right).**

Deposition at Td=500^{O}C results in formation of a 3D ordered structure of QDs. Regular QDs ordering in these samples is evidenced by the appearance of Bragg diffraction peaks (maxima of the interference function) with both q components different from zero.
For Td = 600°C, the QDs formation is very pronounced already during the deposition. Weakly resolved Bragg peaks in the GISAXS spectra indicate that the formed QDs have a poor in-layer ordering, as well as a disturbance of the layer structure. For Td = RT QDs, poorly arranged, and form only after annealing. Annealing at Ta=800°C results in spherical QDs in all samples. The ordering of the QDs and their size distribution was successfully explained in terms of diffusion mediated nucleation and surface morphology effects. The growth model based on these two mechanisms is given in [6]. The basic assumptions of the model are: (i) the nucleation of QDs is mediated by the diffusion of atoms coming on the surface during the deposition process; (ii) the probability of QD nucleation is enhanced in the

regions of negative curvature (troughs) on the surface. Combination of these two effects can lead to a self-organized growth and to the formation of QD superlattices with rhombohedral structure. The film deposited at 500^{o}C represents well the applicability of the model.
Four 1D intensity profiles, Fig. 1 (middle), extracted from the 2D GISAXS maps (Fig. 1 left) along the lines indicated in the inset, are fitted simultaneously to the model function given in [6]. This model assumes the arrangement of dots in a 3D lattice with a disorder degree described by the in-layer and inter-layer disorder parameters σ_{LL} and σ_{LV}, respectively. The input parameters for the fitting process are the primitive cell vectors of an ideal rhombohedral lattice. $R_{L,V}$ and σ_R denote the lateral and vertical radii of the QD and the rms deviation, respectively. The best-fit parameters are given in the Table, in Fig. 1, right.
Additional information on QDs and their properties and self-organization were obtained using additional methods. TEM cross-sections (Fig. 1, left, up); Raman spectroscopy results and Rutherfort Back-Scattering (RBS) results (not shown) excellently agreed with the data from GISAXS and TEM measurements.
In summary, the self-ordering growth of 3D Ge QD superlattices in amorphous SiO_2 matrix is achieved during deposition at Td= 500^{o}C. For lower or higher deposition temperature the deposited Ge atoms also aggregate to form Ge QDs after annealing but the QDs are mostly randomly distributed. The deposition temperature T_d, together with an appropriate thickness of the spacer layers and the Ge/SiO_2 molar ratio, are found essential for achieving the self-organized growth. The superlattices show collective behavior properties [6]. The physical background, the description and explanation of the observed 3D ordering is given in Ref [6], and the technological aspects and possible consequences in Ref [7]. The reported processes open new opportunities in numerous existing and new Ge/SiO_2 system applications, and can be applied more generally for the production of new materials with crystalline QDs in amorphous matrix.
This work was a continuation of previous work at the SAXS beamline in Elettra on semiconductor nanoparticles, which during 2003-2009 resulted in 18 papers (please see Elettra Database); and in particular on Ge QDs, obtained either by magnetron sputtering [8,9] or ion implantation [10].

References:

[1] A. P. Alivsatos, Science 271, 933-937 (1996), R.F. Service, *ibid*. 929-932
[2] W. Scorupa, L. Rebohle, T. Gebel, Appl. Phys. A 76, 1049-1059 (2003)
[3] C. Boested, et al., *Appl. Phys. Lett*. 84 4065-69 (2004)
[4] M. Elhassan et al. Phys. Rev. B 70, 205341 (2004); D. V. Talapin and C.B. Murray, Science 310, 86 (2005).
[5] K. Karral et al., Nature 427, 135 and 432, 81(2004) , M. Perrini et al., Appl. Phys. B 81, 905 (2005).
[6] M. Buljan, U.V. Desnica, M. Ivanda, N. Radić, P. Dubček, G. Dražić, K. Salamon, S. Bernstorff, V. Holy, Formation of three-dimensional quantum-dot superlattices in amorphous systems:Experiments and Monte Carlo simulations, *Phys. Rev. B* 79 (2009) 035310 (Also the same paper is included in the selection of : *Virtual Journal of Nanoscale Science & Technology,* Volume 19, Issue 4, 2009)
[7]M. Buljan, U. V. Desnica, G. Dražić, M. Ivanda, N. Radić, P. Dubček, K. Salamon, S. Bernstorff and V. Holy , The influence of deposition parameters on the correlation of Ge quantum dot positions in amorphous silica matrix, Nanotechnology 20 (2009) 085612 (Selected as one of Journal Highlights articles (LabTalk March 10, 2009 - http://nanotechweb.org/cws/article/lab/38162))
[8] K. Salamon, O. Milat, M. Buljan, U.V. Desnica, N. Radić, P. Dubček, S. Bernstorff, Grazing incidence X-ray study of Ge-nanoparticle formation in (Ge:SiO2)/SiO2 multilayers, *Thin Solid Films* 517 (2009) 1899
[9] U.V. Desnica, K. Salamon, M. Buljan, P. Dubcek, N. Radic, I.D. Desnica-Frankovic, Z. Siketic, I. Bogdanovic-Radovic, M. Ivanda, S. Bernstorff, *Superlattices and Microstructures* 44 (2008) 323-330
[10] U V. Desnica, P. Dubcek, K. Salamon, I.D. Desnica-Frankovic, M. Buljan, S. Bernstorff, U. Serincan, R. Turan, The evolution of the morphology of Ge nanocrystals formed by ion implantation in SiO_2, *Nucl. Instr. Methods Phys. Res. B*, 238 (2005) 272-275 and 249 (2006) 843-846

ORIGIN OF QUANTUM CONFINEMENT EFFECTS IN THIN FILM SILICON

D. Gracin[1], K. Juraić[1], P. Dubček[1], A. Gajović[1], B.Etlinger[1] and S. Bernstorff[2]

1.) Ruđer Bošković Institute, Bijenička 54, 10000 Zagreb, Croatia
2.) Sincrotrone Trieste, SS 14 km 163.5, 34012 Basovizza (TS), Italy

Thin amorphous-nano-crystalline silicon films were deposited on glass substrate under various conditions. According to Raman spectroscopy, their crystal fraction and individual crystals sizes were different from sample to sample. The photo-current induced in the layers using various photon energies showed that the optical gap of the deposited films changed by increasing the crystal fraction. Typical amorphous Si layer have an optical gap, E_G, around 1.6 eV, while the optical gap for crystal Si is 1.1 eV. It could be expected that an increase of the crystal fraction moves the average E_G of a layer that contains an amorphous-crystalline mixture from 1.6 eV towards 1.1 eV. However, the spectral distribution of the normalized photo-current response showed a "blue shift", e.g. indicated an increase of the average optical gap [1] .

The samples were measured by simultaneous GISAXS and GIWAXS in order to find the origin of the "blue shift" and test the Raman results, in particular the estimation of the Raman crystal size.

GISAXS measurements were performed using a X-ray beam energy of 8 keV (λ= 0.154 nm). The grazing angle of incidence, α_i, was selected in the range $0.4^0 < \alpha_i < 1.4^0$. X-ray scattering intensity pattern were acquired by a two dimensional position sensitive charge-coupled device (CCD) detector, at a detector-to-sample distance L = 2 m. The depth distribution of the 'particle' sizes was obtained by changing the grazing incident angle. Since the GISAXS intensity is a convolution of scattering contributions from different depths attenuated according to the incoming and scattering angle, an evaluation of the precise values is very demanding and time consuming. However, for a first approximation, the dominant contribution at the critical grazing incident angle comes from the near surface layer while at the widest measured angles the contribution from the layer that is 300–400 nm below the surface becomes significant. The 'particle' sizes in the direction parallel to the surface, R_{GH} and perpendicular to it, R_{GV}, were estimated by using the Guinier approximation for the analysis of the one-dimensional intensity distribution in these two characteristic directions.

GISAXS showed that the material contained nano-sized objects of similar size and with an electron density different than the average one of the matrix. Measurements performed at various grazing incidence beam angles showed that the size and size distribution of the nano-objects are not uniform across the depth of the sample. Furthermore, the analysis of the particles shape showed a change from spherical symmetric for low concentration of nano-particles towards elongated in directions parallel or perpendicular to the surface for higher concentration. As an example, the average R_G values and ratio between R_{GH} and R_{GV} are plotted in Fig.1 for a sample with 46% crystal fraction as a function of the grazing incidence angle. The angles close to zero correspond to the surface of the sample while the highest angle in the plot corresponds to the part of the sample that is several hundreds of nano-meters below the surface. From Fig. 1 it can be seen that the average crystal sizes (full circles) are larger for lower angles, e.g. closer to surface. The shape of the crystals is ellipsoidal, as can be seen from the ratio between the size in horizontal (R_{GH}) and vertical direction (R_{GV}) plotted as open circles. This anisotropy is larger for lower angles.

The GIWAXS signal, recorded simultaneously with GISAXS, indicated that the nano-sized objects are most probably silicon nano-crystals. Their average sizes, $2R_{GAV}$=2r were compared with the average dimensions estimated from Raman spectroscopy, D_R, in Fig.2. D_R

was estimated from the shift of the transversal optical vibration (TO) of Si bonds in the Raman spectra, assuming only quantum confinement due to the crystal size as a possible cause of the shift. The crystal sizes obtained by Raman and GISAXS are very similar as can be seen from Fig. 2., thus confirming the influence of size effects on the distribution of vibrational states in small crystals. The disagreement between them at higher D_R values could be a consequence of two effects. One is a possible strain in the samples that could result in an overestimation of the crystal sizes calculated by Raman spectroscopy (the points below the unit slope line in Fig.2). The other source of error in the estimation of D_R could be the sample in-homogeneity. As can be seen from Fig.1, the crystals are larger when closer to the surface while Raman is more sensitive for the part of the sample that is closer to the surface.

In a further step, the average GISAXS diameter, "r", is compared in Fig. 3 with the optical gap of the samples. The line in Fig. 3 is plotted in accordance with the effective mass theory that assumes an infinite potential barrier and the optical energy gap in a three dimensional (3D) quantum dot with radius r, as [2]:

$$E_{Gopt} = E_{G\,bulk} + C/r^2 \qquad \text{(eq.1)}$$

where E_{Gopt} is the value for a 3D quantum dot, $E_{G\,bulk}$ is the value for the bulk material, and C is the confinement parameter in the range between 2 and 2.4 eV nm^2 [2]. The comparison of the averaged values for "r" estimated from GISAXS with the values for E_{Gopt} from optical measurements plotted in Fig 3 well supports the theoretical prediction by eq.1, identifying the nano-crystals in the amorphous matrix as "quantum dots".

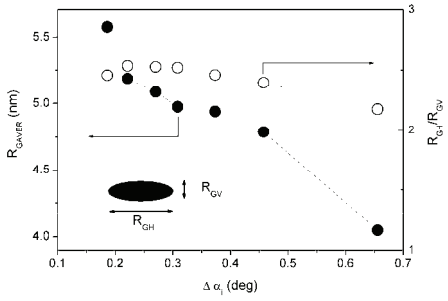

Figure 1. Average gyration radii T_{GAV} versus difference between measured grazing and critical angle, $\Delta\alpha_i$.

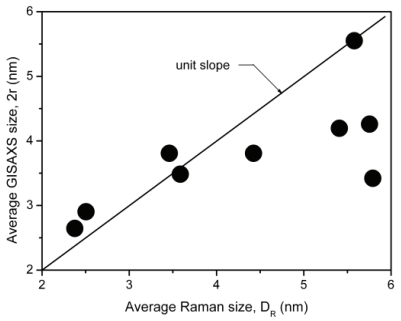

Figure 2. Average crystals size 2r as estimated by GISAXS, versus size of crystals obtained by Raman spectroscopy, D_R

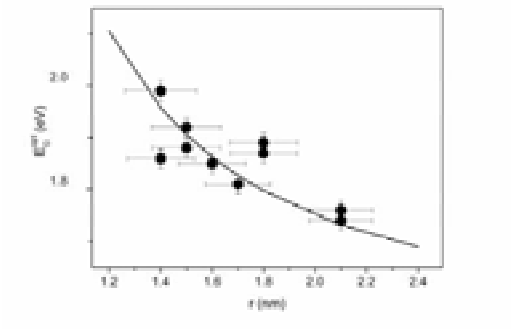

Figure 3. Optical gap EG_{opt} versus crystal size, r, estimated by GISAXS; the full line is a graphical representation of eq.1.

References:

[1] D.Gracin, A.Gajović, K.Juraić, M-Čeh, Z.Remeš, A.Poruba, M.Vaneček, J.Non-Cryst.Solids 354, 2286-2290 (2008)

[2] E.Anastassakis, A.Pinczuk , E.Burstein, F.H.Pollak and M.Cardona, Solid State Commun. 8, 133-138 (1970)

SIMULTANEOUS GISAXS/GIXRD MEASUREMENTS OF LOW-DIMENSIONAL NANOSTRUCTURES IN ZINC OXIDE FILMS

M. Lučić Lavčević[1], S. Bernstorff[2], P. Dubček[3], M. Pavlović[3], and A. Šreder[1]

1.) Faculty of Chemical Technology, University of Split, Teslina 10, 21000 Split, Croatia
2.) Sincrotrone Trieste, SS 14 km 163,5, 34012 Basovizza (TS), Italy
3.) Rudjer Bošković Institute, Bijenička 54, 10000 Zagreb, Croatia

In the frame of investigation of metal oxide nanostructures, we prepared wurtzite-type of zinc oxide films with nanocrystalline units of various morphologies, varying in shape from rods to sheets and particles. Generally, films were grown on substrates by slow, low temperature hydrothermal processes. Nanometric morphology and orientation of nanocrystals were controlled by the choice of precursors and conditions of deposition on seeded non-epitaxial (glass, silicon, ITO) and epitaxial (ZnO thin films derived by e-beam evaporation) substrates. The focus of performed simultaneous GISAXS/GIXRD measurements was on films with high surface area, which is the consequence of the specific arrangement of nanostructures in film, but can also be caused by the inner porosity of nanostructure. The potential application of such architectures is in optoelectronic and sensing devices, as well as in solar cells. The differences needed for specific use of porous ZnO films have to be obtained by fine tuning of the morphology and the thickness of the film. A typical example is formation of films with ZnO nanosheets (sheets with thickness less than 100 nm), constituted of nanograins. The formation process of such quasi two-dimensional nanostructures has not be sufficiently investigated and information about the dependence of their morphology parameters on preparation routes should help in the clarification of their growth. Depending on the preparation route, we obtained thin (few hundred of nanometers) and relatively thick (several micrometers) films, with different dimensions and orientations of both constituent nanostructures - nanosheets and nanograins. GISAXS and GIXRD analysis, performed at the SAXS beamline, give an insight in this complex morphology on the basic level. For example, Fig. 1 presents the FESEM image of a film sample constituted of nanosheets, which are arranged as a microporous system, and Fig. 2 presents a GIXRD pattern of that film. The GIXRD data indicate the presence of crystal grains in the film, of approximately 10 nm in size. The GISAXS pattern of the same sample, in Fig. 3, shows the presence of a porous structure, exhibiting scattering on spheroidal entities with average sizes of 10 nm, which correspond to the grains "seen" by GIXRD, forming a mesoporous sheet.

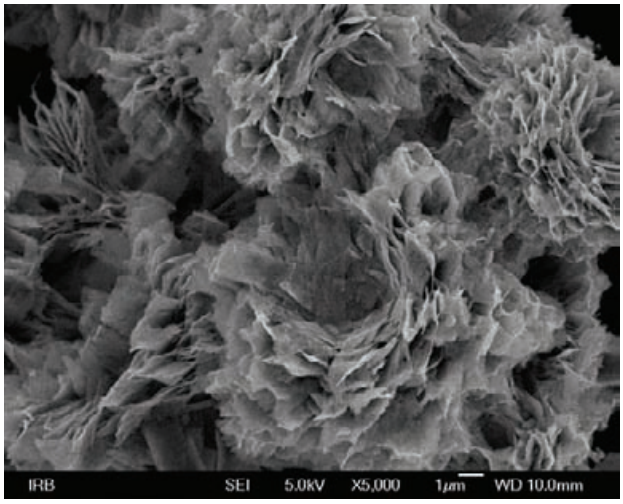

Figure 1. FESEM image of nanosheets

Beside this general view of the existence of the substructure of sheets on the nanometric level, GISAXS/GIXRD data give a detailed description: information about the size distribution of grains in sheets, their direction of growth and surface characteristics (quality of grain/pore interfaces).
In case of thin films on epitaxial substrates, grazing incidence measurements enable separating and comparing the scattering signals from the film and the substrate, giving an advantage in analysis of the influence of substrate morphology on the formation of nanostructures of different shapes and arrangement in the film. Such, a more detailed analysis of the large number of examined samples is in progress.

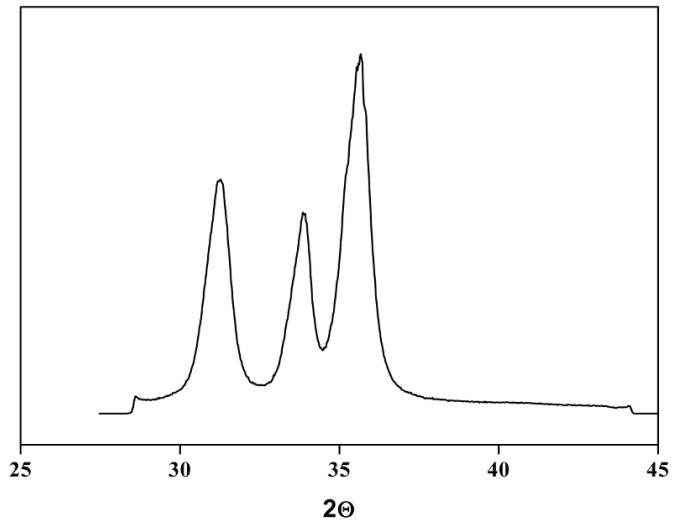

Figure 2. GIXRD pattern of film constituted of nanosheets

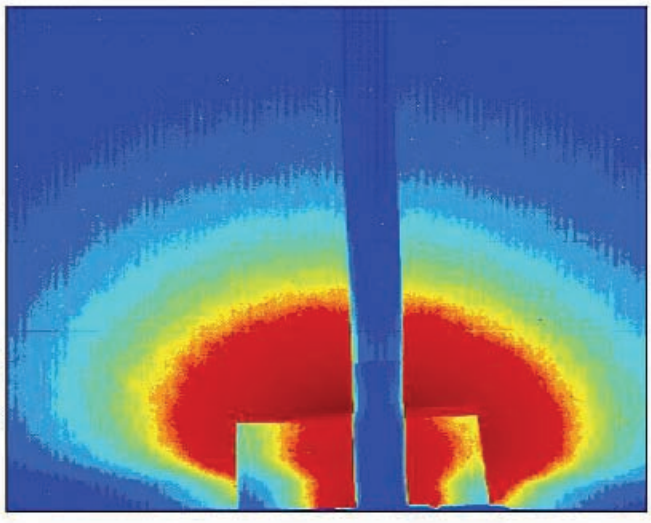

Figure 3. 2D GISAXS pattern of film constituted of nanosheets

TIME RESOLVED SAXS STUDIES OF NANOPARTICLES FORMATION USING A FREE-JET MICROMIXER

B. Marmiroli, G. Grenci[2], F. Cacho- Nerin[1], B. Sartori[1], P. Laggner[1], E. Ferrari[2], L. Businaro[2] and H. Amenitsch[1]

1.) Institute of Biophysics and Nanosystem Research, Austrian Academy of Sciences, Schmiedlstraße 6, Graz, Austria
2.) TASC-INFM-CNR at Elettra Synchrotron, S.S. 14 km 163.5, Trieste, Italy

Understanding the kinetics of nanoparticles formation and the effect of additives is fundamental to control the synthesis, purification, and application of solid substances [1]. In particular, Calcium carbonate (CaCO3) is widely used in medical, polymer, iron, paper, and chemical industry, due to its low cost and physical and chemical properties: it presents polymorphism, which can be controlled by various additives. The initial stages of formation of CaCO3 nanoparticles are therefore an attractive subject [2-4]. We have conducted our investigation by time resolved SAXS. Due to the availability of high brilliance X-rays at synchrotron radiation facilities, SAXS measurements of crystallization kinetics of CaCO3 have become feasible with a time resolution in the millisecond range [5]. Recently, we have combined the state of the art in terms of synchrotron SAXS measurements, rapid mixing through microfluidics and free micro jets in air to push the limits of time resolved measurements of fast chemical reactions. We designed, fabricated and tested a micromixer based on laminar flow and producing a free jet. We achieved a mixing time < 40 μs and a time of first accessible measurement of 75 μs, to our knowledge the fastest obtained up to now for SAXS measurements following up mixing processes [6]. We now improved both the geometry of the device and the connection to the external pumps in order to smooth the fluidic paths. A detail of the channels of the modified micromixer after fabrication by DXRL is shown in figure 1. Then the evolution and stability of the jet, which exits the mixer nozzle at 13 m/s, have been characterized. The transition of the jet cross section from a rectangular shape at the nozzle exit to the circular shape of the free jet in air, as well as the jet breakup distance (indicating the stability of the jet in terms of length), have been examined. It has then been demonstrated that the jet shape curvature does not give rise to a scattering signal. Finally we have conceived a new alignment system based on two cameras, in order to use a smaller x-ray beam dimension and therefore to have a better SAXS signal. This system has successfully been tested first with a gold nanoparticles solution, and then with the study of the formation of Calcium Carbonate, where scattering curves could be fitted and we could calculate the radius of gyration of the nanoparticles, as shown in figure 2. Next step will involve the detailed study of the early stages of formation of Calcium Carbonate in presence of various additives.

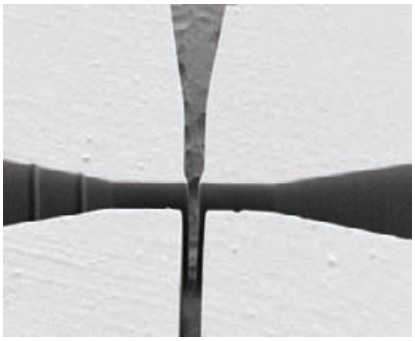

Figure 1. Detail of the channels of the new improved micromixer fabricated by DXRL.

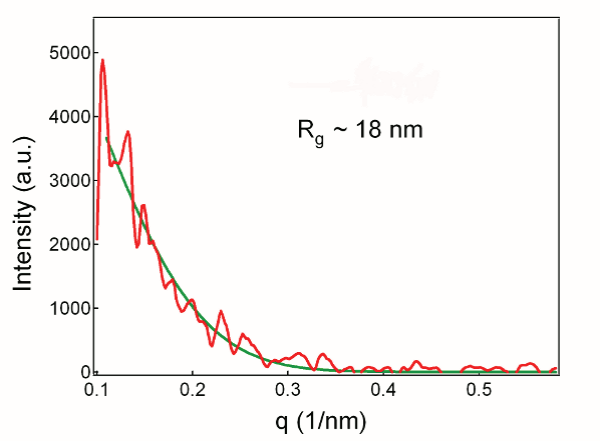

Figure 2. Scattering curve of the calcium carbonate formation at 190 μs.

Acknowledgements

We would like to thank M. Rappolt for useful discussion, and C. Morello and A. Allemandi for the precious technical support.

References

[1] T. Wang, M. Antonietti, H. Cölfen; Calcite Mesocrystals: Morphing Crystals by a Polyelectrolyte; Chem Eur. J.12, 5722 (2006)
[2] F. C. Meldrum, and R. P. Sear ; Now you see them ; Science 322 1802 (2008)
[3] D. Gebauer, A. Völkel, and H. Cölfen, Science 322 1819 (2008)
[4] E. M. Pouget , P. H. H. Bomans, J. A. C. M. Goos, P. M. Frederik, G. de With, and N. A. J. M. Sommerdijk; The Initial Stages of Template-Controlled CaCO3 formation Revealed by Cryo-TEM; Science 323 1455 (2009)
[5] J. Bolze, B. Peng, N. Dingenouts, P. Panine, T. Narayanan, and M. Ballauff; Formation and Growth of Amorphous Colloidal CaCO3 Precursor Particles as Detected by Time- Resolved SAXS; Langmuir 18 8364 (2002)
[6] B. Marmiroli, G. Grenci, F. Cacho- Nerin, B. Sartori, P. Laggner, E. Ferrari, L. Businaro and H. Amenitsch; Lab Chip, DOI:10.1039/B904296B (2009)

CONTROL OF POLYMER MORPHOLOGY THROUGH ADDITIVE

Geoffrey R. Mitchell[1], Robert H. Olley[1], Donatella Duraccio[2] and Sigrid Bernstoff[3]

1.) University of Reading, Whiteknights, RG6 6AF UK
2.) Instituto di Chimica e Tecnologia dei Polimeri, via Campi Flegrei 34, 80078 Pozzuoli, Napoli, Italy
3.) Sincrotrone Trieste, Area Science Park, Basovizza/TS, I-34012, Italy

The properties of semi-crystalline polymers such as polyethylene, polypropylene or poly(ε-caprolactone) depends as much on the processing conditions as they do on the chemical configuration of the polymer. We show that small quantities of dibenzylidene sorbitol dispersed in poly(ε-caprolactone) provide a very effective self-assembling nanoscale framework which, with a flow field, yields extremely high levels of polymer crystal orientation. During modest shear flow of the polymer melt, the additive forms highly extended nano-particles which adopt a preferred alignment with respect to the flow field. On cooling, polymer crystallisation is directed by these particles. The objective of this proposal was to explore this very recent discovery that a mixture of small quantities of special additives in conjunction with flow can be used to control the development of the morphology of semi-crystalline polymers.

We were able to successful mount our special shear stage on the SAXS beam line and obtain quantitative time-resolved SAXS data as well as some 1d-WAXS data. We used a 2s or 4s time slice in these experiments but in some subsequent data analysis we combined frames to give an enhanced signal to noise ratio with a modest reduction in time resolution. In particular, we were able to follow the crystallisation processes from the very earliest stages which enabled us to identify the orientation of the dominant structures which grew first.

We were able to successfully confirm our initial discovery and show that the additives directed the crystallisation process and in particular the alignment of the crystal lamellae.

We use time-resolved small-angle x-ray scattering (SAXS) to quantitatively follow the development of the nanoscale fibrils and the subsequent directed crystallisation. The simultaneous WAXS capability available on the SAXS beamline at Elettra allow us to follow the development of crystallinity in both the nanoscale fibrils and the polymer matrix. The 2-d nature of the SAXS data collection allows us to evaluate the length scales and the level of orientation present before, during and after shear flow.

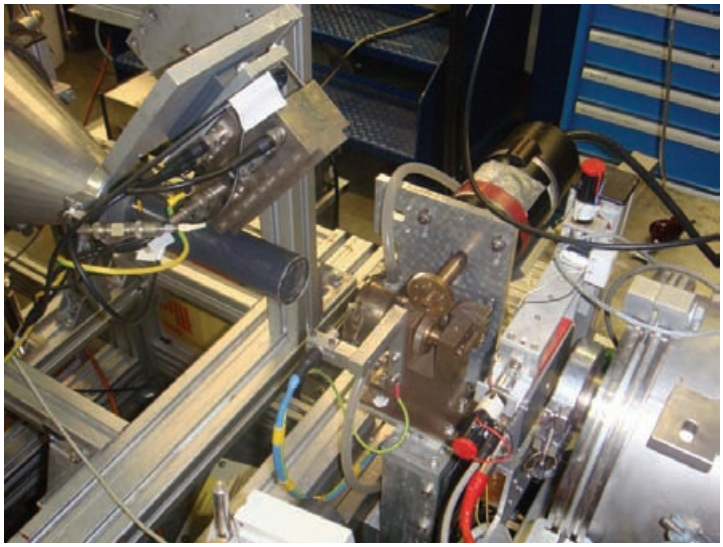

Figure 1 shows the special shear flow cell developed at Reading mounted on the SAXS beamline at Elettra showing the WAXS detector mounted (upper left) above the vacuum chamber leading to the SAXS detector

We were able to explore the effects in samples prepared with different fractions of dibenzylidene sorbitol and other additives in polycaprolactone. In fact the behaviour was exhibited by a wider range of compositions than we had anticipated which provide a very useful insight to the mechanism underlying this novel behaviour.

There was a delay in starting the beam-line experiments and although we were provided with an additional morning to complete the work we decided to focus on the PCL system and therefore we did not have the opportunity to explore the effects in polyolefin based systems.

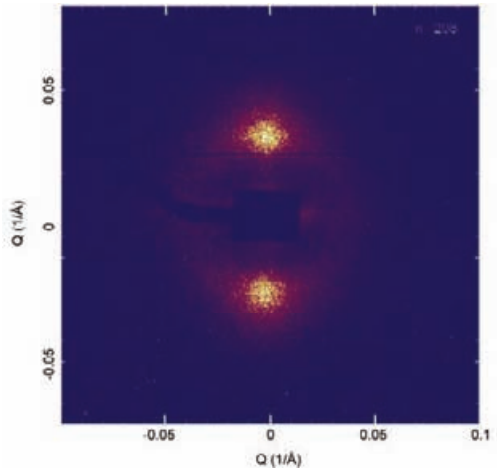

Figure 2: SAXS pattern of Poly(ε-caprolactone) with 3% DBS crystallised after a shear flow of 10s-1 with a shear strain of 1000 shear units

Figure 2 shows a SAXS pattern obtained for a sample of poly(ε-caprolactone) containing 3% DBS which has been crystallised from the melt after shear flow had been applied some 20ºC above the melting point of the poly(ε-caprolactone) crystals. The pattern is typical of a semi-crystalline polymer – the peaks correspond to the lamellar stacks of crystals directed with a common growth direction by the nano-fibrils of DBS aligned by the shear flow. In fact the horizontal streak to the right of the beam-stop arises from the aligned nano-fibrils and can be used to both identify the formation of the fibrils and evaluate their size and orientation.

We have used this capability to map out the relationship between the size and shape of the DBS fibrils and the consequent crystallisation pf the matrix PCL.

The work has enable us to more fully understand the formation of the nano-fibrils [1] and the subsequent matrix polymer crystallisation processes directed by those nano-fibrils [2].

References:

[1] G.R.Mitchell, F.J.Davis, R.H.Olley and S.Wangsoub presented at the EUROMAT2009 International Congress on Advanced Materials and Processes Glasgow Scotland September 2009 'Controlled preparation of nanofibrils from low molar compounds in a polymer matrix'

[2] G.R.Mitchell, R.H.Olley and S.Wangsoub presented at the IOP Polymer Physics Conference Bristol UK September 2009 'Directing polymer crystallisation using low molar mass additives'

GISAXS STUDY OF SILVER METAL ISLAND FILMS ON GLASS SUBSTRATES

M. Pavlović[1], H. Zorc[1], M. Lončarić[1], J. Sancho-Parramon[1], P. Dubček[1], A. Turković[1], G. Jakopic[2], A. Haase[2] and S. Bernstorff[3]

1.) Rudjer Boskovic Institute, Bijenicka c. 54, 10000 Zagreb, Croatia
2.) Institute of Nanostructured Materials and Photonics, Franz-Pichler-Straße 30. 8160 Weiz, Austria
3.) Sincrotrone Trieste, in AREA Science Park, 34012 Basovizza / Trieste, Italy

Metal island films (MIFs) consist of metal clusters deposited on a substrate and represent one of the most basic cases of nanostructured matter. They present unique optical properties, related to the surface plasmon (SP) resonance of metal clusters electrons. In this study, the optical and structural properties of silver metal island films obtained by evaporation process in high vacuum are studied. The samples characterization evidences that the evolution of SP characteristics with the fabrication parameters is explained by the differences in the concentration, shape and size of the islands.

Silver was deposited in three different mass thicknesses (3 nm, 7 nm and 12 nm) and at three different substrate temperatures: 25 °C, 120 °C and 215 °C. Over the silver layer a protective capping layer of 13 nm SiO_2 was deposited. The SP absorption (*A*) properties of the samples were studied using optical spectroscopy in the 300 nm – 1100 nm spectral range. GISAXS measurements were performed at the Austrian SAXS beam line at the Synchrotron ELETTRA, Trieste, Italy [1]. The GISAXS setup data were as follows: 2 GeV electron beam energy, 200 mA beam current, the X-ray photon energy was 8 keV (wavelength $\lambda = 0.154$ nm), the energy resolution ($\Delta E/E$) was $\leq 2.5 \times 10^{-3}$, the spot size FWHM at the sample was 4 x 0.15 mm^2, and the photon flux on the sample was in the order of 10^{12} ph/s. The GISAXS intensity curves are obtained from the scattering pattern recorded by a two-dimensional charge-coupled device (CCD) detector (with image sizes of 1024 x 1024 pixels), which has a 115 mm-diameter input phosphorus screen. The detector to sample distance was L = 1.5 m. A motorized Al beam stop was positioned perpendicular to the sample surface to reduce the very strong transmitted and specularly reflected beams. The samples were mounted on a stepper-motor-controlled tilting stage with a step resolution of 0.001^o and measured at the chosen grazing angles. GISAXS for each sample was measured at two different incident grazing angles, in the 0.050 – 0.310° range. In addition, atomic force microscopy (AFM) was performed with a Dimension 3100 (Digital Instruments) instrument in the tapping mode.

Fig. 1 depicts 2D GISAXS scattering patterns of silver MIFs samples, grouped in columns according to the same nominal mass thickness: 3 nm (first column), 7 nm (second column) and 12 nm (third column) and in rows showing the patterns of the same deposition temperature: 25°C (first row) 120°C (second row) and 215°C (third row). In all cases well defined areas of maximal intensities at both sides of the beam stop can be observed. Each change of colour corresponds to an order of magnitude change in intensity. The scattered intensity concentrates more and more towards the origin of the reciprocal space as the deposited Ag thickness increases (see Fig. 1 from left to the right) as well as the deposition temperature increases, too (see Fig. 1 from top to the bottom). This reveals a growth of the island sizes in all real-space directions. In addition, two maxima situated parallel to the q_y axis are separated by the partly seen (screened by the beam stop) specular rod at $q_y = 0$ nm^{-1}. This interference effect arises because islands are probably separated by a preferential nearest neighbour centre-to-centre distance, *D*, that can be extracted by vector value where the maximum occurs. A quantitative estimation of the lateral (*d*) and vertical size (*H*) of the islands can be obtained in the framework of the Guinier approximation [2] by analysis of vertical and horizontal cuts of the 2D pattern at the wave-vector where the maximum intensity

takes places. Additional interference fringes observed above and parallel to the horizontal axis probably come from the capping protective layer of SiO_2. Table 1 summarizes the characterisation results obtained by spectroscopy, AFM and GISAXS, for all measured silver island samples. λ_{peak} is the position of the absorption peak maximum, $\Delta\lambda_{FWHM}$ shows the respective peak width. *D* represents the average interparticle centre-to-centre distance, R_{rms} is the roughness, *H* is the island vertical size (height) of and *d* is their horizontal (lateral) size.
The first trend of the islands morphology (deduced from GISAXS and AFM) dependence on the above mentioned parameters is the increase of the interparticle distance and of all sizes with the increase of the deposited mass thickness. This could be explained by the greater amount of available deposited material used for the particle nucleation. The second trend is an increase of the particle size and the degree of island sphereicity, and the interparticle distance, as the deposition temperature increases. This is explained by the higher energy amounts available to the Ag atoms when arriving to a hotter substrate. It must be noticed that the GISAXS technique provides a more complete description of the clusters geometry than AFM. Owing to the presence of the protective SiO_2 layer, no information on the vertical and horizontal dimensions of the islands is available from AFM since the bottom of the islands is not reachable by an AFM tip, and only the centre-to-centre distance can be estimated. The connection between the SP characteristics and the deposition conditions is explained by the evolution of the morphological properties of clusters. Thus the increase in particle concentration induces a red shift and broadening of the SP absorption. The SP absorption is blue-shifted as the deposition temperature is increased, what can be related to the change in particle shape, reduction of the interparticle distance and appearance of size effects due to the variation of island size [3].

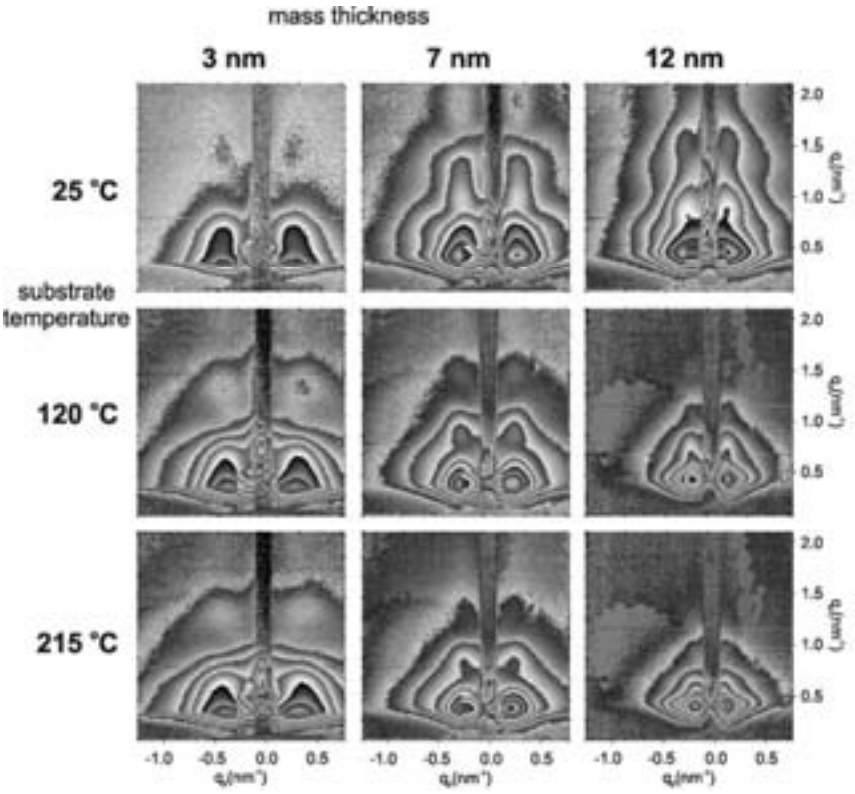

Figure 1. 2D GISAXS scattering patterns for all measured samples. The first column presents samples with 3 nm deposited mass thickness, the second with 7 nm and the third with 12 nm. The first row presents samples deposited at 25°C, the second at 120°C and the third at 215°C.

Methods / Ag samples		Spectroscopy		AFM		GISAXS		
		λ_{peak} / nm	$\Delta\lambda_{FWHM}$ / nm	D / nm	R_{rms} / nm	H / nm	d / nm	D / nm
3 nm	25 °C	497	297	15,7	0,98	5,6	8,2	17
3 nm	120 °C	464	170	22,1	1,10	7,4	9,4	17
3 nm	215 °C	455	126	20,8	1,13	7,8	9,2	17
7 nm	25 °C	591	–	17,7	0,79	14,0	11,2	24
7 nm	120 °C	490	212	27,1	1,52	13,0	14,0	30
7 nm	215 °C	461	171	32,0	1,27	14,8	14,8	30
12 nm	25 °C	940	–	24,3	0,70	10,0	13,4	39
12 nm	120 °C	547	398	40,7	1,72	14,2	21,0	41
12 nm	215 °C	476	248	51,9	2,42	18,6	23,0	47

Table 1. Characterisation results obtained by three methods (spectroscopy, AFM and GISAXS), for all measured silver island samples. λpeak is the position of absorption peak maximum, ΔλFWHM is the respective peak width. D represents the average interparticle centre-to-centre distance, Rrms is the roughness, H is the islands' average vertical size (height) and d is their average horizontal (lateral) size, all in nanometers (nm).

References:

[1] H. Amenitsch, M. Rappolt, M. Kriechbaum, H. Mio, P. Laggner, S. Bernstorff, J. Synchrotron Rad. 1998; 5: 506

[2] A. Guinier and G. Fournet, Small Angle Scattering of X-rays, Wiley, New York (1955)

[3] M. Lončarić, J. Sancho-Parramon, M. Pavlović, H. Zorc, P. Dubček, A. Turković, S. Bernstorff, G. Jakopic, A. Haase; Optical and structural characterisation of silver islands films on glass substrates, Vacuum, In press.

CHARACTERIZATION OF Si_XGe_{1-X} NANOCRYSTALS EMBEDDED IN SiO_2 AND Al_2O_3 THIN FILMS

S. R. C. Pinto[1], S. Levichev[1], A. Khodorov[1], S. Bernstorff[2], M. Buljan[3], R. J. Kashtiban[4], A. G. Rolo[1], U. Bangert[4], and M.J.M. Gomes[1]

1) Centro de Física, Universidade do Minho, 4710-057 Braga, Portugal
2) Sincrotrone Trieste, SS 14, km 163.5, Basovizza (TS), Italy
3) Charles University in Prague, Ke Karlovu 5, 121 16 Prague, Czech Republic
4) Nanostructured Materials Research Group, School of Materials, The University of Manchester, P.O. Box 88, Manchester, M1 7HS, UK

It is well known that, as a result of quantum confinement effects, the emission wavelength of semiconductor nanocrystals (NCs) is shifted to the short wavelengths compared with bulk material and can be tuned by adjusting NCs size [1, 2]. This is the main reason why they have a high potential for applications in optoelectronic and nanoelectronic devices. Metal–Insulator–Semiconductor (MIS) structures using Si and Ge NCs have been reported to show good memory effects and low power operation at room temperature [3]. One of the most common structures used for memory or light emitting diodes applications is the metal or poly-Si/SiO_x/Si structure with Si NCs embedded in the SiO_x layer. SiGe nanocrystals embedded in Al_2O_3 or stacked dielectrics were shown to improve the performances of the flash memory based devices [4]. Since alumina presents a high dielectric constant as big as two times more than that of SiO_2, which makes reducing of thickness of oxide layer to as low as 2-3 nm possible. Moreover, Al_2O_3 presents good mechanical properties, and supports high temperature, which leads it to be a good candidate to replace silica in flash memory systems, and therefore improve their performances. Majority of investigations about Ge NCs have done on Ge NCs embedded in SiO_2 system [5-7]. However, a few studies have been reported on Ge NCs embedded in Al_2O_3 matrix [8, 9]. In this work we studied Ge NCs embedded in alumina grown by RF-magnetron co-sputtering technique.

Conventional RF-magnetron co-sputtering method was used to grow Si_xGe_{1-x} (x=0 to 1) NCs embedded in SiO_2 and Al_2O_3 by Alcatel SCM650 machine. SiO_2 or Al_2O_3 (99,99%) plates with several polycrystalline Si and Ge (99,99%) chips on the surface were used as the target. The samples were produced on n-type Si(111) substrates at 500°C. In order to improve the crystallinity of the Si_xGe_{1-x} phase and control the NCs size the samples were annealed at 800 – 1000 ºC, during one hour in a commercial oven. The high resolution transmission electron microscopy (HRTEM) images were recorded with Tecnai FEGTEM microscope operating at 300 kV. A 2D CCD camera and a 1D gas filled detector were used for simultaneous measurements of grazing incidence small angle X-ray scattering (GISAXS) and wide angle X-ray scattering (WAXS) studies. The X-ray photon energy was 8 keV. An Al stripe was inserted in front of the 2D camera in order to reduce the very intense reflected beam and increase the sensitivity for the scattered signal outside of the specular plane.

The measured GISAXS data were analyzed assuming that the NCs are randomly distributed in the volume of the layer and introducing a depleted region around each NC, where no other particles can occur (so called ideal gas model). We performed fitting and simulation of the whole 2D GISAXS maps. Some of the experimental results together with theoretical calculations are shown on the Fig.1. From the fittings according the procedure described in Ref [10] we determined the NCs shape, the NCs size (R), NCs size distribution (σ), and the distance between NCs (L), see table 1.
The diffraction data were used for the determination of the NCs composition and their crystalline structure. For analyzing of the diffraction spectra of Si_xGe_{1-x} NCs, we developed a

special model based on the Debye-Scherrer approach. Using this model we assume a random distribution of Si atoms within the lattice. It can be used for the full-profile analysis, in which we determine the sizes of the NCs, the chemical composition (especially Si percentage in Si_xGe_{1-x}), the concentration of plane defects and the lattice constant of the nanocrystals. Some typical WAXS result is shown in Fig.2. The NCs radius from the fit, R = 2.5 nm is in a good agreement with the GISAXS finding (R = 2.3 nm). Fig. 3 shows a HRTEM were it is possible to see the lattice fringes of these nanocrystals corresponding to the (111) plane of Si_xGe_{1-x}. The HRTEM data is in good agreement with the GISAXS and WAXS findings.

Table 1. Parameters of fitting process obtained for different samples.

Sample	Technique	R(nm)	σ (nm)	L(nm)
J32	Diffraction	1.99		
	GISAXS	2.27	0.2	10.9
M32	Diffraction	2.05		
	GISAXS	2.35	0.8	12.2
M31	Diffraction	---		
	GISAXS	2.25	0.2	12.1
G21	Diffraction	---		
	GISAXS	2.03	1.1	11.3

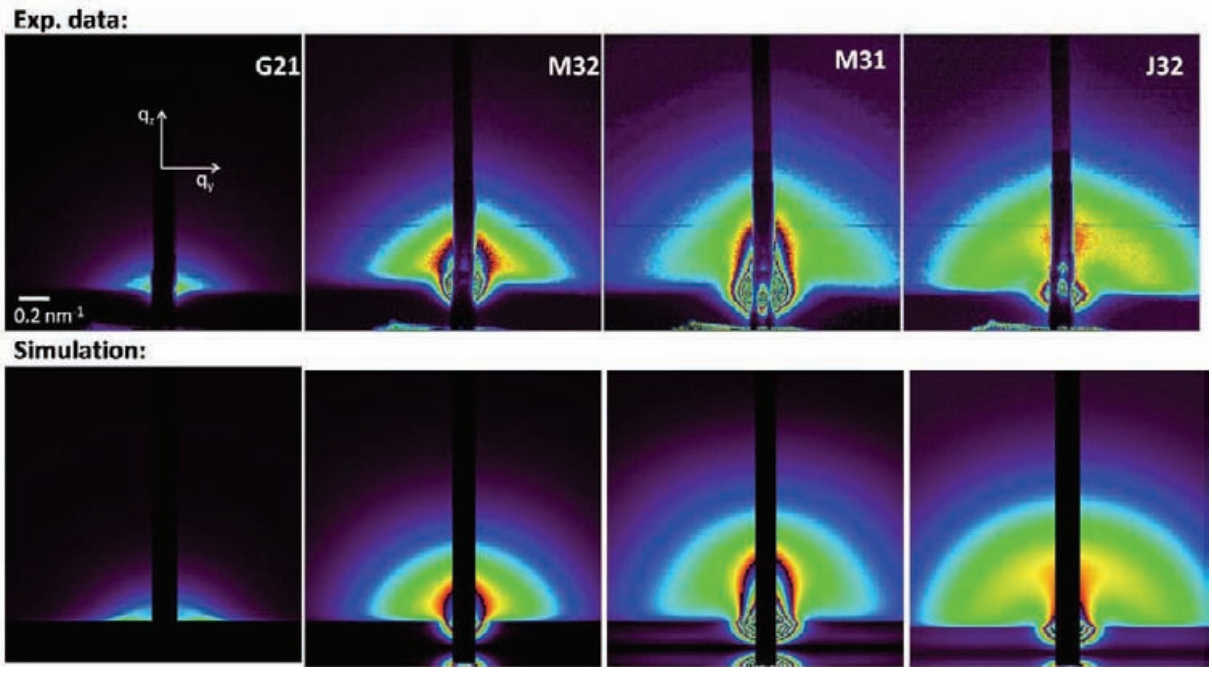

Figure1. Experimental (upper row) and simulated GISAXS maps (down) of Si_xGe_{1-x} NCs in SiO_2 deposited at different conditions.

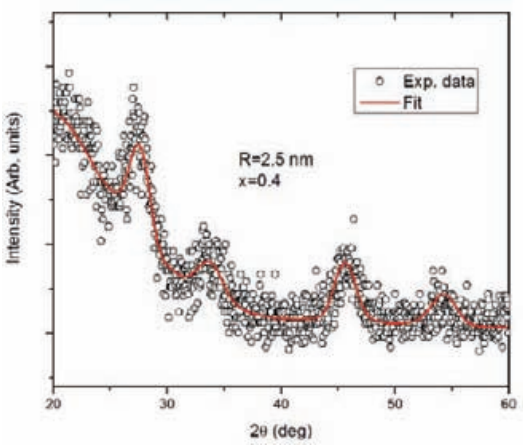

Figure 2. Measured diffraction data (circles) for the Si_xGe_{1-x} nanocrystals in SiO_2 matrix and their fit (continuous line).

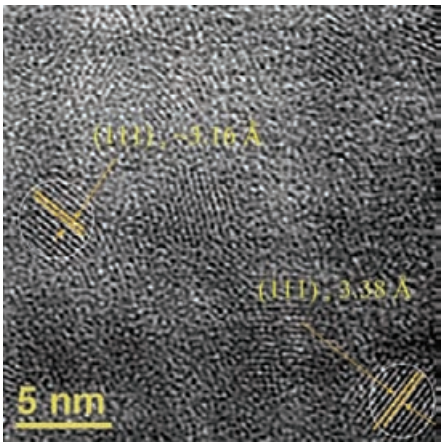

Figure 3. HRTEM of Si_xGe_{1-x} NCs. The lattice fringes correspond to the (111) plane of NCs.

GISAXS data from the Ge NCs formed in Al_2O_3 matrices show the presence of strong lateral peaks. Bragg peaks are visible in GISAXS maps of these samples, which show the existence of correlations in the dots positions (see the Fig. 4). Figure 5 shows a typical WAXS for Ge NCs in Al_2O_3 matrix. The presence of Ge nanocrystals was confirmed by HRTEM measurements (Fig. 6).

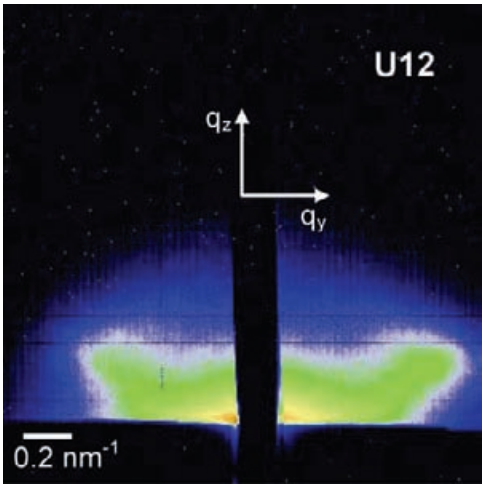

Figure 4. Experimental 2D GISAXS pattern of Ge NCs in Al_2O_3 matrix.

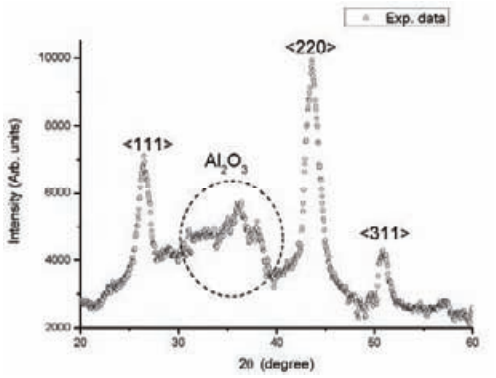

Figure 5. WAXS diffraction data for Ge NCs in Al_2O_3 matrix, the <111>, <220> and <311> are the planes associated to Ge NCs

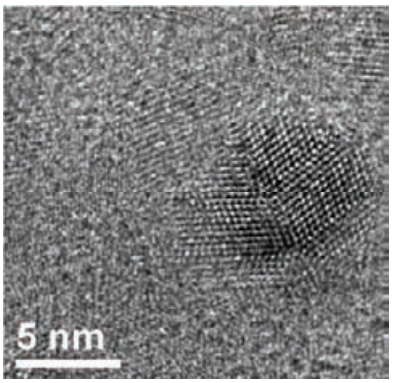

Figure 6 Typical HRTEM image of Ge NC in Al_2O_3 matrix.

References

[1] A.P. Alivisatos, Science, 271 (1996) 933.
[2] J.D. Budai, C.W. White, S.P. Wiothrow, M.F. Chisholm, J. Zhu, and R.A. Zuhr, Nature, 390 (1997) 384.
[3] S. Tiwari, F. Rawa, H. Hannafi, A. Harstein, E. F. Cabbe, and K. Chan, Appl. Phys. Lett., 68 (1996) 1377.
[4] Zs.J. Horváth, Current Applied Physics, 6 (2006) 145.
[5] A. Kanjilal, J.L. Hansen, P. Gaiduk, A.N. Larsen, N. Cherkashin, A. Claverie, P. Normand, E. Kapelanakis, D. Skarlatos, and D. Tsoukalas, Appl. Phys. Lett., 82 (2003) 1212.
[6] T. Baron, B. Pelissier, L. Perniola, F. Mazen, J.M. Hartmann, and G. Rolland, Appl. Phys. Lett., 83 (2003) 1444.
[7] C.J. Park, K.H. Cho, W.C. Yang, H.Y. Cho, S.H. Choi, R.G. Elliman, J.H. Han, and C. Kim, Appl. Phys. Lett., 88 (2006) 71916.
[8] P. Caldelas, A.G. Rolo, M.J.M. Gomes, E. Alves, A.R. Ramos, O. Conde, S. Yerci, and R. Turan, Vacuum, 82 (2008) 1466.
[9] S. Yerci, M. Kulakci, U. Serincan, R. Turan, M. Shandalov, and Y. Golan, J. Nanosci. Nanotechnol., 8 (2008) 759.
[10] M. Buljan, U. V. Desnica, M. Ivanda, N. Radić, P. Dubček, G. Dražić, K. Salamon, S. Bernstorff, and V. Holý, Phys. Rev. B, **79** (2009) 035310.

NANO Si SUPERLATTICES FOR THE NEXT GENERATION SOLAR CELLS

B. Pivac[1], P. Dubček[1], I. Capan[1], I. Zulim[2], T. Betti[2], H. Zorc[1], and S. Bernstorff[3]

1.) Ruđer Bošković Institute, P.O. Box 180, 10000 Zagreb, Croatia
2.) FESB, University of Split, R. Boškovića b.b., 21000 Split, Croatia
3.) Sincrotrone Trieste, SS 14, km 163.5, 34012 Basovizza /Trieste, Italia

A new method based on the preparation of SiO/SiO_2 superlattices which enables the independent control of size, size distribution, position and density of the nanocrystals was suggested [1,2]. However, the diffusion and phase separation process in such confined geometries and in the presence of SiO_2 nearby the interface is not yet completely understood. In addition there is no theoretical work available to our best knowledge, which describes both the phase separation and the crystallization process in the limit of ultrathin layers. For a better understanding of that problem, it is necessary to learn more about the structural changes occurring during the annealing of such superlattices, which we shall present in this work.

Amorphous SiO/SiO_2 superlattices were prepared by high vacuum evaporation of alternating films of SiO_2 and SiO, each 4 nm thick (forming a stack of 10 bilayers) on clean Si (100) substrate held at room temperature. After deposition, the samples were annealed from 600°C to 1100 °C for 1h in vacuum better than 10^{-2} Pa to induce Si nanocrystals formation.

The measured X-ray reflectivities for the as prepared sample and those annealed at different temperatures are shown in Fig. 1. as open circles, together with the calculated reflectivities shown as solid curves and obtained by fitting using the standard calculation procedure. Since our samples are stacks of 10 bilayers, one would expect Bragg type reflections to occur at odd indexes. The first one is visible at about q = 0.8 nm^{-1}, but the third one at q =2.4 nm^{-1} is apparently missing. The relatively weak first Bragg peak could be attributed to the small difference in electron density of the evaporated SiO and SiO_2, but the absence of the third Bragg peak suggests that the roughness of the interfaces between the layers is also significant.

If we follow the strength of the first Bragg peak in Fig. 1. we can se that it gets stronger after annealing at 600ºC, and weakens again after annealing above 1000ºC. The fringes that are present in all reflectivity curves can be a good measure of the overall film thickness. Their dominance in the reflectivity curves suggests that the electron densities of SiO and SiO_2 are similar and significantly lower than the density of the substrate (monocrystalline silicon).

In Fig. 2 the thickness of the SiO and SiO_2 layers is plotted as a function of the annealing temperature. These values were obtained by fitting. What we have observed by X-ray reflectivity is a destruction of the SiO layer: its thickness is reduced to the benefit of the SiO_2 layer thickness and its roughness is increased. The initial SiO layer thickness was chosen in order that the diffusing silicon would form nanoparticles of similar size positioned at the center of the ex SiO layer.

We performed GISAXS experiments in order to verify that silicon particles have been formed. The absence of the correlation peak reveals a poor vertical correlation. However, when the intensities along q_z = 1.3 nm^{-1} are plotted, we can clearly see a difference in the diffuse scattering, as shown in Fig. 3. The scattering intensities are apparently very similar for all annealing temperatures, only for the as received and the 1100ºC annealed sample they differ. Without going into details of the origin of the scattering, one can conclude that the lower annealing temperatures cause structural relaxation (hence the lower intensity from the

as received sample), and only at 1100ºC the particles are actually formed, although distributed quite irregularly through the ex SiO layer.

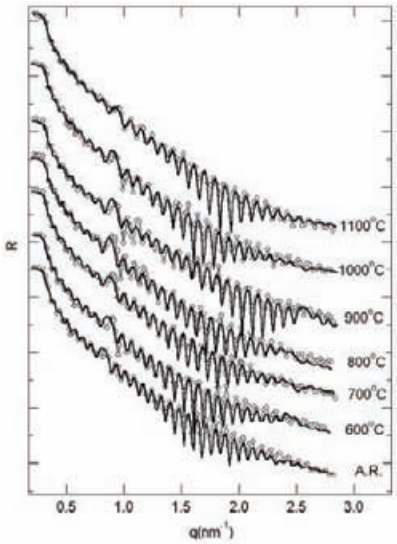

Figure 1. X-ray reflectivity (open circles) for 10 SiO/SiO_2 bilayers together with the best fit (full lines) as a function of the grazing wave vector. The annealing temperatures are indicated at the corresponding curves, and the curves are offset vertically for the sake of clarity.

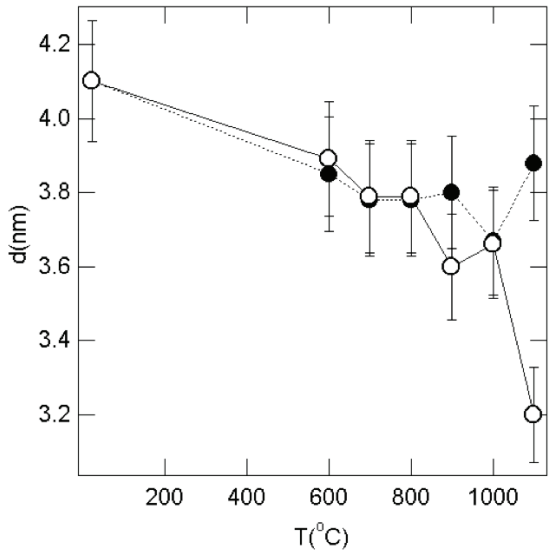

Figure 2. X-Thickness of SiO (open circles) and SiO_2 (full circles) as a function of annealing temperature.

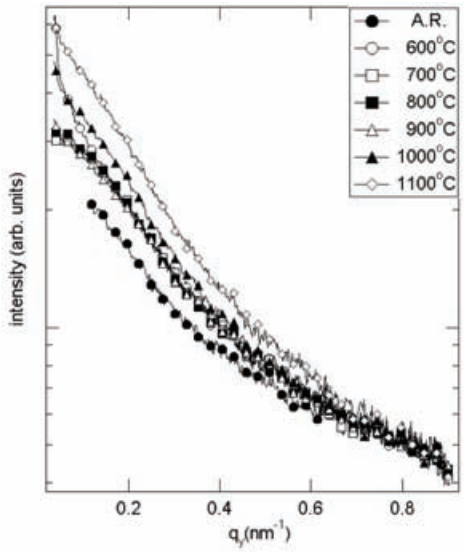

Figure 3. 1-D scattering intensities taken at qz = 1.3 nm-1. vs the scattering wave vector in the direction parallel to the sample surface. The annealing temperatures are indicated in the insert.

References:

[1] L. Tsybeskov, K.D. Hirschman, S.P. Duttagupta, M. Zacharias, P.M. Fauchet, J.P. McCafrey, D.J. Lockwood, Appl. Phys. Lett. 72, 43 (1998)

[2] M. Zacharias, J. Heitmann, R. Scholz, U. Kahler, M. Schmidt, J. Blaesing, Appl. Phys. Lett. 80, 661 (2002)

SURFACE LAYER MORPHOLOGY OF TUNGSTEN-CARBON THIN FILMS

N. Radić[1], P. Dubček[1], M. Jerčinović[1], M. Ristić[1], S. Musić[1], A. Tonejc[2] and S. Bernstorff[3]

1.) Rudjer Boškovi Institute, Bijenicka 54, HR-10000 Zagreb, Croatia
2.) Faculty of Sciences, Zagreb University, Bijenicka 34, HR-10000 Zagreb, Croatia
3.) Sincrotrone Trieste, I-34012 Basovizza (TS), Italy

Transition metals carbides, and tungsten carbides in particular, exhibit many properties of interest to technology - high melting point, extreme hardness, low friction coefficient, chemical inertness, oxidation resistance, and good electric conductivity. The surface conditions of these materials are critical for some applications, and preparation processes are optimized to meet such requirements. Surface layer of W-C thin films prepared by reactive magnetron sputtering (argon + benzene) on monocrystalline silicon substrates have been examined by GISAXS, XRR, AFM and SEM methods. The preparation conditions have been varied in a wide range of deposition parameter values: the benzene partial pressure in the 1-10% range, the substrate temperature in steps RT, 200°C, and 400°C, and beside deposition onto substrates at floating potential also a substrate bias of -70 V has been applied. The discharge power has been 2 x 25-40 W, yielding a deposition rate of about 5 nm/min. The final film thickness was about ≤ 250 nm.

A dominant carbide in all prepared films is WC1-x, with (111) preferential orientation in films deposited at room temperature. The surplus/unreacted carbon forms a fine dispersion of graphitic nanoparticles imbedded in the intergranular space. The surface of the samples has been examined by AFM and SEM methods. The pertinent results are summarized as: The AFM examination shows roughness depending upon the preparation conditions - from about 0,5 nm on films prepared at low benzene partial pressure increasing towards a few nanometers when high benzene partial pressure was used. A corresponding average lateral grainsize has been estimated at 10-20 nm, revealing a scale-like morphology of the film surface. The SEM results corroborate the surface morphology, but reveal the subsurface film structure: at the top of the film there is a 10-20 nm thick layer which clearly differs from the main body of the film beneath.

The GISAXS and XRR examination has been performed at the SAXS beamline of the Elettra Synchrotron, at 8 keV (λ = 0,154 nm), and using a 2-dim CCDdetector (1024 x 1024 pixels). The goal was to determine the average size of the WC-grains and of segregated carbon inclusions, to check the propagation of the bulk grain caracteristics towards the surface and to characterize the surface in terms of roughness and the thickness of distinctive top surface layer. The GISAXS results can be summarized as: the W-C grainsize is determined at about 3 nm by the GISAXS method, with a very smooth surface - roughness about 0,5 nm - and a very short height-height correlation length at the surface. However, the XRR method yielded a somewhat increased roughness (Fig. 1). The roughness derived from AFM measurements is given in each panel for comparison. The observed difference between the AFM- and XRR-roughness is probably due to the difference in spatial resolution of the probes: 10-20 nm tip of the probe of the AFM vs 0,154 nm wavelength used in the XRR. However, the trend of the roughness variation is similar - the higher the substrate temperature during the deposition, the smoother is the surface. In that way one might control the surface morphology when it is required.

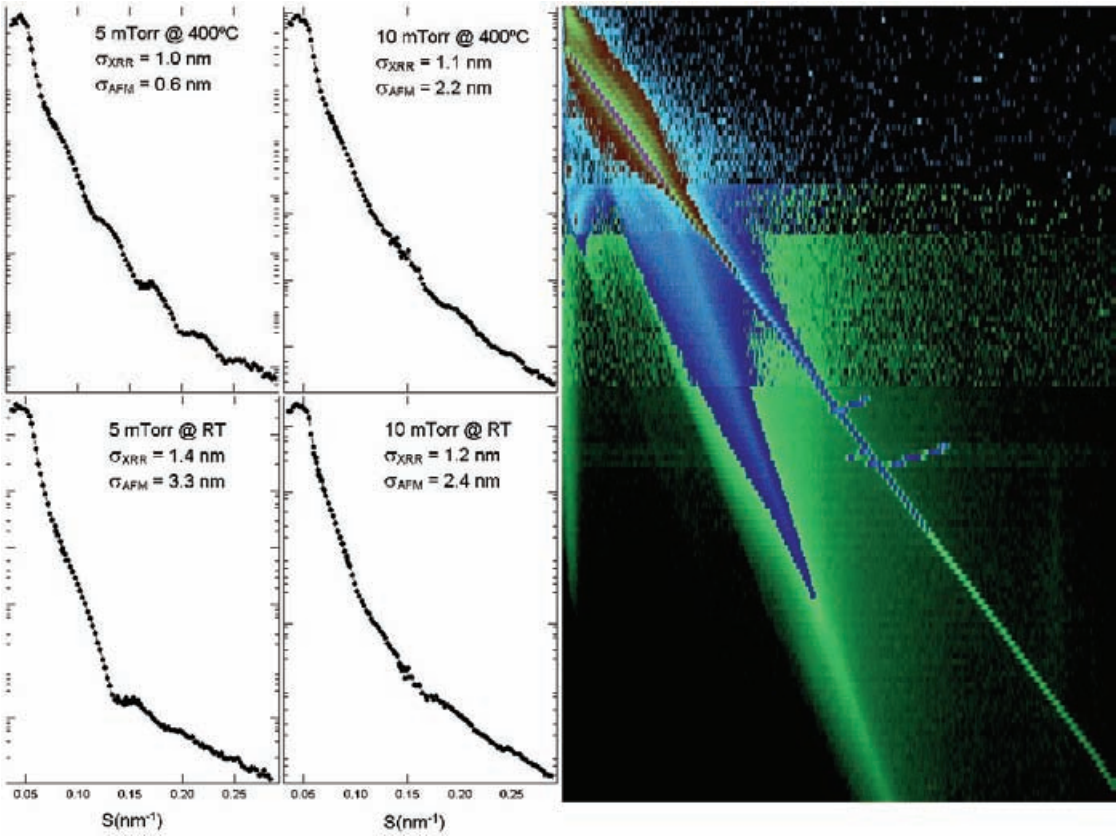

Figure 1: Contour plot of SAXS intensities (right) for a range of incident angles, wherefrom the XRR intensities are extracted as shown left for two different benzene pressures and two substrate temperatures, as indicated in the insert. The comparison of the surface roughness obtained from XRR and AFM is also shown**.**

References:

[1] N. Radic, P. Dubcek, M. Jercinovic, M. Ristic, S. Music, A. Tonejc, and S. Bernstorff; Surface Layer Morphology of Tungsten-Carbon Thin Films, Proceedings of ICTF14 & RSD2008, Ghent, 2008. 299-299

[2] N. Radic, P. Dubcek, M. Ristic, S. Music, A. Tonejc, and S. Bernstorff;Surface characterization of carbon-tungsten alloys prepared by reactive sputtering // E-MRS 2008 Spring Meeting BOOK OF ABSTRACTS, Strasbourg, 2008

IN SITU ANALYSIS OF SILICA MESOSTRUCTURING OF AEROSOLS INSIDE THE DRYER

I. Shyjumon, M. Rappolt, B. Sartori, P. Laggner, and H. Amenitsch

Institute of Biophysics and Nanosystems Research, Austrian Academy of Sciences, Graz, Austria

Analysis of mesostructured particles inside the dryer helps to follow *in situ* the structuring of these particles during the heating phase; where the evaporation induced self assembly (EISA) [1] process takes place. Figure 1 shows the schematic of the set-up with a modified dryer, a slit serving as X-ray window is constructed in the dryer with a ceramic separation for temperature insulation. This provides a sharp temperature step corresponding to a residence time of the aerosol particles of ~ 270 ms in this temperature regime, which should be fast enough to follow the fast self assembly process (i.e. much faster than 8 s from our previous experiments). By regulating the initial (T_1) and final temperature (T_2) as well as the temperature gradient along the slit we are able to tune the self assembly process and therefore understand better the phase changes.

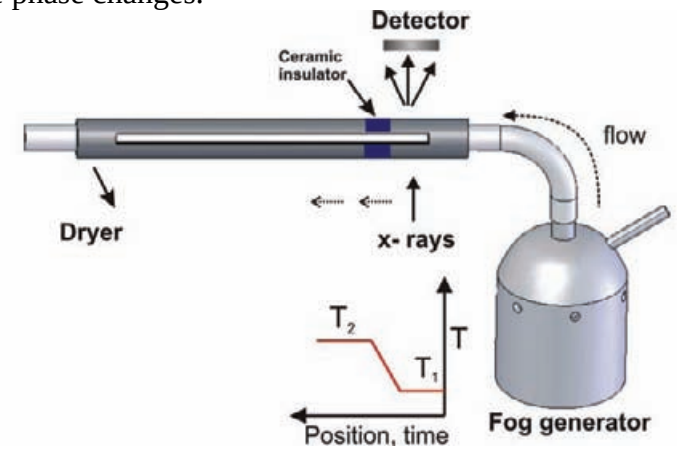

Figure 1: *In situ* set-up with the modified dryer for the online analysis of the self assembly process. The in-set shows the temperature profile within the dryer.

The temperature has been measured carefully along the axis of the modified dryer; figure 2 shows the temperature ramp inside the dryer at different positions inside the dryer with the corresponding residence time assuming a flow of 5 SLM.

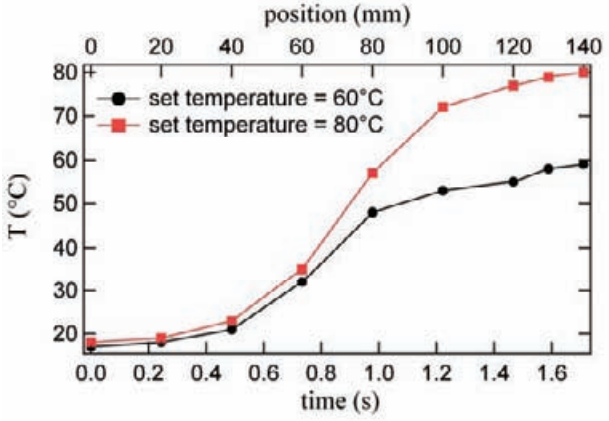

Figure 2: Temperature calibration inside the dryer at different final temperatures T2 and with a nominal inlet temperature of 15 °C.

Using this modified dryer the self assembly inside the dryer is investigated at different final dryer temperatures, which corresponds to different temperature ramps. The typical solution

prepared contain CTAB:TEOS:H_2O:HCl with molar ratio 0.14:1:41:0.13 (water rich) [2,3]. Aerosol is created using in house built aerosol generator (~ 4×10^8 droplets/s, with an average droplet size of ~ 2.5 μs) with the CTAB-TEOS solution, and the dense mist so produced is carried by air at a flow of 5 standard liter per minute (SLM). Figure 3 (left) shows the scattering profile measured inside the dryer at different positions of the temperature ramp and at a dryer set temperature of 80 °C, figure 3 (right) includes the corresponding *d* space shifting at different set temperatures. A clear shrinkage of *d* spacing can be seen in the regime of sharp temperature jump. This might be an indication of the phase changes from wormlike to 2 D hex during self assembly process of the silica mesophase.

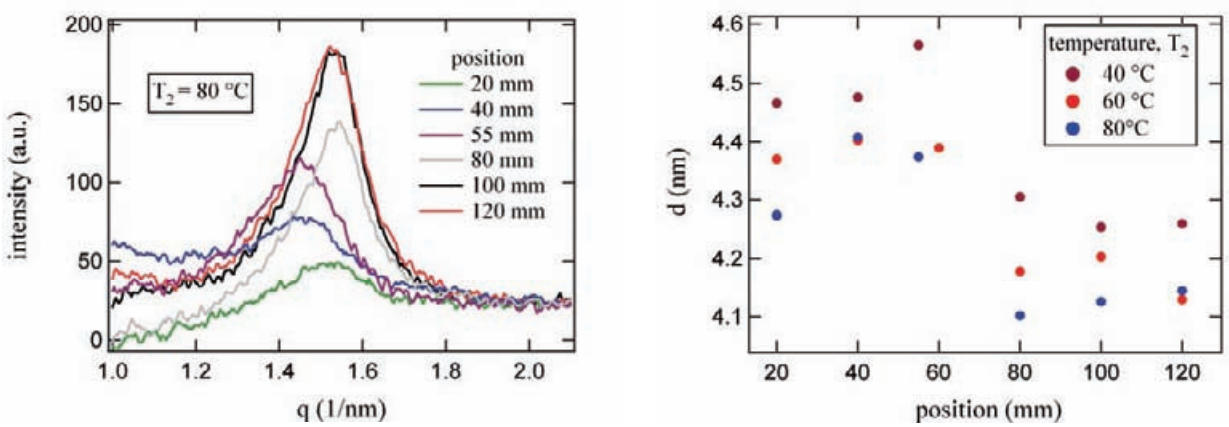

Figure 3: Left*:* Scattering profile at different positions inside the dryer at a final dryer temperature T_2 of 80 °C. Right: *d* spacing shrinkage with temperature ramp at different final dryer temperatures T_2.

Reference:

[1] Y. Lu, et.al.; Nature; 398, 223-226 (1999)
[2] C. Boissiere, et al.; Chemical Communications ; 22, 2798-2799 (2003)
[3] M. T. Bore, et al.; Langmuir; 19, 256–264 (2003)

STUDY OF EVAPORATION CONTROLLED MESOPHASES OF SILICA IN AEROSOLS USING *IN SITU* SAXS

I. Shyjumon, M. Rappolt, B. Sartori, P. Laggner, and H. Amenitsch

Institute of Biophysics and Nanosystems Research, Austrian Academy of Sciences, Graz, Austria

Surfactant templated mesostructured silica particles have received much attention because of their potential applications as sensors, as optoelectronic devices, and in selective catalysis [1,2]. A. Gibaud et al [3] have demonstrated the phase evolution of silica mesostructure from a selected reference solution, to either the 2D hexagonal (*p*6*m*), the 3D hexagonal (*P*63/*mmc*), the cubic (*Pm*3*n*), or mixed structures depending on the evaporation conditions on silica films. But tracking these phase changes *in situ* in the gas phase with a controlled evaporation will give insights on the phase evolution of mesostructure in particular if different mesophases of silica are formed.

In our previous studied we investigated the mesostructuring of CTAB, TEOS and water system (water rich) [4] which results in a fully condensed honeycomb hexagonal structure. Using ethanol rich solution (CTAB, TEOS and ethyl alcohol) in place of water rich will lead to different regimes of evaporation conditions as well as different phase evolutions. A commercial TSI 3079 aerosol generator is used for the ethanol rich solutions. Scattering data were acquired at the end of the dryer using an image plate. Experiments are performed with aerosol flow (5 slm) only and aerosol flow (5 slm) plus a humid air flow (4 slm) to understand the influence of humidity inside the dryer. Figure 1 (left) shows the scattering profile at different dryer temperatures with an aerosol flow of 5 slm only. The corresponding *d* spacing behavior with dryer temperature for only aerosol flow and aerosol flow plus humid air flow are shown figure 1 (right), the solution aging was 54-56 hours. A pronounced decrease in *d* spacing is observed between 100 and 150 °C, similar to the water rich solution. This shrinkage is mainly due to the presence and the evaporation of water (below/above 100 °C) in the system. Also can be seen in figure 1 (right) that additional humidity inside the dryer has little effect on the final structure.

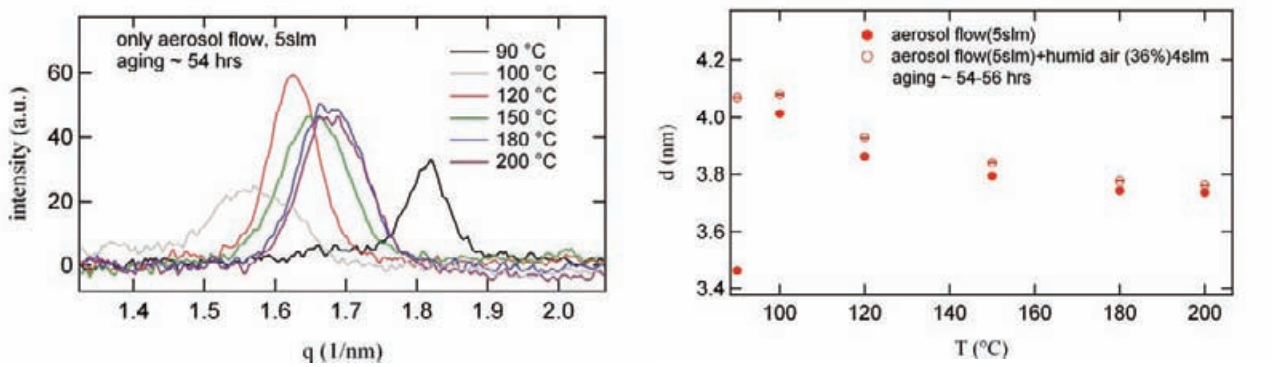

Figure 1: Left – Scattering profile at different dryer temperatures with only aerosol flow (5 slm). Right – d spacing shrinkage with dryer temperatures for aerosol flow (5 slm) only and both aerosol flow and humid air flow (4 slm).

Experiments were repeated with different solution aging, figure 2 shows the *d* spacing behavior at two different solution aging for only aerosol flow and both aerosol and humid air

flow. And the results indicates nearly no dependence with solution aging for ethanol rich solution, which is very different the aging effects of water rich solutions [4].

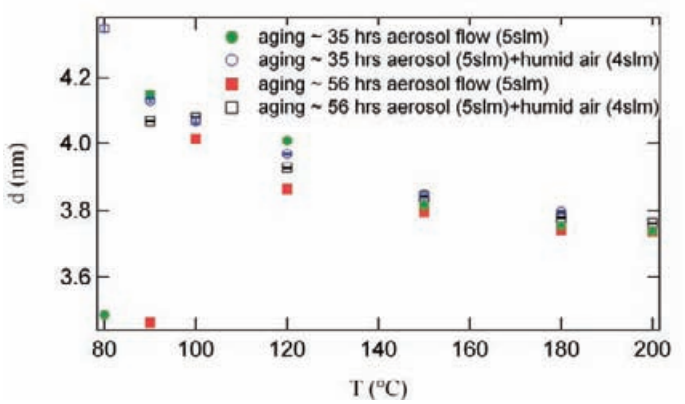

Figure 2: d spacing shrinkage with dryer temperature at two different solution aging for only aerosol flow and for both aerosol and humid air flow.

Reference:

[1] J. Lopez, et al., J. Mater. Chem; 17, 1563 (2007)
[2] M.T. Bore, T. L. Ward, A. Fukuoka, and A. K. Datye; Catal Lett., 98; 167 (2004)
[3] A. Gibaud, et al.; J. Phys. Chem. B; 107, 6114 (2003)
[4] I. Shyjumon, et al.; In preparation (2009)

INVESTIGATION OF THE EXISTENCE AND OF THE KINETICS OF DISLOCATION GENERATION IN BIODEGRADABLE SEMICRYSTALLINE POLY(3-HYDROXYBUTYRATE) (PHB) BY IN-SITU WAXS DEFORMATION

F. Spieckermann[1], H. Wilhelm[1], E. Schafler[1], M. Kerber[1], S. Bernstorff[2] and M. J. Zehetbauer[1]

1.) Research Group Physics of Nanostructured Materials, Faculty of Physics, University of Vienna, A-1090 Wien, Austria
2.) Sincrotrone Trieste SCpA, I-34012 Basovizza / Trieste, Italy

Using a specially designed miniature compression machine enabling in-situ WAXS and SAXS measurements, investigations on the biodegradable polymer poly(3-hydroxybuthyrate) (PHB) were carried out . Different experimental conditions were chosen in order to study the strain rate sensitivity as well as relaxation effects. Cyclic step cycle tests were giving insight into the morphological and micro-structural changes related to the loaded and unloaded state of the material (which were found to differ considerably) and tests at different strain rates were designed in order to capture dynamical effects. The recorded profiles were evaluated by means of Multi-Reflection X-ray Line Profile Analysis (MXPA) [1]. The results of these initial evaluations are quite surprising as the change of the profile broadening induced by plastic deformation found in the material seems to be very small.

Earlier investigations of X-ray line broadening in crystallized isotactic α - polypropylene (iPP) yielded a strong deformation induced increase of the broadening. This could be related to the formation of dislocations while the coherently scattering domain size (CSD) which is also responsible for an important part of the broadening remained nearly constant. Also the CSD was found to correspond very well to the lamella size of the material as determined by DSC or SAXS [2].

The present experiments yield a similar behavior for the CSD in PHB but the broadening related to dislocations does not seem to be affected by deformation (Fig. 1). Although in absolute terms the initial dislocation density turns out to be higher in PHB than in iPP it does not change strongly as a function of the compression strain applied. These first results indicate that a deformation mechanism different than dislocation motion might be active in PHB in contrast to the observations in iPP [2]. This is also supported by the only small changes in crystallographic texture that can be derived from the relative change of the diffraction peak intensities of the WAXS signal. The most likely micro-structural quantity which seems to govern the transition from a dislocation controlled deformation to another process is the lamella thickness, which is as low as about 7 nm in PHB.

The opening of the cycles in the cyclic stress-strain curve represented in Fig. 2 increases with the deformation. According to [3], this behavior can be attributed to the viscoelastic properties of the amorphous phase. The strong reduction of the crystalline volume fraction plotted in Fig. 3 is in accordance with this observation leading to a stronger influence of the amorphous phase on the relaxation behavior of the material.

Furthermore with the present experiments the application of MXPA could be extended to a new polymeric material confirming its ability to determine microstructural properties of semicrystalline polymers in a non destructive manner. The restricted evolution of the dislocation density found in PHB is of great interest because it indicates that the crystal size may be the crucial parameter interfering in dislocation based plasticity. This result does not only concern polymers but may also provide valuable input for a better understanding of deformation mechanisms of nano-crystals in general.

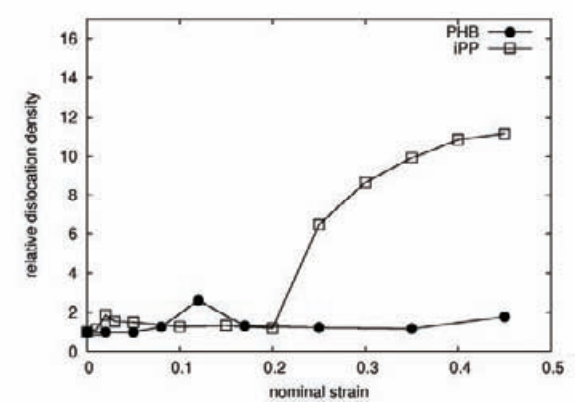

Figure 1: Strain characteristics of the relative dislocation density in unaxial compression for PHB and iPP as a function of the nominal strain.

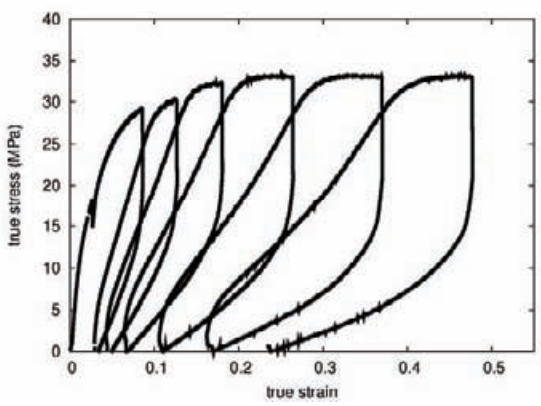

Figure 2: The true stress - true strain curve of PHB in cyclic loading – unloading.

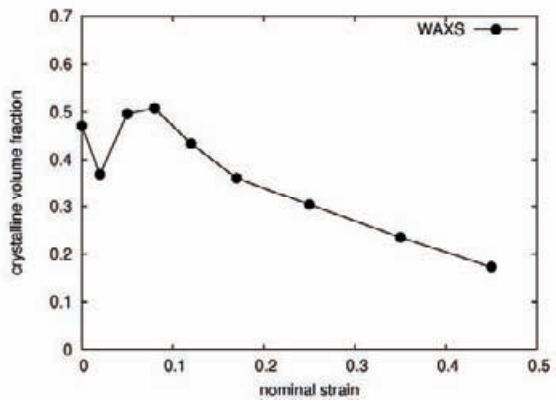

Figure 3: The evolution of crystallinity as a function of the nominal strain as derived from the deconvolution of the amorphous and the crystalline WAXS signals.

Acknowledgments:

Support in the frame of EC contract RII3-CT-2004-506008(IA-SFS) is gratefully acknowledged. Thanks are given to the University of Vienna for providing support within the PhD Program “Experimental Materials Science - Nanostructured Materials” and the Focus Project ”Bulk Nanostructured Materials”.

References:

[1] T. Ungár, J. Gubicza, G. Ribárik, & A. Borbély, Journal of Applied Crystallography 34, 298—310, 43—1699 (2001)

[2] H. Wilhelm, A. Paris, E. Schafler, S. Bernstorff, J. Bonarski, T. Ungar, & M. Zehetbauer, Materials Science and Engineering A 387-389, 1018-1022 (2004)

[3] Spieckermann F., Wilhelm H., Schafler E, Aifantis E. & Zehetbauer M, Journal of Engineering Materials and Technology, 131, 11109-11114 (2008)

GISAXS MEASUREMENTS OF NANOSTRUCTURED TITANIUM DIOXIDE THIN FILMS

A. Turković[1], P. Dubček[1], M. Rakić[1], M. Lončarić[1] and S. Bernstorff[2]

1.) Institute "Ruđer Bošković", P.O. Box, 10002 Zagreb, Croatia
2.) Sincrotrone Trieste, 34012 Basovizza /Trieste, Italy

At the SAXS–beamline at ELETTRA we have measured GISAXS (grazing–incidence small–angle X-ray scattering) of TiO_2 thin film samples on glass substrate at grazing angles from 0.3 to 0.7 degrees. These samples were prepared by CVD (chemical vapour deposition) or by e-beam epitaxy. The goal of this work was to determine the relevant parameters as grain sizes and porosity of all samples and then make a decision about which preparation method is the most suitable for the construction of nanostructured solar cells. The analysis of the data is still in progress, and will be used for publications in some of international scientific journals for materials science and physics.

Figure 1 shows 2D GISAXS patterns of TiO_2 nanostructured porous films on glass substrate obtained by the CVD method. The films have been annealed for half an hour at 100°C, 200°C, 500°C, 700°C, 740°C, 800°C, 900°C, and for 5,5 hours at 900°C. In the upper horizontal row the first sample was kept at room temperature, than follow the samples annealed at 100°C, 200°C, second row 500°C, 700°C, 740°C and third row 800°C, 900°C and 900°C for 5,5 hours. It can be seen that there is a structural phase transition from the low temperature anatase phase to the high temperature rutile phase. The phase transition is starting at 800°C, which could be observed as a change in the GISAXS pattern shape. The nanograin sizes and porosity could be obtained from linear vertical and horizontal cuts taken from the 2D patterns.

Figure 1. GISAXS pattern of CVD obtained samples of TiO_2 nanostructured thin films

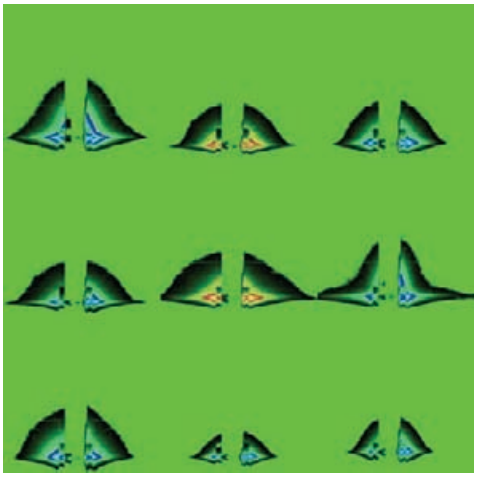

Figure 2.GISAXS pattern of e-beam-epitaxy obtained samples of TiO_2 nanostructured thin films

Figure 2 shows 2D GISAXS patterns of TiO_2 nanostructured porous films on glass substrate obtained by the e-beam epitaxy method. The films have been annealed annealed for half an hour at 100°C, 200°C, 500°C, 700°C, 740°C, 800°C, 900°C, and for 5,5 hours at 900°C. In the upper horizontal row the first sample was kept at room temperature, than follow the samples annealed at 100°C, 200°C, second row 500°C, 700°C, 740°C and third row 800°C, 900°C and 900°C for 5,5 hours. It can be seen that there is a structural phase transition from the low temperature anatase phase to the high temperature rutile phase. The phase transition is

starting at 800°C, which could be observed as a difference in the GISAXS pattern shape. The nanograin sizes and porosity could be obtained from linear vertical and horizontal cuts taken from the 2D patterns.
The GISAXS patterns in Figures 1 and 2 were obtained by the program FIT2D, Version: V12:077.

Life Science

STRUCTURE AND DYNAMICS OF APOPTOTIC MODEL MEMBRANES

B. Boulgaropoulos, E. Gander, H. Amenitsch, G. Pabst and P. Laggner

Institute of Biophysics and Nanosystems Research, Austrian Academy of Sciences, Graz, Austria

Life is based on cell division, proliferation and cell death (apoptosis). Amongst the three phases of apoptosis (initiator, effector and execution phase), the effector phase is of particular interest, because its detailed understanding may be fundamental for novel therapeutic approaches for various diseases, including atherosclerosis, cancer, or Alzheimer to name but a few. During the effector phase the bilayer looses its asymmetric lipid distribution and neutral sphingomyelinase (nSMase) hydrolyses bulk sphingomyelin (SM) to Cer, which in turn may lead to apoptotic body formation (van Blitterswijk et al. 2003, 369:199-211), (Rudolf and Cervinka 2005, 48:29-34), (Coleman et al. 2001, 3:339-345). The structural changes occurring on the supramolecular level and the involved time scales are, however, largely unknown.

Therefore, we focussed on the structural changes in membranes during the SM conversion to Cer using the well characterized nSMase from Bac cereus. Mammalian membranes were mimicked by an equimolar mixture of palmitoyl oleoyl phosphatidylcholine (POPC)/SM. The structural reorganization occurring within the membranes during the enzyme reaction was followed by time-resolved small- and wide-angle X-ray-scattering (SWAXS). Cer levels and reaction kinetics were determined by high performance thin layer chromatography.

We found, that the enzyme hydrolyzed about 60 % of the total SM-amount of the membrane to Cer and water soluble phosphocholine after approximately 100 min of reaction time. Interestingly however, the membrane structural reorganization takes about two to three times longer than the enzymatic formation of Cer. The reason is most likely hindered lateral diffusion due to Cer induced phase separation into gel-like Cer/SM-rich and fluid-like POPC-rich lipid domains. These results strengthen the alternative approach of apoptosis induction through the plasma membrane in cancer therapy.

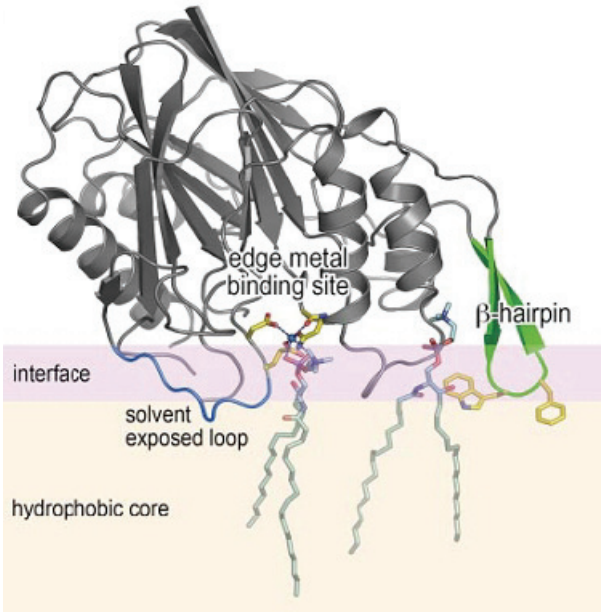

Figure 1. Binding model of Bc-SMase to the SM membrane, (Ago et al. 2006, 281:16157-16167)

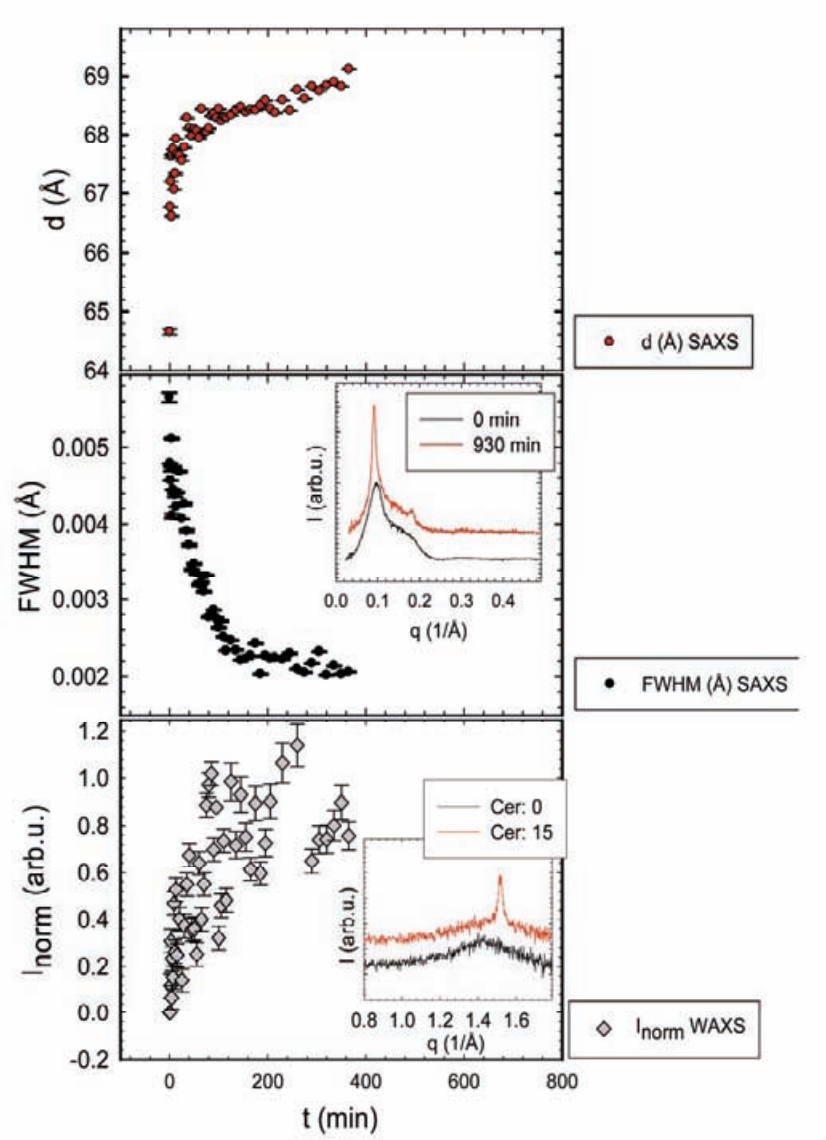

Figure 2: Changes of the structural parameters as a function of time during the reaction course. (10 Units Enzyme/ 2 mg Lipid (ULVs consistent of POPC/SM), which is one enzyme per about 300 SM molecules in the outer leaflet of the vesicles) A: Lamellar repeat distance d (Å), taken from the SAXS data as a function of reaction time. B: FWHM of the SAXS Bragg peak as a function of time. The insert shows SAXS patterns for the binary system with 0 mol % Cer (in black) and the one for a ternary lipid system with 15 mol % Cer (in red). The saturation value for the FWHM of this curve is given by the instrumental resolution of $\delta q = 2.23 \times 10-3$ Å−1. C: Changes of the normalized intensities of the WAXS gel peaks which emerge in the presence of Cer as a function of reaction time. The insert presents two WAXS patterns, horizontally shifted for better graphical presentation. The black pattern belongs to the binary sample without Cer (in black) and the red one (top) to a ternary lipid system with 15 mol % Cer.

References

[1] Ago, H., M. Oda, M. Takahashi, H. Tsuge, S. Ochi, N. Katunuma, M. Miyano, and J. Sakurai. 2006. Journal of Biological Chemistry 281, no. 23:16157-16167.
[2] Coleman, M. L., E. A. Sahai, M. Yeo, M. Bosch, A. Dewar, and M. F. Olson. 2001. Nat.Cell Biol. 3, no. 4:339-345.
[3] Rudolf, E. and M. Cervinka. 2005. ACTA MEDICA 48, no. 1:29-34.
[4] van Blitterswijk, W. J., A. H. van der Luit, R. J. Veldman, M. Verheij, and J. Borst. 2003. 23. Biochemical Journal 369:199-211.

NEW INSIGHTS INTO THE MECHANICAL PROPERTIES OF THE HUMAN ADVENTITIA FROM ITS NANO/MICROSTRUCTURAL RESPONSE

F. Cacho-Nerin[1], F. Schmid[1], B. Sartori[1], M. Rappolt[1], G.A. Holzapfel[2], P. Laggner[1] and H. Amenitsch[1]

1.) Institute of Biophysics and Nanosystems Research, Austrian Academy of Sciences, Schmiedlstr. 6, Graz, Austria
2.) Institute of Biomechanics, Graz University of Technology, Kronesgasse 5-I, Graz, Austria

Like most soft biological tissues, blood vessels are very elastic under normal working conditions, but become progressively stiffer as the load increases. This characteristic behavior is widely attributed to the collagen fibers present in the tissue [1,2], and constitutes a protection mechanism against excessive deformations. The case of the blood vessels, however, is significant because of their ability to withstand extreme conditions without damage or malfunction. These range from everyday situations such as an occasional jump down the stairs, to extraordinary circumstances such as balloon angioplasty procedures, surgical interventions or high-speed impact due to e.g. a car accident. While some damage may occur to other tissues under these conditions (broken bones, distended muscles, ruptured tendons, liver and lung trauma), the integrity of blood vessels is usually preserved without malfunction.

The need to study, model and predict the mechanical behavior of the arteries at macroscopic scales arises in many different academic, medical and industrial contexts (e.g. implant design), and has led to a variety of constitutive models that successfully describe the main features from a continuum perspective, explicitly accounting for the contribution fibers [3,4]. These formulations assume that the motion of any material point during the deformation can be described by an affine transformation from a reference configuration. Based on this, the orientation of the collagen fibers and cells, and their associated mechanical environment, are deduced from the motion of the body at macroscopic scale. However, the corresponding experimental data relating the fiber kinematics to the macroscopic biaxial deformations was missing in the literature.

For the present experiment, a vertically mounted biaxial testing machine was designed and constructed that allows arbitrary deformations in two independent axes. Deformations in the illuminated region are tracked with a video extensometer. The sample is kept in a constant-temperature chamber filled with physiological solution (NaCl 0.9% or PBS). A unique feature of this machine is that the sample chamber can be easily detached from the motors and load cells, so that the sample can be changed rapidly without affecting the setup. The device was used to perform time-resolved fiber diffraction measurements of porcine aortic adventitia under a variety of loading protocols. The samples were harvested at the local slaughterhouse upon sacrifice of the animals, and immediately processed (removal of loose connective tissue and fat) before storage at -80ºC. Immediately before testing, the samples were thawed at +4ºC and the adventitia was dissected from the intima/media. The resulting patch was then cut into a cruciform shape of about 4x4 cm using a scalpel and a custom template.

Under strip-biaxial conditions with pre-stretch, only one fiber distribution is seen initially aligned with the pre-stretch direction. As the deformation progresses, the distribution “unfolds” into two distinct distributions (Fig. 1). Under equibiaxial conditions, two

distributions are seen, which is consistent with histological findings [5]. These results indicate that the fibers rotate towards the local stretch direction at a rate that is initially much higher than that predicted by affine transformations, until a locking state is reached where the fibers cannot rotate anymore [6]. This locking state is independent of the sample and the loading direction (along the circumferential or longitudinal vessel axes). These findings are similar to results previously obtained from samples of the human arteries.

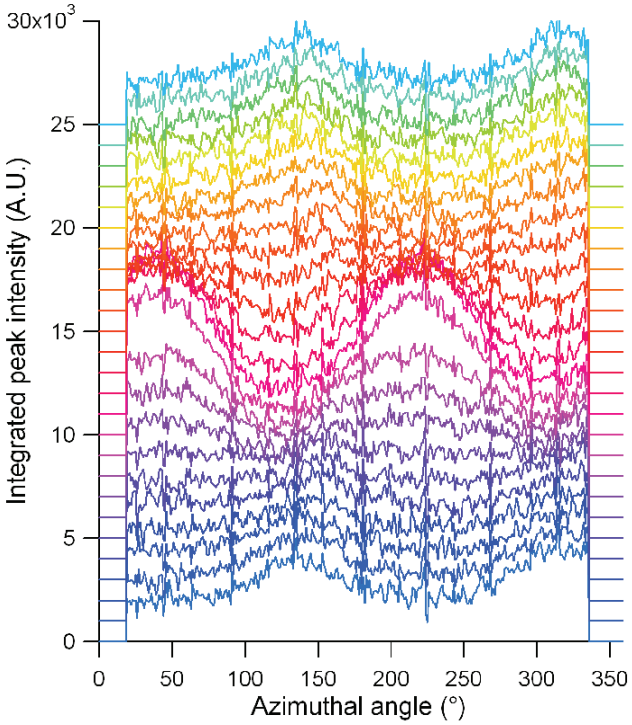

Figure 1: Integrated azimuthal peak intensity for a strip biaxial test in the circumferential direction, where the longitudinal direction had been pre-stretched. The curves are stacked vertically according to increasing experiment time (both the loading and unloading protocols are shown). The change in the distribution of the collagen orientations can be clearly seen, shifting from the longitudinal direction (135º due to the biaxial machine setup) to 45º (circumferential direction). All curves have the same (arbitrary) scale, and as a result the results corresponding to the equibiaxial stress state appear as a nearly uniform distribution.

Acknowledgments

We would like to thank C. Morello for the technical support.
This research has been funded by the FWF Austrian Science Fund under Project No. FWF P17922-N02.

References

[1] P. Fratzl, Collagen: Structure and Mechanics, Springer, 2008.
[2] P.P. Purslow, T.J. Wess, and D.W.L. Hukins, “Collagen Orientation and Molecular Spacing During Creep and Stress-Relaxation in Soft Connective Tissues,” J. Exp. Biol., vol. 201, 1998, pp. 135-142.
[3] G.A. Holzapfel, T.C. Gasser, and R.W. Ogden, “A new constitutive framework for arterial wall mechanics and a comparative study of material models,” J. Elasticity, vol. 61, 2000, p. 1—48.
[4] F. Cacho, J. Elbischger, F. Rodríguez, M. Doblaré, and A. Holzapfel, “A constitutive model for fibrous tissues considering collagen fiber crimp,” Int. J. Non-Linear Mech., vol. 42, 2007, pp. 391-402.
[5] J.A.G. Rhodin, “Architecture of the vessel wall,” Handbook of Physiology, The Cardiovascular System, D.F. Bohr, A.D. Somlyo, and H.V. Sparks, eds., Bethesda, Maryland: American Physiologial Society, 1980, p. 1—31.
[6] F. Cacho-Nerin, F. Schmid, B. Sartori, M. Rappolt, G.A. Holzapfel, P. Laggner and H. Amenitsch, “New Insights into the Mechanical Properties of the Human Adventitia from its Nano/microstructural Response”, Submitted

EFFECT OF PH ON THE STRUCTURE OF LIPOPLEXES

G. Caracciolo[1], D. Pozzi[1], R. Caminiti[1], C. Marchini[2], M. Montani[2], A. Amici[2] and H. Amenitsch[3]

1.) Department of Chemistry, University of Rome "La Sapienza", P.le Aldo Moro 5, 00185 Rome, Italy
2.) Genetic Immunization Laboratory, Department of Molecular Cellular and Animal Biology, University of Camerino, Via Gentile III da Varano, 62032 Camerino (MC), Italy
3.) Institute of Biophysics and Nanosystems Research, Austrian Academy of Sciences, Schmiedelstrasse 6, A-8042 Graz, Austria

At present, there is a high level of interest in complexes consisting of DNA mixed with cationic liposomes (CLs) [1]. This extraordinary interest arises because the complexes mimic natural viruses as carriers of DNA into cells in worldwide human gene therapy clinical trials. Mixing CLs and DNA results in their spontaneous self-assembling into highly organized liquid crystalline complexes (lipoplexes). For transfection purposes, positively charged lipoplexes are used as they bind electrostatically to the negatively charged cell surface proteoglycans with sulfated groups [2,3]. However, to meet therapeutic requirements, the efficacy of lipoplexes needs major improvement, and a detailed comprehension of the mechanism of entry in relation to eventual transfection efficiency (TE) could be part of such a strategy. Endocytosis is recognized as the major pathway of entry. After internalization via endocytosis, the internalized complexes exist in endosomes with no virtual access to the cytosol or the nucleus. Endosomes either fuse with lysosomes for degradation or recycle their content back to the cell surface. Unfortunately, lipoplexes lack a protein machinery to destabilize the endosomal membrane. Therefore, the escape of DNA from endosomal compartments is thought to represent a critical barrier to lipoplex-mediated transfection [4,5]. Recently, it has been postulated that a primary importance of the pH is for accomplishing efficient translocation of nucleic acids across the endosomal membrane into the cytosol. Lipids that form a stable bilayer at physiological pH~7 can undergo, at an acidic pH, a transition from a bilayer to an inverted hexagonal structure, which fuses and destabilizes the endosomal membrane [6]. Such an interaction between the nonlamellar lipoplex structure and the endosomal membrane may promote gene translocation. As a result, the ability of specific lipid species (such as the widely used dioleoylphosphatidylethanolamine) to promote, when protonated, lamellar-to-nonlamellar phase transitions may be a key parameter for DNA transfection. However, unambiguaous evidences of a correlation between successful formation of nonlamellar phases, DNA release, and efficient transfection are still largely lacking.

In the present study, we employed 1,2-dioleoyl-3-trimethylammonium-propane–dioleoylphosphocholine/DNA (DOTAP–DOPC/DNA) and 3β-[N-(N',N'-dimethylaminoethane)-carbamoyl]-cholesterol–dioleoylphosphatidylethanolamine/DNA (DC-Chol–DOPE/DNA) lipoplexes. Such lipid formulations, largely used for gene delivery in vitro and in vivo, exhibited very different levels of transfection in mouse fibroblast NIH 3T3, ovarian CHO, and tumoral myofibroblastlike A17 cells. In detail, in all the cell lines, TE of DC-Chol–DOPE/DNA lipoplexes is about one order of magnitude higher than that of DOTAP–DOPC/DNA ones.

With the aim of providing insight into the postulated correlation between TE, the phase evolution of lipoplexes upon acidification, and the DNA release, we investigated the pH dependence of the lipoplex structure by high-resolution synchrotron small-angle x-ray scattering (SAXS), and we estimated the extent of DNA release by means of electrophoresis on agarose gels.

Here we show that upon acidification from physiological to acidic values (as those characteristic of endosomes), (i) the lamellar structure of DOTAP–DOPC/DNA and DC-

Chol–DOPE/DNA lipoplexes is essentially preserved and that no lamellar-to-hexagonal phase transition occurred (Figure 1), (ii) the one-dimensional (1D) DNA packing density within lamellar lipoplexes increases, probably reflecting a contraction of interfacial area of lipid headgroups (a schematic illustration of the proposed mechanism for the reduction in DNA spacings upon acidification is reported in Figure 2), and (iii) DNA is not released from employed lipoplexes. Thus, our data suggest that acidification of lipoplexes within the endosomal compartment is not an obvious prerequisite in a model of a phase-mediated membrane destabilization. Taken together, all our findings seem to suggest that parameters other than simple acidification determine the transfection capacity of a given complex. The present work strongly suggests that such interfering parameters may include the DNA-binding capacity of CLs, which in turn is governed by the chemical nature of the amphiphile. Optimization of cationic lipid/DNA complexes for transfection will require to determine the optimal cationic lipid/DNA charge ratio necessary to complex completely the DNA [7].

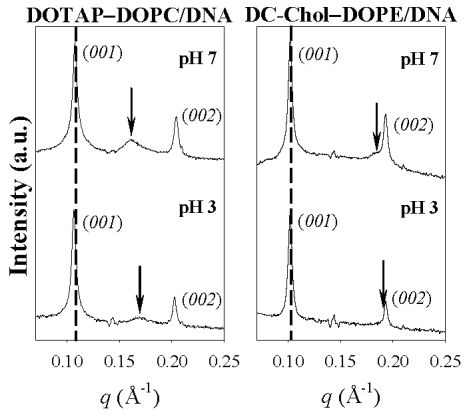

Figure 1. SAXS patterns of DOTAP–DOPC/DNA (left panel) and DC-Chol–DOPE/DNA (right panel) at two different pH values: pH 7 and pH 3. As pH decreases, DNA peak (marked by arrows) shifted to higher q values (i.e., shortest DNA spacings) as a result of the lateral expansion of the lipid headgroups. Vertical dashed line identifies the position of the (001) Bragg peak at pH 7.

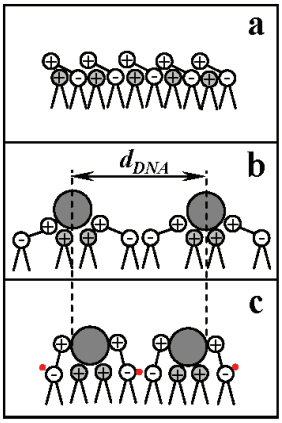

Figure 2. Schematic illustration of the proposed mechanism for the reduction in DNA spacings upon acidification. Panel (a): a mixed cationic-zwitterionic lipid membrane. The headgroup of the cationic lipid species carries one positive charge (gray circle). The headgroup of the zwitterionic lipid consists of a single dipole with spatially fixed negative-charge base and a mobile positive-charge head (white circle). Panel (b): mixing DNA and cationic liposomes results in the formation of locally ordered 1D arrays of DNA chains (dark gray circle) intercalated between charged membrane bilayers. The distance between DNA chains is indicated as d_{DNA}. Panel (c): upon lowering the pH, H_3O^+ molecules (red circle) form hydrogen bonding with P– atomic groups. N^+ atomic groups align the headgroup dipole moment (P→N vector) against the dipole moment created by the H_3O^+ molecules. As a consequence, the interfacial area of lipid headgroups decreases and a lateral contraction of lipid bilayer occurs.

References:

[1] P. L. Felgner; Nonviral strategies for gene therapy; Sci. Am. 276, 102-106 (1997).

[2] A. J. Lin, N. L. Slack, A. Ahmad, I. Koltover, C. X. George, C. E. Samuel and C. R. Safinya; Structure and structure-function studies of lipid-plasmid DNA complexes; J. Drug Target. 8, 13-27 (2000).

[3] G. Caracciolo, R. Caminiti, D. Pozzi, M. Friello, F. Boffi and A. Congiu Castellano; A new approach for the study of cationic lipid-DNA complexes by energy dispersive X-ray diffraction; Chem. Phys. Lett. 351, 222-228 (2002).

[4] D. P. Siegel and R. M. Epand; The mechanism of lamellar-to-inverted hexagonal phase transitions in phosphatidylethanolamine: implications for membrane fusion mechanisms; Biophys. J. 73, 3089-3111 (1997).

[5] S. Audouy and D. Hoekstra, Cationic lipid-mediated transfection in vitro and in vivo; Mol. Membr. Biol. 18, 129-143 (2001).

[6] I. M. Hafez, S. Ansell, and P. R. Cullis; Tunable pH-sensitive liposomes composed of mixtures of cationic and anionic lipids; Biophys. J. 79, 1438-1446 (2000).

[7] G. Caracciolo, D. Pozzi, R. Caminiti, C. Marchini, M. Montani and Heinz Amenitsch; Effect of pH on the structure of lipoplexes; J. Appl. Phys. 104, 014701 (2008).

STRUCTURAL STABILITY AND INCREASE IN SIZE RATIONALIZE THE EFFICIENCY OF LIPOPLEXES IN SERUM

G. Caracciolo[1], D. Pozzi[1], C. Marchini[2], M. Montani[2], A. Amici[2], C. Marianecci[3] and H. Amenitsch[4]

1.) Department of Chemistry, University of Rome "La Sapienza", P.le Aldo Moro 5, 00185 Rome, Italy
2.) Genetic Immunization Laboratory, Department of Molecular Cellular and Animal Biology, University of Camerino, Via Gentile III da Varano, 62032 Camerino (MC), Italy
3.) Dipartimento di Chimica e Tecnologie del Farmaco, Faculty of Pharmacy, University of Rome "La Sapienza", P. le Aldo Moro 5, 00185 Rome, Italy
4.) Institute of Biophysics and Nanosystems Research, Austrian Academy of Sciences, Schmiedelstrasse 6, A-8042 Graz, Austria

Cationic liposomes (CLs) have become widely used as nonviral gene vectors for both in vitro and in vivo applications [1]. Because of their positive charge, they spontaneously associate with negatively charged DNA, thereby forming lipoplexes [1]. The ease of cationic lipid synthesis and the availability of lipid technologies resulted in a huge number of lipid transfection reagents. Unfortunately, the absence of supporting biology of transfection resulted in plateauing of transfection efficiencies by lipoplexes. As a result, understanding the mechanisms of lipid mediated delivery is definitely more compelling now. Among the barriers to transfection, serum has been reported to exert its inhibitory effect [2]. Serum components interact with the lipoplex in a nonspecific manner. Two kinds of effects of serum have been reported. First, serum proteins such as albumin, lipoproteins, fibrinogen, and heparin can bind to lipid membranes, causing aggregation of lipoplexes and resulting in size increases and decreases as a function of the zeta potential [2,3]. As a result, the interaction of lipoplexes with the cell or the interaction of DNA with the cationic lipid is weakened. The second effect is a destabilization of the lipoplex structure, which may induce the dissociation of DNA from the complexes. Lipoplexes can be arranged into lamellar or inverted hexagonal phases depending on lipid composition. A serum-induced lamellar-to hexagonal phase transition of lipid membranes has been also proposed [3] but, to the best of our knowledge, has not been reported so far. The presence of serum at the time of lipoplex incubation with cells, in general, was found to decrease the transfection [4], hence the desire to develop formulations of lipoplexes that are unaffected by serum [5]. Unfortunately, the mechanisms that regulate the stability of lipoplexes in serum as well as the details of lipoplex-serum interaction are still poorly understood.

In this work we investigated the effect of fetal bovine serum (FBS) on the colloidal stability (structure, size, zeta potential, and DNA-binding capacity) of lipoplexes and we tried to correlate it with transfection efficiency (TE). Because of the amphiphile-dependent nature of the interaction of lipoplexes with serum proteins, we prepared different lipoplex formulations by fixing the neutral helper lipid dioleoylphosphatidylethanolamine (DOPE) but varying the cationic lipid (by incorporating dimethyldioctadecylammonium bromide (DDAB) or 3β-[N-(N',N'-dimethylaminoethane)-carbamoyl]-cholesterol (DC-Chol) in the binary mixtures). Some authors have suggested that serum stability may be dependent on the membrane charge density of lipoplexes [6]. To test this suggestion, we maintained a constant quantity of the cationic lipid (alternatively DDAB or DC-Chol) and varied the amount of DOPE within the formulation. Structural changes of lipoplexes in serum were investigated by means of high-resolution synchrotron small-angle X-ray scattering (SAXS). The effect of serum on the size of the complexes was assessed by dynamic light scattering (DLS), whereas the association between lipid and DNA in serum was evaluated by agarose gel electrophoresis. These physicochemical properties were compared with the transfection of NIH 3T3 cells. In the absence of serum, all tested formulations were found to be very efficient in trasfecting NIH

3T3 cells with varying efficacy, and this is mainly dependent on the lipid phase behaviour and DNA-binding capacity of cationic liposomes. Despite most previous results [4], the transfection efficiency of all lipoplex formulations increased in the presence of FBS (Figure 1). Investigated lipoplexes were stable in serum, and no appreciable changes in lamellar structure and DNA packing density were detected. Synchrotron SAXS data indicated that serum promoted the lamellar-to-inverted hexagonal phase transition in DDAB–DOPE/DNA lipoplexes at Φ=0.5 (Figure 2). It has recently been proposed that serum protein intercalation within lipid bilayers can induce the formation of nonlamellar motifs in the membranes of lipoplexes [3]. Mixing molecules within the lipid bilayer can reduce the bending rigidity of membranes and, in turn, can result in a reduction in the elastic energy barrier to the formation of the hexagonal phase. Inverted hexagonal phases are proposed to play a key role in the endosomal escape of DNA and to display high transfection efficiency. The formation of the fusogenic inverted hexagonal phase may therefore be taken into account to explain why DDAB–DOPE/DNA lipoplexes at Φ=0.5 exhibited the highest increase in efficiency in the presence of serum.

Neither DNA released from lipoplexes nor the morphology of DNA protected by cationic lipids was affected by serum. We believe that such a marked stability of tested lipoplex formulations in serum is a reasonable explanation of their efficiency. Major changes in lipoplex size were induced by serum. According to the established viewpoint of the size-dependent entry mechanism of lipoplexes, our results seemingly suggest that the increase in transfection efficiency in serum may be due to a serum-induced switch from a clathrin-dependent to caveolae-mediated mechanism of internalization of lipoplexes. If further confirmed, these results imply that, by controlling lipoplex stability and size in serum, an efficient lipid delivery system may be achieved [7].

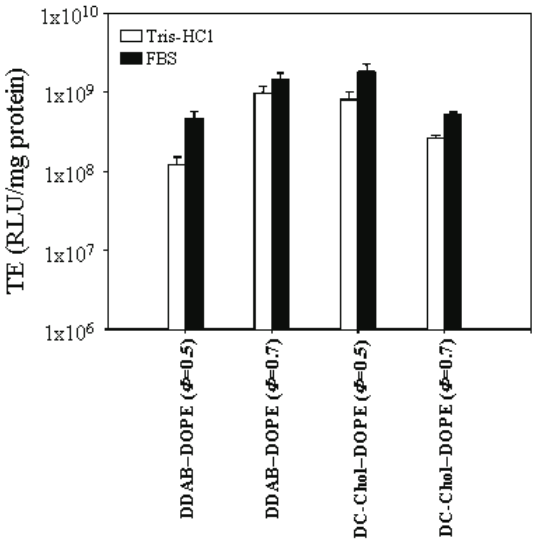

Figure 1. Transfection efficiency in RLU/mg of cellular proteins of DDAB–DOPE/DNA (Φ=0.5), DDAB–DOPE/DNA (Φ=0.7), DC-Chol–DOPE/DNA (Φ=0.5), and DC-Chol–DOPE/DNA (Φ=0.7) lipoplexes in the absence (white histograms) and in the presence of serum (black histograms).

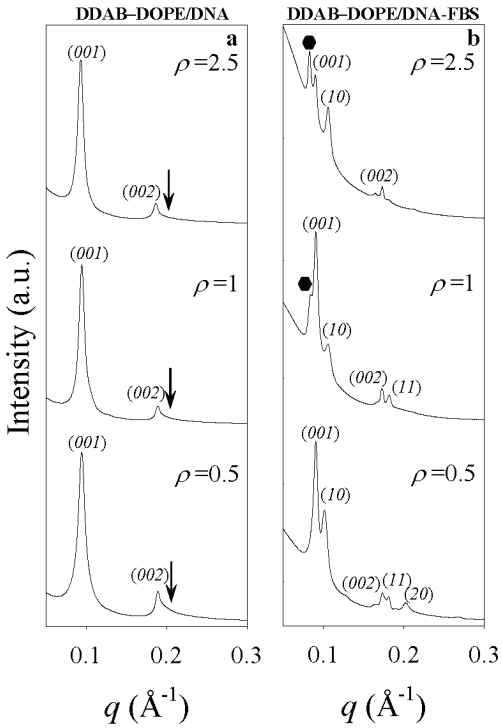

Figure 2. Synchrotron SAXS patterns of DDAB–DOPE/DNA lipoplexes at Φ=0.5, as a function of increasing ρ (from bottom to top), in the absence (a) and in the presence of serum (b). The interhelical DNA-DNA distance peak is marked with an arrow.

References:

[1] P. L. Felgner; Nonviral strategies for gene therapy; Sci. Am. 276, 102-106 (1997).

[2] D. Simberg, S.Weisman, Y. Talmon, A. Faerman, T. Shoshani and Y. Barenholz; The role of organ vascularization and lipoplex-serum initial contact in intravenous murine lipofection; J. Biol. Chem. 278, 39858–39865 (2003).

[3] L. Wasungu, M. Scarzello, G. van Dam, G. Molema, A. Wagennar, J. B. F. N. Engberts and D. Hoekstra; Transfection mediated by pH sensitive sugar-based Gemini surfactants; potential for in vivo gene therapy applications; J. Mol. Med. 84, 774–784 (2006).

[4] J. Turek, C. Dubertret, G. Jaslin, K. Antonakis, D. Scherman, and B. Pitard; Formulations which increase the size of lipoplexes prevent serum-associated inhibition of transfection; J. Gene Med. 2, 32–40 (2000).

[5] S. Audouy, G. Molema, L. de Leij and D. Hoekstra; Serum as a modulator of lipoplex-mediated gene transfection: dependence of amphiphile, cell type and complex stability; J. Gene Med. 2, 465–476 (2000).

[6] D. Simberg, A. Weiss, and Y. Barenholz; Reversible mode of binding of serum proteins to DOTAP/Cholesterol lipoplexes: a possible explanation for intravenous lipofection efficiency; Hum. Gene Ther. 16, 1087–1096 (2005).

[7] C. Marchini, M. Montani, A. Amici, H. Amenitsch, C. Marianecci, D. Pozzi and G. Caracciolo; Structural stability and increase in size rationalize the efficiency of lipoplexes in serum; Langmuir 25, 3013-3021 (2009).

PHASE BEHAVIOR OF A MYVEROL/SALINE MIXTURE AS A FUNCTION OF TEMPERATURE

C.J. Garvey[1], A. Duff[1], T. Larkin[2] and P. Kuchel[2]

1.) ANSTO, PMB 1 Menai, NSW 2234, AUSTRALIA
2.) School of Molecular and Microbial Biosciences, University of Sydney NSW 2006, AUSTRALIA

We are investigating of the phase behavior of a Myverol, a food emulsifier rich in monoacylglycerols with the aim of preparing macroscopic crystals of the cubic phase for small angle crystallography measurements. In principle the production of well oriented samples will allow separation of important length scales more clearly than isotropic/powder samples. A fundamental question that will ultimately limit the application of this approach is competition between thermal motions of the lattice and the forces which assemble the lattice [1].

Measurements have been made using 8 keV x-rays on samples of 73% Myverol and 27% 154mM saline over the range of scattering vectors 0.09 to 3.5 nm-1 using an image plate detector. The image plate detector gives a large q-range, and better resolution, q, afforded by most area detectors. Two-dimensional scattering patterns have been collected from the sample in a capillary heated from 20°C in 5°C increments to 80°C every 5 minutes. The resulting scattering patterns are shown in Figure 1. The sample was then quenched to 20°C, allowed to equilibrate for 60 minutes, and then raised 10°C every 5 minutes. The system was then again quenched to 20°C. At 20°C and above we observe sharper and more peaks than was measured in a lab. The data is radially symmetric around the direction of the incident x-ray beam which is indicative of sample which consists of numerous crystalline domains isotropically oriented (powder pattern). As the sample is heated phase transitions are observed between 50°C and 55°C; and 70°C and 75°C. According to Qiu and Caffrey [2] these transitions would be from the Ia3d to hexagonal; and the hexagonal to fluid isotropic transition respectively. The data from the "isotropic" phase above 70°C is clearly aligned.

In the Ia3d phase we find that the number of peaks is greater than the corresponding data from a lab based SAXS camera. This is due to the highly monochromatic nature of the synchrotron x-ray beam, and the superior Δq of the image plate detector. As the sample is heated in the Ia3d phase, some of the peaks disappear, presumably to broadening as the size of the ordered regions of the cubic phase decrease. Those reflections which are clearly visible shift to higher q with temperature. The size of the unit cell of the cubic crystal decreases with increasing temperature.

In the interpretation of small angle scattering generally it is the radial average of the data and the attending imposition of the powder average. We find that heating the sample and cooling in cycles produces as anisotropic scattering pattern from Ia3d phase (Figure 3).

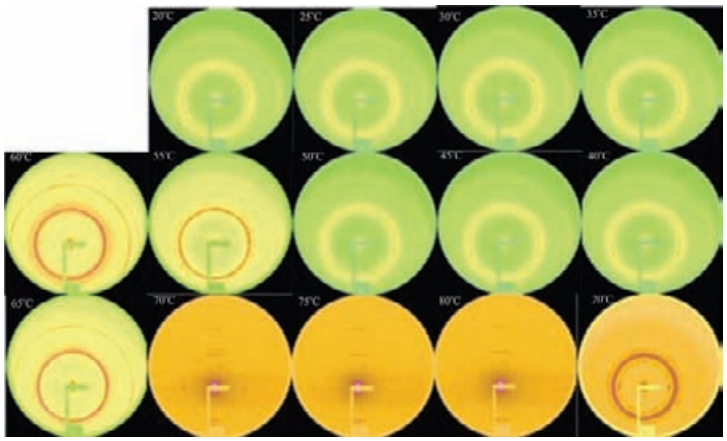

Figure 1. X-ray scattering patterns from 73% Myverol and 27% 154mM saline heated through 5°C steps to 80°C, and then quenched to 20°C in the final step.

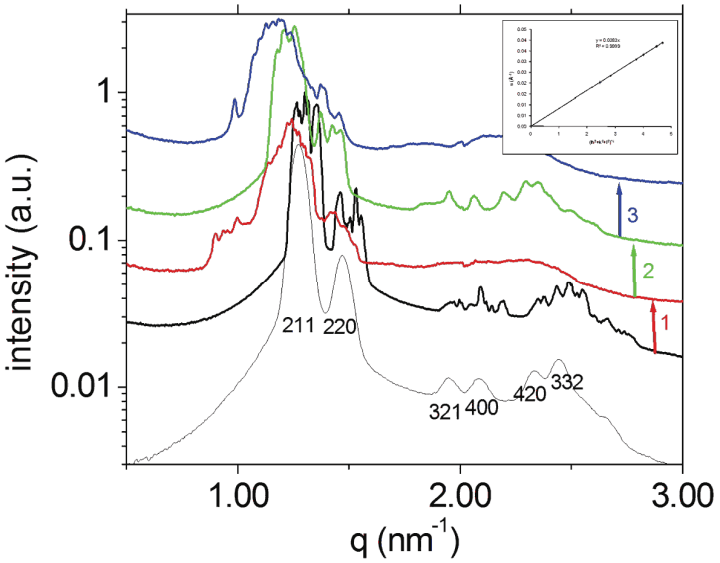

Figure 2. Radial averages of data from: lab-based SAXS camera and crystallographic assignment of peaks (thin line); initial sample at 20°C (thick line); heated to 80°C and then quenched to 20°C (2); allowed to equilibrate for 20 minutes (3); and then heated again to 80°C and quenched (4). The data from the lab based measurement allowed us to assign the Ia3d cubic phase (inset).

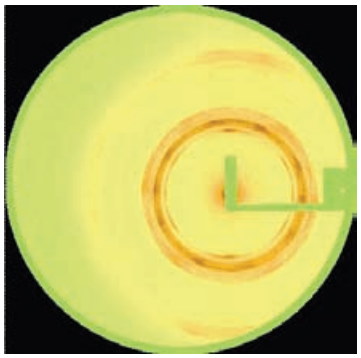

Figure 3. Scattering pattern used to produce the top curve in Figure 1

References:

[1] Saksena, R. S. and P. V. Coveney (2009). "Rheological response and dynamics of the amphiphilic diamond phase from kinetic lattice-Boltzmann simulations." Proceedings of the Royal Society a-Mathematical Physical and Engineering Sciences 465(2106): 1977-2002 (2009).

[2] Qiu, H. and M. Caffrey (2000). "The phase diagram of the monoolein/water system: metastability and equilibrium aspects." Biomaterials 21(3): 223-234 (2000).

CHARACTERIZATION OF DIFFERENT CONFORMATIONAL FORMS OF MALARIAL ANTIGEN

C.J. Garvey[1], A. Duff[1], T.Larkin[2], G. Bryant[3], R. Anders[4], and R. Norton[5]

1.) ANSTO, PMB 1 Menai, NSW 2234, Australia
2.) School of Molecular and Microbial Biosciences, University of Sydney NSW 2006, Australia
3.) Applied Physics, RMIT University, Melbourne VIC 3001, Australia
3.) Department of Biochemistry, La Trobe University, Victoria 3086, Australia
4.) Structural Biology Division, Walter and Eliza Hall Institute of Medical Research, Parkville, Victoria 3050, Australia

Malaria caused by infection with the protozoan parasite P. falciparum remains one of the world's most serious public health problems. Young children who have not developed protective acquired immune responses to the parasite are particularly susceptible to developing life-threatening disease and more than 1 million children die from malaria each year. Malaria is most prevalent in poor rural populations of African and other tropical developing countries and has been recognised recently as a significant cause of this poverty [2]. More effective deployment of existing control methods and the development of new tools to control malaria are needed urgently to improve population health and facilitate economic development in many of the poorest countries of the world. Immunization is a particularly cost-effective means of controlling infectious diseases and the development of an effective malaria vaccine is a major global public health priority. Although there have been increased resources available recently for malaria vaccine development and important progress made with some efficacy demonstrated in field trials, major issues still need to be addressed before a malaria vaccine that can be widely deployed against this disease becomes a reality. The impact of antigen conformation and polymorphisms on vaccine efficacy are two such issues.

Acquired specific immune responses developing in individuals as a result of recurrent infection with malarial parasites are particularly directed against asexual blood-stage antigens, and antibodies to merozoite surface antigens, including merozoite surface protein 2 (MSP2), appear to be important components of effector mechanism that inhibit the disease causing asexual blood-stage parasites. The studies on MSP2 proposed here build on our long-term interest in this antigen, which has involved their cloning, characterization, preclinical evaluation and early clinical development, and has been a major factor in establishing MSP2 as a leading malaria vaccine candidate.

MSP2 is an integral membrane protein anchored by a C-terminal glycosylphosphatidylinositol (GPI) moiety to the surface of the merozoite stage of P. falciparum [3]. MSP2 is considered to be essential for invasion of erythrocytes by P. falciparum. It is expressed approximately 12 h after invasion begins, during the late ring stage, reaching a maximal concentration after about 42 h [4]. MSP2 appears to be essential for parasite viability as attempts to produce a "knock-out" of this gene result in non-viable parasites. Because of its location on the merozoite surface, MSP2 is directly accessible to immune attack by antibodies in the host plasma, and antibodies to both native and recombinant MSP2 can block merozoite invasion of erythrocytes in vitro. MSP2 is therefore being assessed as a candidate for inclusion in a multi-valent vaccine against malaria [5, 6].

In this study we examine the solution scattering of two isoforms of MSP2 FC27 and 3D7 in two different buffers, an acetate buffer and a phosphate buffer. Scattering curves for the protein at different concentrations between 0.5 to 5 mg.ml-1 are shown on an absolute scale of intensity with background of capillary and buffer subtracted. The scattering curves are show in Figure 1a-c. There are some problems with background subtract for the mid-protein concentrations (Figure 1c), nether the less, the Guinier analysis of the initial slope of the curve

is used to calculate the radius of gyration, r_{gyr}, is compared to the hydrodynamic radius, r_{hydro}, calculated from pulse field gradient NMR measurements of the diffusion co-efficient and the Stokes equation [7]. A linear relationship of concentration to I(0) and consistency of r_{gyr} indicate the samples did not aggregate or dissociate during the experiment. The values of $r_{gyr} < r_{hydro}$ (Table 1). This is because the hydrodynamic radius contains a contribution from strongly bound water molecules. The trends for different buffers are the same as those found from NMR measurements.

Further physiochemical characterizations of the two isoforms are consistent with relatively unstructured proteins with small amount of residual structure [7]. The Kratky plots of the two proteins in different buffers (Figure 2a-c) are also consistent with relatively unstructured proteins containing more rigid linker regions.

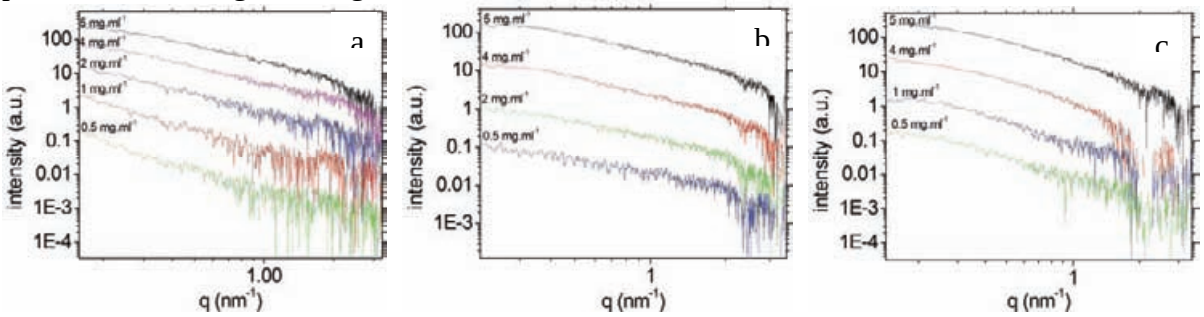

Figure 1. Radially averaged small angle X-ray scattering from different concentrations of: 3D7 in acetate buffer, a); FC27 in acetate buffer, b); and FC27 in phosphate buffer, c).

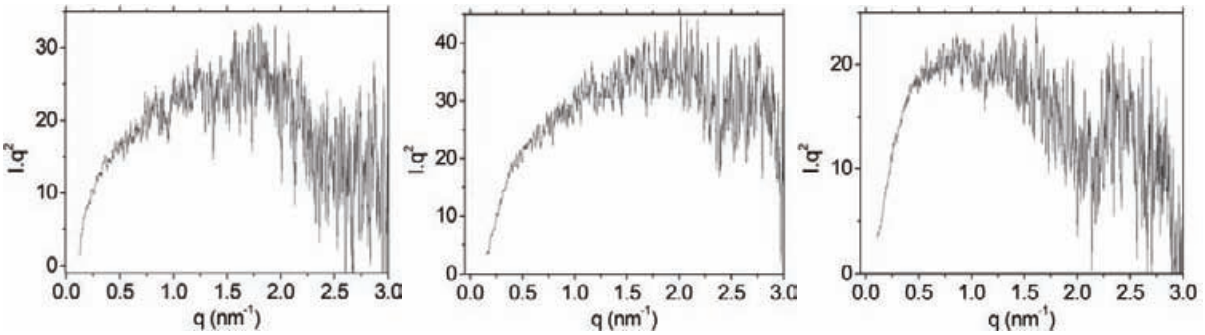

Figure 2. Kratky plot of X-ray scattering from: 3D7 in acetate buffer, a); FC27 in acetate buffer, b); and FC27 in phosphate buffer, c).

Table 1. Comparison of radius of gyration with hydrodynamic properties of protein.

Sample	Buffer (pH)	rgry (±0.01 nm)	rhydro (nm)
3D7	Acetate (3.6)	3.80	4.10
	Phosphate (7.25)	-	3.49
FC27	Acetate (3.6)	3.50	3.91
	Phosphate (7.25)	3.27	3.39

References:

[1] Genton, B., et al., J Infect Dis, 2002. 185: 820-7.
[2] Sachs J, Malaney P. Nature. 2002 415 :680-5.
[3] Smythe, J.A., et al., Proc Natl Acad Sci U S A, 1988. 85: 5195-9.
[4] Heidrich, H.G., et al., J Parasitol, 1983. 69: 360-7.
[5] Hoffmann, E.H., et al., Ann Trop Med Parasitol, 2001. 95: 117-32.
[6] Genton, B., et al., Vaccine, 2000. 18: 2504-11.
[7] Zhang, X., et al., J. Mol. Biol. 2008. 379, 105-121.

SAXS INVESIGATION INTO THE INTERACTION OF ANTIMICROBIAL PEPTIDES WITH ENDOTOXINS

J. Howe[1], M. Rappolt[2], T. Gutsmann[1], and K. Brandenburg[1]

1.) Forschungszentrum Borstel, LG Biophysik, Parkallee 10, D-23845 Borstel, Germany
2.) Institute of Biophysics and Nanosystems Research, Austrian Academy of Sciences, Graz, Austria

The particular glycolipid lipopolysaccharide (LPS) from Gram-negative bacteria is an amphiphilic macromolecule located in their outer membrane. LPS, which is released by the attack of the immune cells or simply by dividing cells, is able to induce a variety of biological effects. The result of the specific interaction of LPS with cells was found to be the activation of cells such as cellular proliferation of murine B-lymphocytes and the formation and secretion of bioactive mediators (cytokines). At low concentrations these mediators are beneficial for the proper functioning of the immune system and its fight against invading microorganisms, at high concentrations, however, these mediators cause toxic effects such as pyrogenicity, leukopenia, and irreversible shock. For a fight against infection and in particular against Gram-negative sepsis, a new strategy is the development of suitable peptides based on the binding domains of human proteins such as lactoferrin. From the observed biological properties of LPS it can be concluded that an understanding of the aggregate structure of LPS molecules and its interaction with natural antibiotic proteins or synthetic peptides is of high important with respect to an characterization of the interaction mechanism leading to cell activation.

We have found that general properties of the aggregate structures of these molecules govern their biological effectiveness, and that these characteristics are changed due to binding of antimicrobial agents. We have also found that a necessary but not sufficient prerequisite for the inactivation of a given LPS/lipid A due to peptide/protein binding is the conversion of the LPS aggregates into multilamellar structures. A detailed analysis of the kind of multilamellar structure is therefore of high importance. This comprises the number of lamellae, the aggregate (vesicle)size, and the bilayer thicknesses. The meausrements are performed with synchrotron SAXS, analysing various LPS chemotypes differing in the length of the sugar chains and their interactions with some model peptides. The experimental results are then compared with theoretical calculations, which should allow to get an estimate of the aggregate fine structures. Furthermore, from these data we will deduce electron density maps of the LPS: peptide multilamellae, which should allow to elucidate the interaction sites of the peptides within the LPS molecules. In first experiments the interaction of lipopolysaccharide Re from Salmonella minnesota R60 was studied with the peptide Pep19-2, a compound which has been found to drastically reduce the LPS-induced cytokine production in human mononuclear cells. The SAXS experiments, performed at a [LPS]:[peptide] ratio of 10:1 molar, showed an excellent conversion of the cubic structure for pure LPS (data not shown) in the presence of already a low amount of the peptide (see Fig. 1). Therefore, these data make it possible to directly deduce from the SAXS measurements the effeicifity of any antimicrobial compound.

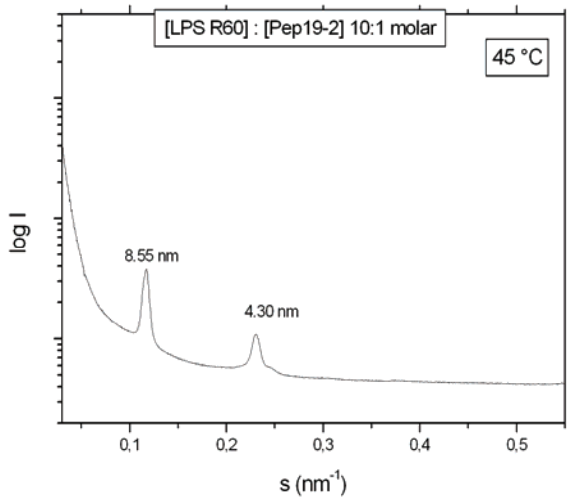

Figure 1. SAXS pattern of the interaction of lipopolysaccharide R60 with antimicrobial peptide Pep 19-2. The reflection maxima at 8.55 and 4.30 nm are indicative of a multilamellar aggregate structure, while pure LPS forms cubic structures (not shown).

CHARACTERIZATION OF THE INTERNAL STRUCTURE OF LIPIDIC NANOPARTICLES BY SYNCHROTRON SAXS

M. Monduzzi[1], S. Murgia[1], P. Mariani[2], M. Rappolt[3], and S. Bernstorff[4]

1.) Dip. Scienze Chimiche, University of Cagliari, Monserrato (CA), Italy
2.) Dip. Scienze Applicate ai Sistemi Complessi, Univ. Politecnica delle Marche, Ancona, Italy
3.) Austrian Academy of Sciences, Inst. Biophysics anad Nanosystems Research, Graz, Austria
4.) Sincrotrone Trieste, Basovizza, (TS), Italy

Nanostructured lipid aggregates constitute an important challenge to engineering biomaterials for nanobiotechnological applications such as innovative drug delivery systems. Nowadays, intelligent biomaterials would combine molecular recognition properties with controlled drug release. In general molecular recognition can be attained through different molecular mechanisms driven by electrostatic and H-bonding interactions mainly.

Surface properties and interfacial interactions of nanostructured mesophases with the biological environments are crucial to determine the bioadhesion, and then the release performance of the drug.

Monoolein (MO)-based liquid crystalline (LC) phases, particularly bicontinuous cubic and hexagonal LC types, have been shown to be suitable for drug inclusion and controlled release [1-6]. Due to the difficulty in the direct use of LC phases as drug delivery systems, several groups have developed new technologies to prepare fluid dispersions of LC nanoparticles (cubosomes and hexosomes) using a triblock copolymer (typically Pluronic F127) as dispersing agent. These methods, however, do not allow to enclose very hydrophilic drugs such as nucleotides.

The focus of this project was the entrapment of four mononucleotides, namely AMP, GMP, UMP, and CMP inside the cubic LC phase of MO/Water systems. Indeed, these molecules may play a significant role in molecular recognition thus enhancing the already high bioadhesion properties of monoolein. The nanoparticle dispersions were prepared through the fracture (via ultraturrax) of LC massive phases using Pluronic F127, PEG-monooleate (PMO) and lauroyl choline chloride (LCh) as dispersing agents. In this context, it is worth noting that some preliminary results of biological tests (3T3, Hela and HEK cell lines) indicated high viability of dispersions stabilized by LCh (no enclosed drugs - manuscript in preparation). The preservation of the LC matrix is crucial to assure controlled and gradual release when the formulations are projected for drug delivery systems.

SAXS synchrotron beamline measurements were performed on several aqueous dispersions of cubic and hexagonal LC prepared using the different emulsifiers. The preservation of the liquid crystalline (LC) structure of Monoolein-based nanoparticles dispersed in water was ascertained only in few cases where hexagonal LC were used. As an example, Figure 1 shows the SAXS patterns of two old samples of monoolein-water-CMP for which a cubic-to-hexagonal phase transition was observed with time. The left diffractogram refers to the hexagonal LC phase, whereas the right one shows the sample dispersed using the PEG-MO emulsifier. These results clearly indicate that the high energy process used to produce lipid nanoparticles directly from massive LC phases causes the loss of the original LC nanostructures in most cases.

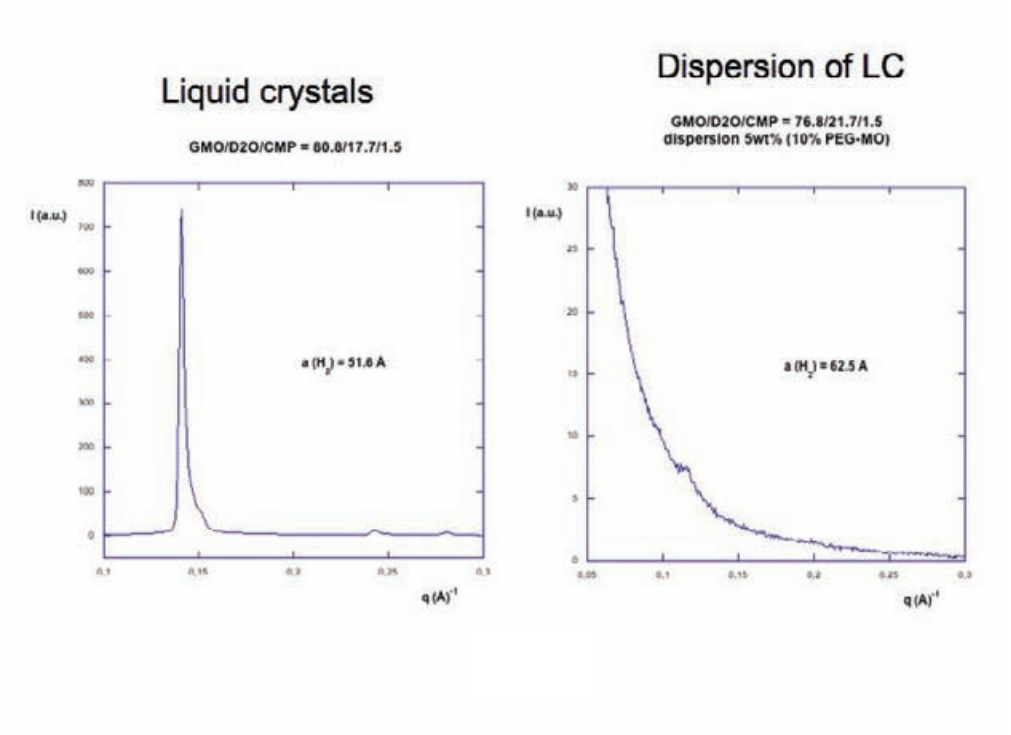

Figure 1. SAXS pattern of a hexagonal LC phase (left), and of a PEG-MO stabilized lipid dispersion (right).

References:

[1] K. Larsson, Cubosomes and hexosomes for drug delivery. Proc. Int. Symp. Control Rel. Bioact. Mater Mater. 24, 198–199 (1997).

[2] M. Monduzzi, H. Ljusberg-Wahren, K.Larsson, A 13C NMR study of aqueous dispersions of reversed lipid phases. Langmuir, 16, 7355–7358 (2000).

[3] P.T. Spicer, K.L. Hayden, M.L. Lynch, A. Ofori-Boateng, J.L. Burns, , Novel process for producing cubic liquid crystalline nanoparticles (cubosomes). Langmuir 17, 5748–5756 (2001).

[4] J. Barauskas, M. Johnsson, F. Joabsson, F. Tiberg, Cubic Phase Nanoparticles (Cubosome): Principles for Controlling Size, Structure, and Stability. Langmuir 21, 2569-2577 (2005).

[5] B.J. Boyd, D. Whittaker, S.M. Khoo, G. Davey, Hexosomes formed from glycerite surfactants- formulation as a colloidal carrier of irinotecan. International Journal of Pharmaceutics 318, 154-162 (2006).

[6] G. Popescu, J. Barauskas, T. Nylander, F. Tiberg, Liquid Crystalline Phases and Their Dispersions in Aqueous Mixtures of Glycerol Monooleate and Glyceryl Monooleyl Ether, Langmuir, 23, 496-503 (2007).

TRIACYLGLYCEROL CRYSTALLIZATION AND TEMPERING IN EMULSION

M. Ouattara[1], D. Kalnin[2], V. Faivre[1]

1.) Laboratoire de Physico-Chimie des Systèmes Polyphasés, UMR CNRS 8612 – IFR 141, Université Paris-Sud, 5 rue J.B. Clément, 92296 Châtenay-Malabry, France
2.) Life Science and Chemical Industries Section YKI, Ytkemiska Institutet AB (YKI, Institute for Surface Chemistry) P.O. Box 5607, SE-114 86 Stockholm, Sweden

Lipid-based drug delivery systems have been demonstrated to be useful in enhancing the bioavailability of highly lipophilic and hence water insoluble active molecules. Among them, solid lipid nanoparticles, e.g. based on triglycerides, waxes or fatty acids are being extensively investigated as potential carrier systems however part of those investigations show that micro-phase separation, due to confined space, leads to expulsion of the incorporated drug and hence a uncontrolled release. This small particle size moreover makes them interesting as delivery systems for different routes of administration, including the intravenous one.
In our group, we develop particles containing cocoa butter and medium-chain triglycerides as soft matter matrix, which are partially liquid at room temperature, have been used to increase the drug incorporation and retention in nanoseized particles

Because of the important dilution of the dispersion (20% of lipid content) and the small particle size (100-300nm), the high flux of ELETTRA BL 5.2 has been used to study the effect of different tempering procedures on particles of different size (200 vs. 300 nm) or composition (native cocoa butter (CB) or fractionated cocoa butter (FCB)). Furthermore, crystallisation rate upon rapid cooling have been checked and evaluated for each formulation.

Sample Preparation

Hot emulsions (60°C) were prepared with a two-stage homogenization, using an APV 2000 homogenizer, after a pre-emulsification step (Ultraturrax). After initial preparation emulsions were kept at 4°C during 48h in order to crystallize the CB based high melting part of the soft matter matrix inside particles. After this low-temperature crystallization step, half of the particles have been stored at 21°C during 5 days and the other ones at 31°C during 5 days and then all the sample were stored(and transported) 2 days at room temperature prior to analysis. Depending on the homogenization procedure, two sizes of stable emulsions have been obtained (±200 and ±300 nm). The formulations contained always 24% of Labrafac, 3% of surface active agents and 73% of cocoa butter; this CB being native or fractionated (FCB) in order to increase its melting temperature of solid fraction [1].
The samples were analyzed at fixed temperature, 20°C or 4°C (in crystal growth rate experiments), and DSC were performed using Microcalix [2], a microcalorimeter especially designed for installation in an X-ray beam.

Results

A typical diffractogram of the particles obtained 9 days after their initial preparation is presented in the figure 1. A peak indicating a lamelar order is clearly apparent in the SAXS domain while the WAXS pattern shows more than one phase which could be attributed to both crysatllization of CB and labrafac at the interface or inside the emulsion droplet. Following static measurements, samples have been heated for melting point determination. All the results are summarized in the table 1. A d-spacing between 44-48Å could be measured, corresponding to the classical 2L arrangement of the cocoa butter. The melting temperatures are around 25-27°C. For the two studied particle sizes, no strong effects of the

composition on d-spacings and melting temperatures (with or without Labrafac, native or fractionated CB), or tempering conditions should be noticed. This behavior is completely different compared to similar formulations studied as bulk material (data not shown).
The crystal growth kinetics of CB- or FCB-based droplets, obtained after quenching from 60°C to 4°C, are shown in the figure 2. No size effect could be observed. However a strong dependence on the composition can be noticed

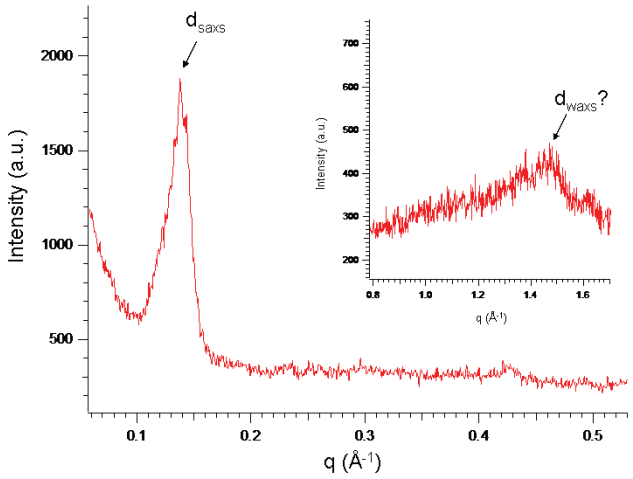

Figure 1. Typical X-ray scattering pattern of the nanoparticle suspensions (composition CB/labrafac; size: 200 nm, tempering condition: 31°C).

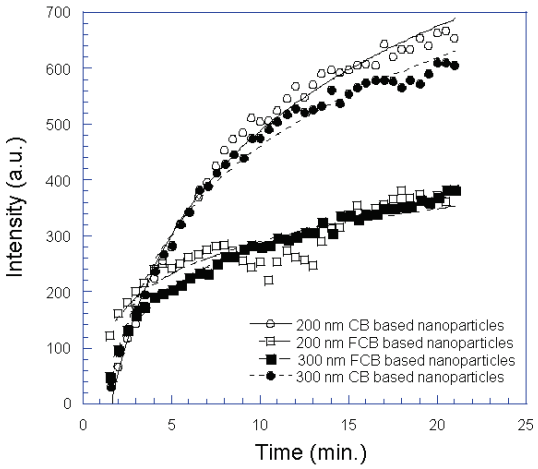

Figure 2. Crystallization kinetics following the quenching of the droplets from 60°C to 4°C.

Table 1. Short description of the particle compositions, sizes and tempering conditions and summary of the main results.

	Labrafac	Size	Tempering conditions	d-SAXS (Å)	Melting T (°C)
CB based nanoparticles	+	200 nm	21°C	45.8	25.0
	+		31°C	44.6	-
	-	214 nm	21°C	45.0	25.5
	-		31°C	45.4	-
	+	290 nm	21°C	44.6	26.0
	+		31°C	44.6	-
	-	312 nm	21°C	44.4	-
	-		31°C	44.4	-
FCB based nanoparticles	+	199 nm	21°C	48.7	27.0
	+		31°C	45.0	-
	-	187 nm	21°C	49.4	26.1
	-		31°C	49.7	-
	+	280 nm	21°C	45.0	27.2
	+		31°C	44.8	-
	-	340 nm	21°C	45.0	-
	-		31°C	45.4	-

References:

[1] M. Ouattara, V. Faivre, D. Kalnin and M. Ollivon; Multiple fractionation of cocoa butter for pharmaceutical and food applications; in preparation

[2] G. Keller, F. Lavigne, L. Forte, K. Andrieux, M. Dahim, C. Loisel, M. Ollivon, C. Bourgaux and P. Lesieur; DSC and X-ray diffraction coupling : specifications and applications. J. Therm. Anal., 51, 783-791 (1998).

STRUCTURAL ELUCIDATION OF LIGHT-ACTIVATED LIPOSOMES

L. Paasonen[1], M. Yliperttula[1], A. Yaghmur[2,3], M. Rappolt[2], A. Urtti[1]

1.) Centre for Drug Research, University of Helsinki, Helsinki, Finland
2.) Institute of Biophysics and Nanosystems Research (IBN), Austrian Academy of Sciences, Graz, Austria
3.) Present address: Department of Pharmaceutics and Analytical Chemistry, Faculty of Pharmaceutical Sciences, University of Copenhagen, Universitetsparken 2, DK-2100 Copenhagen, Denmark

Liposomal formulations are well known as attractive candidates for forming drug delivery systems and for targeting [1]. For some medical indications, it would be beneficial to trigger the drug release at specified times and sites of the body [2]. In this context, there is an intriguing approach based on light activation of the drug release from lipid liposomes, in which small gold nanoparticles are embedded in the liposomal bilayer [2]. In principle, the applied light energy is absorbed by the nanoparticles and then released as heat to the surrounding lipid/water system thereby causing drug release through the molten lipid bilayers. In these liposomal formulations, the localization of the small nanoparticles is playing an important role and it could be found in one of the following compartments: A) the hydrophobic internal region of the bilayer, B) the internal core (or pool), or C) the water-lipid bilayer interfacial area (see Fig. 1).

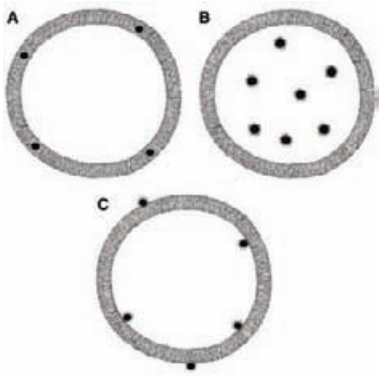

Figure 1: Schematic representation of the localization of different types of gold nanoparticle-functionalized liposomes: (A) hydrophobic small nanoparticles in the hydrophobic region of the lipid bilayer, (B) anionic hydrophilic nanoparticles in the liposome core, and (C) nanoparticles in the water-lipid bilayer interface (this figure is taken from [2]).

In a recent study at Elettra. We carried out both static and time-resolved investigations on different gold nanoparticle-functionalized liposomes. The static investigations were be helpful to understand the effect of loading different gold nanoparticle on the lipid bilayers, whereas the time-resolved studies demonstrated the importance to explore the light-induced structural changes and the behavior of the lipid bilayer. The obtained results are not shown in this contribution because we need more time for the data analysis.

References:

[1] P. Couvreur, C. Vauthier; Pharm. Res. 23, 1417 (2006)
[2] L. Paasonen, T. Laaksonen, C. Johans, M. Yliperttula, K. Kontturi, A. Urtti; J. Control. Release 122, 86 (2007)

STRUCTURE OF NEW PEGYLATED NANOPARTICLES OF GEMCITABINE SQUALENE AND EVALUATION OF INTERACTION BETWEEN GEMCITABINE SQUALENE NANOPARTICLES AND PHOSPHOLIPID BILAYERS

B. Pili[1], C. Bourgaux[1], H. Amenitsch[2] and M. Ollivon[1]

1.) Univ .Paris-sud XI, Faculté de Pharmacie, UMR CNRS 8612, Châtenay-Malabry, France
2.) Austrian Academy of Sciences, Institute of Biophysics and Nanosystems Research, Graz, Austria

Introduction

Squalenoyl gemcitabine (SqGem) is a new molecule obtained by the coupling of gemcitabine, a nucleoside analogue with antineoplastic activity, with squalene, a precursor in the biosynthesis of sterols. SqGem is a prodrug able to protect gemcitabine from its rapid metabolic inactivation. It exhibits greater anticancer activity than free molecule in vitro in human cancer cells and, in vivo, in experimental leukemia [1]. SqGem molecules spontaneously form nanoassemblies (NAs) of about 130 nm in water. Previous synchrotron studies have demonstrated that the pro-drug is packed in an inverted hexagonal phase [2]. The covalent coupling of poly(ethylene glycol) (PEG) at the surface of nanoparticles is a known strategy to reduce their opsonisation and blood clearance. Newly synthesized squalene-PEG (SqPEG) was used for PEGylation of SqGem NAs. A single population of NAs with an efficiently incorporation of SqPEG, as shown by size distribution analysis and by radioactivity measurements, has been obtained by co-nanoprecipitation. The SqGem-SqPEG NAs displayed a higher cytotoxic effect on a resistant leukemic cell line (L1210 10K) compared to that of both SqGem NAs (~ 3 fold) and Gemcitabine free (~ 6.4 fold) [3]. The first aim of this project was to determine the supramolecular organization of SqGem–SqPEG NAs and to investigate the influence of increasing amounts of SqPEG on their structure. We have also studied the effect of SqGem NAs on phospholipidic bilayers in excess of water, as a model of biomembrane.

Experimental methods

DPPC (1,2–dipalmitoyl–sn–3- phosphatidylcholine) was purchased from Avanti Polar Lipids (purity 99%), Squalene from Fluka (purity 97%) and Gemcitabine·HCl from Sequoia Research Products. SqGem and SqPEG were synthesized in our laboratory.

SqGem NAs and SqGem-SqPEG NAs were prepared by co-nanoprecipitation [1-3] in order to obtain the following ratio SqGem : SqPEG (w/w) 1:0.1; 1:0.3; 1:0.5 and a SqGem final concentration of 4mg ml^{-1}. Aliquots of the NAs were ultracentrifuged and the sediment phase was placed into quarzt capillaries. Then, 150µL of SqGem NAs were used for hydrating in excess DPPC bilayers. The structural properties of PEGylated nanoassemblies and the interaction of SqGem NAs with DPPC bilayers were examined on the SAXS beamline of Elettra synchrotron using the Differential Scanning Calorimeter (Microcalix) as a sample holder. It allows X-ray diffraction patterns to be recorded as a function of temperature [4].

Results

Three Bragg reflections were observed in the SAXS pattern of SqGem –SqPEG 1:0.1 and 1:0.3 at 20°C (Fig.1). The q values are spaced in the ratio 1 : √3 : 2, indicating the formation of an hexagonal phase; the supramolecular organization is the same as that of SqGem NAs. However, the peaks appear broader and their intensity was decreased compared to SqGem NAs. These effects may be due to disorder induced by PEG. At higher SqPEG concentrations (ratio of 1:0.5) the SAXS patterns showed a very broad bump revealing that the long-range positional order is no longer preserved.

The influence of the temperature (4°C, 20°C and 37°C) on the supramolecular structure of SqGem:SqPEG 1:0.3 NAs has also been investigated (Fig.2). The SAXS patterns exhibit the three Bragg reflections of an hexagonal phase, for the two lower temperatures (4°C and 20°C), and a broad bump at 37°C. This evolution indicates the instability of PEG-NAs as a function of temperature.

Finally, fully hydrated DPPC bilayers have been incubated during 5 days at room temperature in the presence of SqGem NAs. The SAXS pattern of the mixture SqGem NAs/DPPC, recorded at 20°C, shows a lamellar phase strongly perturbed, as indicated by the presence of a shoulder at q~0.09 (Fig.3). It is interesting to compare this pattern with that of SqGem / DPPC mixtures, previously characterized at SAXS Elettra beamline, demonstrating that SqGem was able to induce the formation of a bicontinuous cubic phase in DPPC membranes. This pattern appears similar to that of SqGem/ DPPC at molar ratio 0.045 (Fig 3). This suggests a release of SqGem molecules by the NAs and a progressive uptake of these molecules by the fully hydrated phospholipid bilayers.

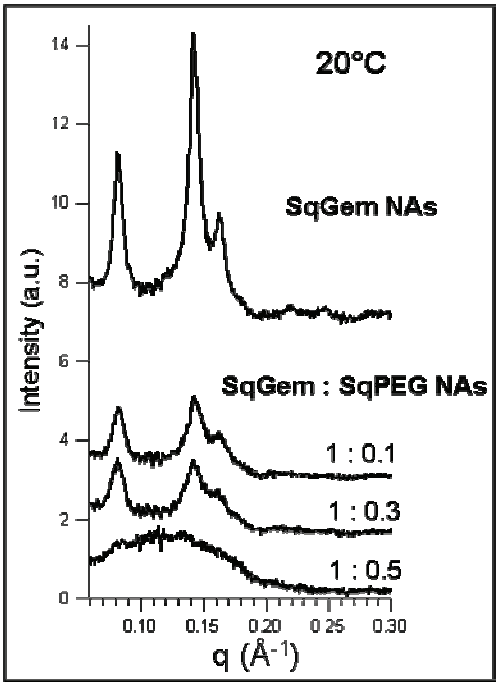

Figure 1. SAXS patterns of SqGem:SqPEG NAs at 1:0.1, 1:0.3, 1:0.5 ratios

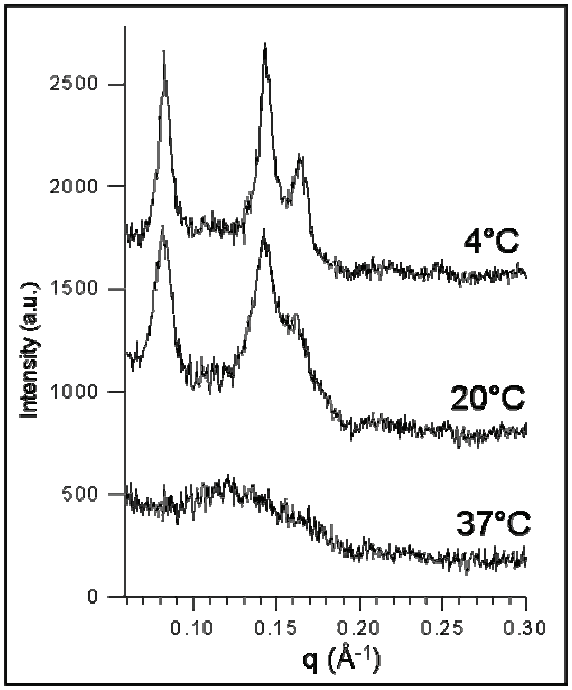

Figure 2. SAXS pattern of SqGem:SqPEG NAs 1:0.3 as a function of temperature.

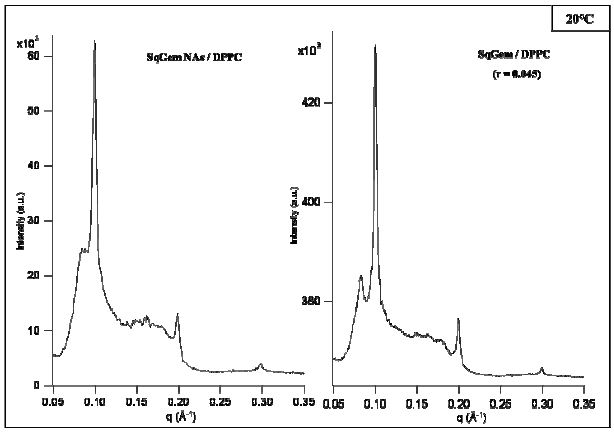

Figure 3. Comparison between the pattern of SqGem: DPPC mixture (r= 0.045) and that of DPPC incubated with SqGem NAs.

Conclusions

The pegylation of SqGem NAs allows to preserve their internal hexagonal organization for ratio < 0.5 but these NAs are strongly influenced by temperature.

The SqGem NAs release progressively the pro-drug that can interact with phospholipidic bilayers and induce the formation of bicontinuous cubic phases in DPPC membranes.

References

[1] P.Couvreur et al; Squalenoyl nanomedicines as potential therapeutics; NanoLetters, 6(11), 2544-2548 (2006).

[2] P.Couvreur et al; Discovery of new hexagonal supramolecular nanostructures formed by squalenoylation of an anticancer nucleoside analogue; Small 4(2), 247-253 (2008)

[3] F. Bekkara-Aounallah et al; Novel PEGylated nanoassemblies made of self-assembled Squalenoyl nucleoside analogues; Adv. Funct. Mater. 18, 3715-3725 (2008)

[4] M. Ollivon et al; DSC and high resolution X-ray diffraction coupling; J. Thermal Anal. and Calor. 85, 219–224 (2006).

SMALL ANGLE X-RAY SCATTERING ON POLYPLEXES

A. Subrizi[1], M. Yliperttula[1], A. Yaghmur[2,3], M. Rappolt[2], A. Urtti[1]

1.) Centre for Drug Research, University of Helsinki, Helsinki, Finland
2.) Institute of Biophysics and Nanosystems Research (IBN), Austrian Academy of Sciences, Graz, Austria
3.) Present address: Department of Pharmaceutics and Analytical Chemistry, Faculty of Pharmaceutical Sciences, University of Copenhagen, Universitetsparken 2, DK-2100 Copenhagen, Denmark

This report describes the self-assembled nanostructures of three different plasmid DNA-cationic polymer complexes: DNA-polyethyleneimine (PEI, 25 kDA), DNA-polyethyleneimine (PEI, 2 kDA), and DNA-poly-L-lysine (PLL, 200 kDA). The present study was undertaken to characterize these attractive systems as nanocarriers in medicine [1;2] by using synchrotron small-angle X-ray scattering (SAXS), and to address also the structural differences that could have an impact on the in-vitro and the in-vivo behavior of these complexes.

The SAXS investigations were carried out on pellets at three different temperatures (10, 25, and 37 °C): the DNA-polymer complexes were centrifuged for an hour at 13000 rpm and thereafter the excess of water was removed. All samples are characterized by a single broad peak at s-value in the range of 0.037-0.041 $Å^{-1}$. Thus the calculated d spacing of these complexes is the range of 24-26 Å (see example given in Figure 1). The parameter FWHM (the full widths at half-maximum of the observed beak) allows estimating the number of repeat units in the crystallites by applying the Scherrer formula, i.e. N = 1/{(FWHM measured - FWHM of our instrument)*d-spacing}. We found that this number is low in all investigated samples: it is in the range of 5-11 repeat units. The crystallite size of these complexes is in the range of 120-260 Å (it is approx. equal to N*d-spacing, N is number of repeat units in the crystallite). The crystallinity has also been judged qualitatively only by calculating the following ratio: (Peak height)/(Imax). Comparison of the calculated ratios in the three complexes clearly indicates that the DNA-PLL complexes shows approx 9-13 times lower crystallinity than the two DNA-PEI complexes. The highest crystallinity was observed in the DNA-PEI complex formed from the interaction of DNA with PEI consisting of 2 kDA.

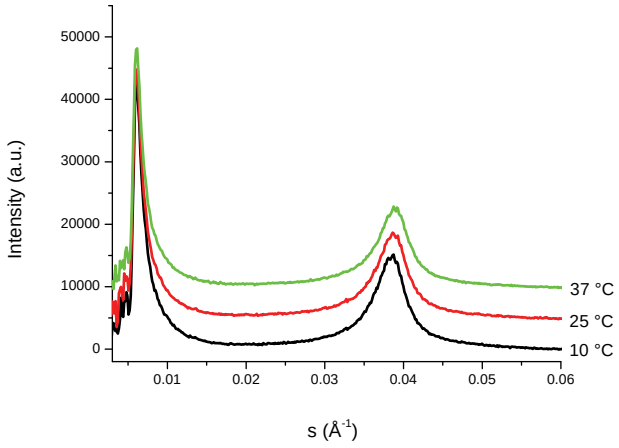

Figure 1. The scattering curves of DNA-polyethyleneimine (PEI, 2 kDA, n/p 8) complex at three different temperatures: 10, 25, and 37 °C. The intensities were shifted by a constant arbitrary factor for better visibility.

References:

[1] M. Männistö, S. Rönkkö, M. Mättö, P. Honkakoski, M. Hyttinen, J. Pelkonen and A. Urtti; The role of cell cycle on polyplex-mediated gene transfer into a retinal pigment epithelial cell line; J. Gene Med. 7, 466-476 (2005)

[2] M. Hornof, M. de la Fuenta, M. Hallikainen, R.H. Tammi and A. Urtti; Low molecular weight hyaluronan shielding of DNA/PEI polyplexes facilitates CD44 receptor mediated uptake in human corneal epithelial cells; J. Gene Med. 10, 70-80 (2008)

THE EFFECTS OF PRESSURE AND TEMPERATURE ON THE SELF-ASSEMBLED FULLY HYDRATED NANOSTRUCTURES OF MONOOLEIN-OIL SYSTEMS

Anan Yaghmur[*1,2], Manfred Kriechbaum[1], Heinz Amenitsch[1], Miloš Steinhart[3], Peter Laggner[1], Michael Rappolt[1]

1.) Institute of Biophysics and Nanosystems Research (IBN), Austrian Academy of Sciences, Graz, Austria
2.) Present address: Department of Pharmaceutics and Analytical Chemistry, Faculty of Pharmaceutical Sciences, University of Copenhagen, Universitetsparken 2, DK-2100 Copenhagen, Denmark
3.) Institute of Macromolecular Chemistry, Academy of Sciences of the Czech Republic, Prague, Czech Republic

In the present study, our main objective is to investigate the effect of pressure variation on the stability of either Fd3m or H_2 phases under high pressure conditions and to explore their pressure- and temperature-dependent phase behaviors. In this context, the pressure-temperature effects on oil-loaded Fd3m phase are interesting since few experimental studies have been carried out to date on the pressure- and temperature- dependence of this phase [1;2]. An investigation of the impact of pressure on such an oil-loaded discontinuous cubic phase should lead to an improved understanding on its destabilization at high pressures. We used the high hydrostatic pressure synchrotron small-angle X-ray scattering (SAXS) cell for studying the pressure-induced structural transitions in two fully hydrated MO/tetradecane (TC)/water systems at fixed MO/TC weight ratios of 7/3 (sample A) and 6/4 (sample B), respectively.

Figure 1a shows the typical structural transitions observed for sample A at 20 °C as pressure increases in the range of 1-1200 bars. At 1 bar, the self-assembled Fd3m phase is identified by recoding at least the first 9 reflections. Following the pressure increase up to 800 bar, the Fd3m structure is retained but the set of the observed peaks shift to low q values indicating an increase in the lattice parameter. At 900 bar, the ternary system displays the two liquid crystalline phases: Fd3m and H_2 nanostructures. The lattice parameter strongly increases from 230.4 to 241.7 Å as the pressure varies in the range of 1-900 bar. Up to 900 bar, the response of the lattice parameter to pressure is linear and the $(\partial a/\partial P)T$ has a value of approximately 13.3 Å $kbar^{-1}$. On further compressing of the sample, the Fd3m phase vanishes and a direct structural transition induces to form pure H_2 phase. We witness also a linear variation of the H_2 lattice parameter upon increasing pressure indicating most probably an increase in the order of the lipid and oil acyl chains (denser chain packing) and an enhancement of swelling water from surrounding excess water. For H_2, the lattice parameter lies in the range of 62.0-65.1 Å and the isothermal change, $(\partial a/\partial P)T$, has a value of approximately 10.3 Å $kbar^{-1}$. Our results reveal that the impact of pressure on Fd3m nanostructure is slightly greater than that observed for the H_2 phase. The effect of pressure variation on the nanostructure of sample A was studied also at 7 °C (Figure 1b). It should be noted that decreasing temperature allows the occurrence of Fd3m → H_2 structural transition at lower pressure values and could lead at relatively higher pressures to the formation of V2 nanostructures. We found indeed as illustrated in Figure 1b that the pressure increase in the range of 1-750 bar induces the Fd3m → H_2 → Pn3m structural transition at lower pressures values.

It is surprising that at higher pressures (above 800 bar in Figure 1a, and at 350 bar in Figure 1b), we witness the appearance of an additional peak at q value of approximately 0.3465 nm^{-1} (a peak marked with * having a d-spacing value of approximately 18.1 Å), which is independent of the pressure variation. This distinct peak disappears during the pressure-cycling as the pressure value reduces to less than 900 bar in the reverse cycle. A possible

explanation for the observation of this peak could be related to the pressure-induced ordering of the TC molecules. It is most likely that part of the alkane molecules begin to crystallize at high pressures and to form probably triclinic structure. This claim is supported by the fact that the d-spacing value of this peak corresponds closely to that of the (001) reflection in the pure triclinic TC crystal as previously reported [3;4].

Further results and experimental details will be published elsewhere (manuscript in preparation). In summary, our present results suggest that heating the oil-loaded samples extends the H_2 and the Fd3m regions. Conversely, compressing the samples enhances the acyl chain stretching and decreases the effective hydrophobic chain volume of the investigated lipid. This explains the tendency to form V_2 and even the more flattened phase, Lα, at high pressures.

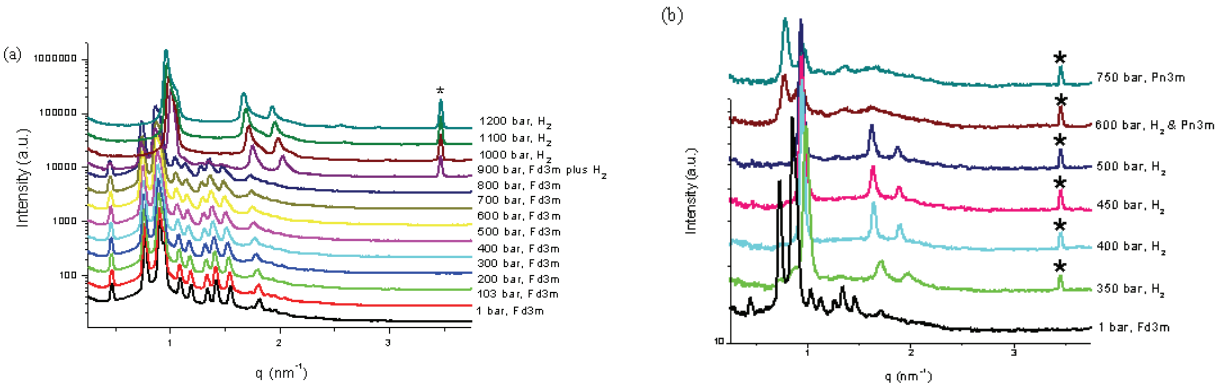

Figure 1: Effect of isothermal changes on modulating the fully hydrated nanostructure of sample A: (a) at 20°C and the pressure value increases in the range of 1-1200 bars. (b) At 7°C and the pressure value increases in the range of 1-750 bars.

References:

[1] S.S. Duesing, J.M. Seddon, R.H. Templer and D.A. Mannock; Pressure Effects on Lamellar and Inverse Curved Phases of Fully Hydrated Dialkyl Phosphatidylethanolamines and β-d-Xylopyranosyl-sn-glycerols; Langmuir 33, 2655-2664 (1997).

[2] A. Yaghmur, L. de Campo, L. Sagalowicz, M.E. Leser and O. Glatter; Emulsified microemulsions and oil-containing liquid crystalline phases; Langmuir 21, 569-577 (2005)

[3] S.C. Nyburg and J.A. Potworowski; Prediction of unit cells and atomic coordinates for the n-alkanes; Acta Cryst. B29, 347-352 (1973).

[4] E. Gilbert, P. Reynolds and J. White; Application of small-angle scattering to the study of graphite-adsorbed hydrocarbons; J. Appl. Cryst. 33, 744-748

Chemistry

IN SITU ZnO / SiO_2 VITROCERAMIC MESOPOROUS THIN FILM STUDIES USING SAXS / WAXS / ELLIPSOMETRY

J. D. Bass,[1] B. Julián-López,[2] P. Evrar,[3] C. Boissière,[1] L. Nicole,[1] C. Sanchez,[1] H. Amenitsch,[4] and D. Grosso[1*]

1.) Chimie de la Matière Condensée de Paris, UMR UPMC-CNRS 7574, Université Pierre et Marie Curie (Paris 6), 4 place Jussieu, Tour 54-5E, 75252 Paris 05, France
2.) Dpto. Química Inorgánica y Orgánica, Universidad Jaume I, Avda. Sos Baynat, s/n, 12071 Castellón, Spain
3.) SOPRA SA, 26, rue Pierre Joigneaux, 92270 BOIS-COLOMBES, France
4.) Institute of Biophysics and Nanosystmes Research, Austrian Academy of Sciences, Schmiedlstr. 6, A-8042 Graz, Austria

We report the formation of ZnO/SiO_2 vitroceramic (or nanocomposite) thin films composed of around 5 nm in size wurtzite ZnO semiconductor nanoparticles nucleated into glassy SiO_2 network, ordered mesoporous or dense, networks. Thin films were prepared by Chemical Solution Deposition of from TEOS and $ZnCl_2$ precursor solutions. Commercial Pluronic-type block copolymers were used as template for the Evaporation Induced Self-Assembly (EISA) to proceed during deposition, while a direct thermal treatment in air was applied to achieve the film's desired characteristics.[1,2] Dense or highly ordered mesoporous (pore size = 6nm and porousvolume = 60%) films with composition ranging from 0 to 90%mol ZnO can be processed with high optical quality. When 50%mol ZnO is used, the mesoporous films exhibit a very low refractive index of 1.17, while the nanoposity allows high accessibility to the ZnO phase. In these films, the similar intensity of the UV and visible emission bands reveals a high amount of oxygen defects making them well suited for applications in stimulated emitters, actuators, and lasing cavities. The present results are supported by original simultaneous in situ time-resolved Grazing Incident Small Angle X-ray Scattering (GISAXS) / Wide Angle X-ray Scattering (WAXS) / Thermal Ellipsometry Analysis (TEA) investigations that allow to study the kinetics of crystallisation of oxide NPs into such mesoporous amorphous matrices. The present work constitutes the first example of vitroceramic mesoporous films, while the approach can virtually be extended to most divalent metal oxide

In situ time resolved GISAWS/WAXS/Ellipsometry investigation during thermal annealing was performed exclusively on 50%mol ZnO films, at the Austrian SAXS beam line of Elettra (Trieste-Italy). The incident X-ray beam (8 KeV) was collimated into a vertical elongated rectangular shape of 400*1000µm. Small angle X-ray diffractions were collected in grazing incidence ($\omega \approx 0.25°$) on a CCD camera (Photonic) placed at a distance of 150cm from the sample, with 10s interval between frame. Wide angle diffraction signals were collected with a linear gas detector placed at 35 cm from the sample (see Figure 1). A SOPRA ellipsometer (GES5E model based on a rotating polarizer which acquires spectra of 1024 wavelengths from 250 to 1000 nm within 1s) was adjusted on the line sample environment as depicted in Figure 1. The direction of ellipsometry analysis was set to be at 90° from the direction of the X-ray analysis. Incident ellipsometer beam was adjusted at 63° to the normal of the sample surface. Variation of ellipsometer parameters were fitted using a Cauchy model suitable for transparent dielectric films. To be able to measure simultaneously the reflected depolarised light (ellipsometer) and the diffracted X-rays (GISAXS and WAXS), it is necessary that the incident X-ray beam illuminates the surface of the film just above the critical angle of penetration ($\omega \approx 0.25°$), while the reflected ellipsometer beam falls in the middle of the detector at normal incidence. These geometrical requirements have to be fulfilled during the whole heating duration of the experiment. To do so, both ellipsometer source and detector were fixed at the right position with respect to the surface of the substrate in order to follow

any movement applied to the sample during alignment with the X-ray beam. The heating was provided by a flat thermal regulated resistance onto which the sample was placed and a ramp of 40°C/min was applied. An aluminum chamber bearing apertures for the incident, the reflected and the diffracted signals to enter and escape respectively, was used to isolate the sample from the cool environment. Misalignment occurs during the thermal treatment as a result of the dilatation-induced displacement of the sample. Due to the shape of the X-ray beam, the latter displacement did not affect the irradiation of the sample, while two to three realignments of the ellipsometer detector had to be done to be able to collect the reflected visible light when heating proceeded. More details on Thermal Ellipsometry Analysis (TEA) can be found in other works dedicated to TiO_2 [3] and MgF_2 [4] porous films. SAXS, WAXS and TEA results are shown in Figure 2. All thermally induced phenomena, such as polymer thermal decomposition (TEA), SiO_2 viscous sintering (SAXS), inorganic centre dehydration (TEA), ZnO crystallisation (WAXS) (nucleation growth of ZnO wurtzite nanoparticles inside the vitreous SiO_2 mesoporous network), and finally the diffusive sintering responsible for the porosity loss (disappearance of the SAXS diffraction signal and dramatic increase of the refractive index by TEA) have been clearly identified. The present results showed that if $ZnCl_2$ is used as ZnO precursor in the initial TEOS solution, less than 5 nm in size Wurtsite nanoparticles are precipitated within the silica network after 500°C. The very high porosity is then retained up to 700°C where a dramatic vitreous transition occurs. Photoluminescent properties of this mesoporous ZnO/SiO_2 vitroceramic films have been investigated but results are presented elsewhere. It revealed that photoluminescent properties can be tuned through thermal annealing conditions.

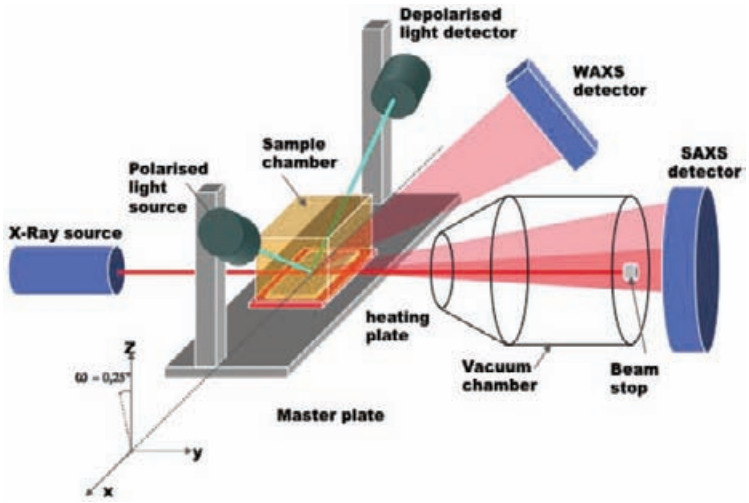

Figure 1. in situ time-resolved SAXS/WAXS/TEA set-up, assembled at the Austrian SAXS beam line of Elettra Synchrotron (Italy). Film samples have been heated under air while Ellipsometry was measuring the variation of optical density and physical thickness. Micro and nano structures evolution were simultaneously deduced from X-ray diffraction collected at wide and small angles respectively.

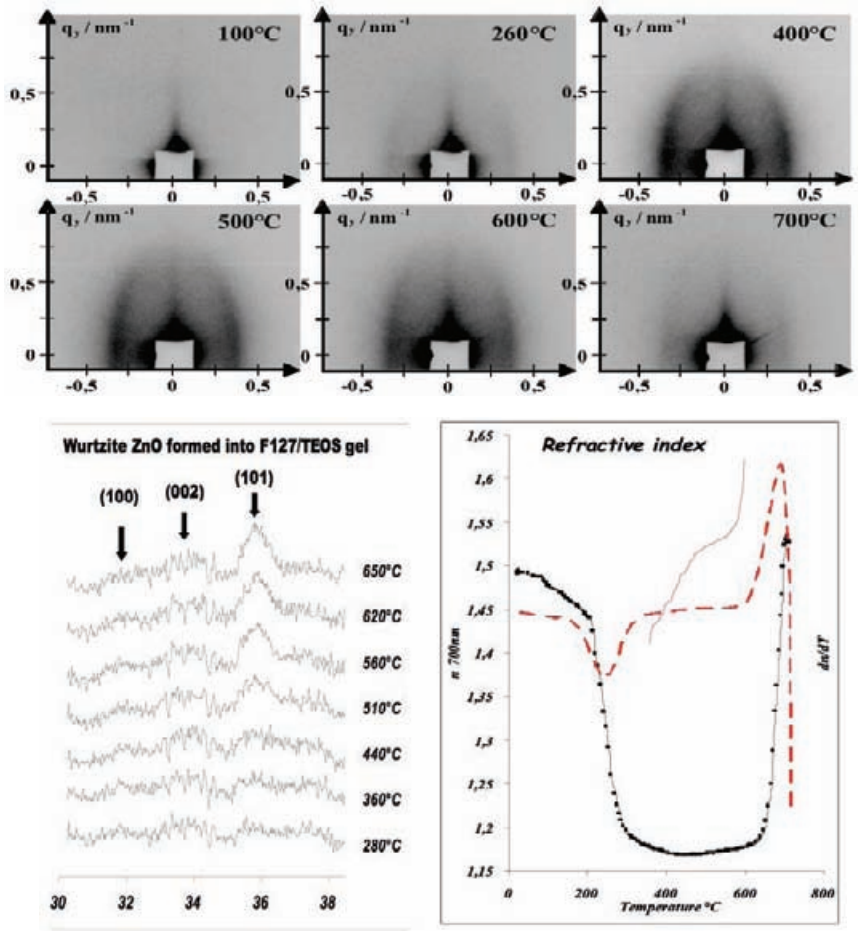

Figure 2. Evolutions of GISAXS patterns (up), WAXS diagram (down left), and refractive index (down right) with temperature during the annealing process of mesoporous SiO_2/ZnO vitroceramic films.

We have presented a simple chemical approach to mesoporous SiO_2-based vitroceramic thin films with very low refractive index, and accessible porosity. The powerful simultaneous in situ time-resolved SAXS/WAXS/TEA investigations clearly showed the influence of the structure on the thermally induced effects (e.g. crystallisation, viscous sintering, decomposition, vitreous transition…) taking place during annealing, and was very useful to understand the related formation kinetics. The latter approach is original and will then be extended to the formation of mesoporous vitroceramic spheres through aerosol generation, and open the route towards nanocrystal reach divalent metal oxide mesoporous materials under film and powder form.

References:

[1] C. Sanchez, C. Boissiere, D. Grosso, C. Laberty, L. Nicole Chem. Mater. special issue 2008, 20, 682.
[2] D. Grosso, F. Cagnol, G. J. de A. A. Soler-Illia, E. L. Crepaldi, P. A. Albouy, H. Amenitsch, A. Brunet-Bruneau, and C. Sanchez. Adv. Funct. Mater. 2004, 14, 309.
[3] J.D. Bass, D. Grosso, C. Boissière, C. Sanchez, J. Am. Chem. Soc. 2008, 130, 7882. 21
[4] J.D. Bass, C. Boissiere, L. Nicole, C. Sanchez, D. Grosso, Chem. Mater. 2008, 20, 5550.
[5] J. D. Bass, B. Julián-López, P. Evrar, C. Boissière, L. Nicole, C. Sanchez, H. Amenitsch, and D. Grosso, Adv. Funct. Mater. (submitted).

GELATION OF SILICA USING STOPPED FLOW SR-SAXS

C. Camerani[1], A. Terry[2], C. Petersen[1] and I. Jansson[1]

1.) Eka Chemicals, 445 80 Bohus, Sweden
2.) ISIS Facility, Rutherford Appleton Lab., Didcot, OX11 0QX, UK

Permeation grouting may be defined as the introduction of low viscosity gelling solutions or particulate suspensions in the ground, e.g. clean sands and gravels or permeable discontinuities in rock, without disturbing the structure of the ground. The types of grout and their material constituents are chosen such that, under relatively low injection pressures, they can flow without difficulty through the pores and fissures. The main objectives are to reduce the permeability or increase the strength and stiffness of the ground [1].

Colloidal Silica sols (CS) are small particles consisting of an amorphous SiO_2 core, which is insoluble in water. The size of the particles can be varied between 1 and 500 nm, hence they are small enough to remain suspended in the fluid medium without settling [2]. In a physical sense CS are "particle-free" and retain a Newtonian flow behaviour during grouting. Consequently, CS grouts, formed by addition of a salt ("accelerator") to CS, easily invade very thin voids. Moreover, their "clean" chemical content makes them ideal if a sustainable permeation grouting has to be obtained. Unfortunately, information about how the particle size distribution varies during coagulation and gelation in permeation grouting is lacking. This is mainly due to the difficulty of recording data at the very first reaction time with small time intervals without introducing sample artefacts.

In this project we seek to mimic the conditions during which CS are coagulated into gels after the addition of an accelerator. To investigate the cluster growth during gelation, we have used time resolved Synchrotron Radiation Small Angle X-ray Scattering (SR-SAXS) measurements. In order to fully characterise the behaviour and to really capture the very onset of gelation, a stopped flow cell was used. The parent solutions were injected directly into the measuring volume and data from the first 100's milliseconds examined. SR-SAXS measurements were performed on a colloidal system containing monodisperse single primary particles (B1). To promote gelation, the sol was mixed with NaCl.

Results

The SAXS data for B1 is fitted well to a spherical form factor, as obtained by the Fish program [3]. Using a hard sphere interaction potential, the particle diameter is found to be 7.8 nm and a relatively low polydispersity (12 %), in agreement with the SEM micrographs (see Fig.1, inset). This estimation of the polydispersity is in agreement with the Gaussian size distribution obtained by GPC technique.

The gelation of the 40 wt.% colloidal silica solution B1 was followed in the stop-flow cell with the CCD detector with the addition of a 10 wt.% NaCl salt solution in the proportion shown in Table 1. This concentration of added accelerator gave a gel time of 2280 seconds and the data collection was stopped after 2480 seconds. Figure 1 shows a sequence of plots of I(q) vs q following this process, each curve is shifted vertically and only every 5th curve (that

is every 50s) is plotted for clarity. The curve with the time nearest to the gel time is shown in bold. In Figure 1 the first curve plotted is at time t = -10 s and was collected before mixing with the salt, in the stop-flow cell. This plot clearly shows changes at time scales much shorter than the nominal gelation time. The initial maximum observed which is due to interparticle interference effects at this high concentration of silica particles appears to shift to lower q only from about 500 seconds after mixing. This initially was surprising since we expect some aggregation to start almost immediately and then the whole structure to slowly grow and evolve to form the space-filling gel. From 1000 seconds, the intensity at low q rises indicating strong aggregation. It is difficult to describe thoroughly the nature of the large aggregates due to the limited q-range for our experiments. However, fitting the data around this time reveals that the structures are evolving very slowly, the average radius of the particles appearing to reduce to 7.1 nm as does the volume fraction if its constraint is released in order to achieve a better fit. It should be noted that the aggregation of the investigated colloidal silica particles during gelation appears to maintain a spherical form factor, that is spherical aggregates of 15 nm in radius are formed. It is interesting to note that even though the structure factor and size of aggregates is changing dramatically during gelation, almost no evolution of the higher q part of the scattering curve occurs above q > 4 nm^{-1}. Very little further evolution of the structure is observed within the curves.

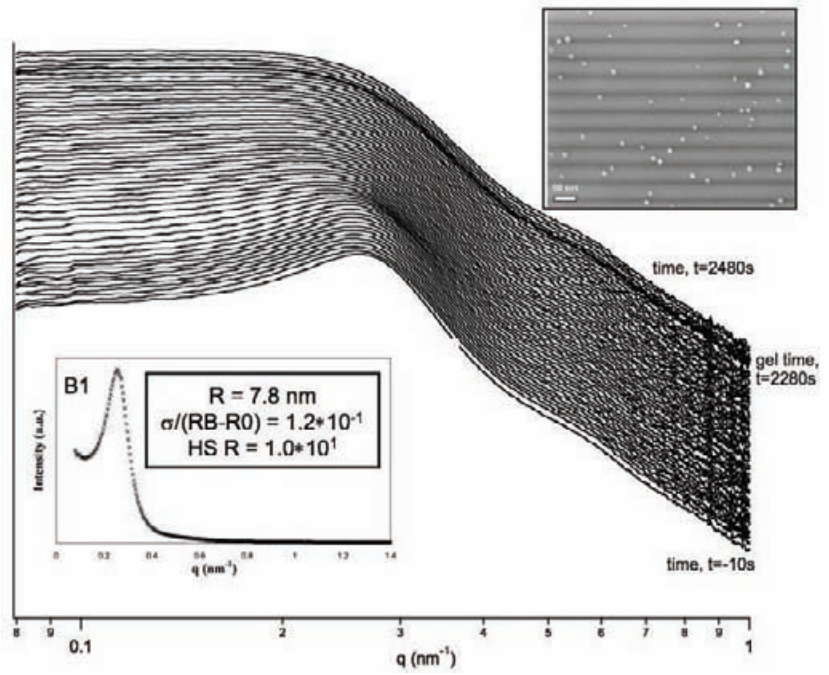

Figure 1: I(q) vs q for the gelation process in B1 upon addition of NaCl.

Table 1. Gelation time and mixing proportions of the investigated colloidal silica sol and accelerator.

Sample	Weight (g)	Gel time (min)
B1 (40% w/w SiO_2)	100	39
NaCl (10% w/w)	13	

References:

[1] S. Littlejohn; "The Development of Practice in Permeation and Compensation Grouting: A Historical Review (1802-2002) Part 1: Permeation Grouting." Grouting and Ground Treatment, Proceedings of the Third International Conference, Geotechnical Special Publication 120, New Orleans, LA, ASCE, p. 50-99 (2003)

[2] R.K. Iler; The Chemistry of Silica, Wiley, USA (1979)

[3] R Heenan; www.isis.rl.ac.uk/largescale/LOQ/FISH/instructions1.htm

GEL PHASE BEHAVIOUR OF MIXED NONIONIC BLOCK COPOLYMERS AND ANIONIC SURFACTANTS

I. W. Hamley[1], V. Castelletto[1], B. M. O'Driscoll[1], C. Chaibundit[2] and H. Amenitsch[3]

1.) Dept of Chemistry, University of Reading, Whiteknights, Reading RG6 1EU, UK
2.) Polymer Science Program, Faculty of Science, Prince of Songkla University, Hat Yai, Songkhla, 90112, Thailand
3.) Austrian Acad Sci, Inst Biophys & Nanosyst Res, A-8042 Graz, Austria

Triblock copolymers of type $E_mP_nE_m$, in which hydrophilic poly(ethylene oxide) is combined with hydrophobic poly(propylene oxide), are widely available commercially from a number of suppliers and cover a wide range of block lengths and compositions. We use the notation E = oxyethylene, OCH_2CH_2, P = oxypropylene, $OCH_2CH(CH_3)$, and subscripts m and n to denote number-average block lengths in repeat units. For convenience we also use the commercial notation of the Pluronic Grid [1] .In many applications these copolymers are used in mixtures with anionic or cationic surfactants: e.g. sodium dodecyl sulphate (SDS) or hexadecyl(cetyl)-trimethylammonium bromide (CTAB). We focused attention on two copolymers of these copolymers, F127 and P123 (Pluronic notation, nominal compositions $E_{98}P_{67}E_{98}$ and $E_{21}P_{67}E_{21}$) in mixtures with SDS [2].

SAXS experiments were performed on beamline A-2 of DESY, Hamburg, Germany and on beamline BL5.2L of ELETTRA, Trieste, Italy. The x-ray wavelength on both beamlines was 1.5 Å. At DESY, the sample-detector distance was 2.2 m, data were collected with a linear detector (M.Braun). Samples were placed in copper cell in an electrically heated sample holder, sandwiched between kapton windows. The sample holder was placed in vacuum in the beamline. At ELETTRA, the sample-detector distance was 2 m, data were collected on a Mar image plate system and subsequently reduced to one-dimensional form. The sample was mounted in a brass liquid cell, between mica windows within a Teflon O-ring. The liquid cell was connected to a water bath for temperature control. At DESY, the q scale was calibrated with collagen (rat tail tendon) and silver behenate, and at ELETTRA it was calibrated with silver behenate.

Examples of SAXS profiles from the gels are shown in Figure 1. The high intensity of the first-order peak of the 50 wt% gel may well be caused by orientation of this very-high-modulus gel during mounting in the sample holder: a similar effect was noted with certain the high-modulus SDS/P123 gels. For all SDS/F127 gels examined values of q/q^* were in sequence $1 : 2 : \sqrt{3}$, consistent with body-centred cubic (bcc) structures. The face-centred cubic (fcc) structure recorded recently for our sample of F127 in water is consistent with recent observations on as-received F127 by Mortensen et al [3]. while the body-centred cubic (bcc) structures found for the SDS/F127 gels conform with previous reports of cubic structures for SDS/F127 gels [4]. Values of q at the first order refraction (q^*) and of the d-spacing (calculated as $d = 2\pi/q^*$) are listed in the Table 1, together with the gel structures.

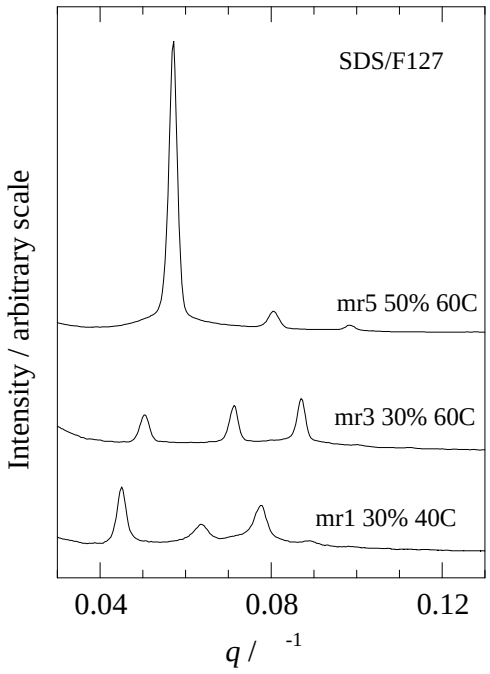

Figure 1. SAXS profiles for SDS/P123/water gels. Values of mole ratio [SDS]/[F127] (mr), wt% solute, and temperature (°C) are indicated. Intensity scales and zeros are arbitrary.

Table 1. SAXS: Structure and Spacings for SDS/F127/water Gels.

[SDS]/[F127]	wt% solute	*T* / °C	Structure	*q** / Å^{-1}	*d* / Å
mr = 0[a]	30	25	fcc	0.0390	161
mr = 1	30	40	bcc	0.0448	140
mr = 3	30	40	bcc	0.0512	123
		60	bcc	0.0504	125
mr = 5	50	60	bcc	0.0569	110

a Data from ref. 24.

References:

(1) Hamley, I. W. Block Copolymers in Solution; Wiley: Chichester, 2005.
(2) Chaibundit, C.; Ricardo, N. M. P. S.; Ricardo, N. M. P. S. et al. in preparation 2009.
(3) Mortensen, K.; Batsberg, W.; Hvidt, S. Macromolecules 2008, 41, 1720.
(4) Hecht, E.; Mortensen, K.; Gradzielski, M.; Hoffmann, H. J. Phys. Chem. 1995, 99, 4866; Ivanova, R.; Lindman, B.; Alexandridis, P. Coll. Surf. A 2001, 183-185, 41.

A NEW LEVEL OF HIERARCHICAL STRUCTURE CONTROL BY USE OF SUPRAMOLECULAR SELF-ASSEMBLED DENDRONIZED BLOCK COPOLYMERS

Chaoxu Li[1], A. Dieter Schlüter[2], Afang Zhang[2]* and Raffaele Mezzenga[1,3]*

1.) Department of Physics and Fribourg Center for Nanomaterials, University of Fribourg, Ch. du Musée 3, CH-1700 Fribourg, Switzerland.
2.) Laboratory for Polymer Chemistry, Department of Materials, ETH-Zurich, HCI J 541, CH-8093 Zurich, Switzerland
3.) Néstlé Research Center, Vers-Chez-Les-Blanc, 1000 Lausanne 26, Switzerland

The design of self-assembled materials with complex three dimensional structures is virtually infinite when constructing units such as mesogens, polymers and colloidal particles of varying length scales are brought together. Typically, block copolymers in which microphase segregation between two chemically incompatible blocks can be combined with supramolecular attachment of side chains or mesogens to one block, constitute very appealing systems to design hierarchically self-assembled macromolecular materials.[1-2] Self-organization of these systems is achieved typically at two length scales: that of the side chains (~10^0nm) and that of the block copolymers (~10^1-10^2nm). Advanced materials with tuneable nanoporosity, switchable conductivity and photonic properties have successfully been prepared using diblock copolymers in which one block is inert, while the other is supramolecularly "hosting" side chain surfactants via either hydrogen bonding or electrostatic binding. However, due to the linear nature of the supramolecular active blocks, the only possibility to control the structure at small length scales is the variation of the type of surfactants or mesogens supramolecularly attached, with the result of observing essentially lamellar phases at these length scales.

Here we demonstrate that by replacing the linear polymer block with a dendronized polymer capable of participating in supramolecular interactions, one additional degree of freedom (the generation of the dendronized polymer) is introduced to engineer the self-assembly into unprecedented hierarchically ordered bulk structures. Not only this allows controlling beyond current possibilities the structures at the smaller length scale, with the introduction for example, of new columnar rectangular, hexagonal and tetragonal phases, but it may also lead to new functional template materials with increased 3D topological complexity for advanced technologies.

The chemical structures of the dendronized block copolymers used was shown in Figure 1, in which one block is a dendronized polymer attached supramolecularly by various length of alkyl tails, while the other is a spacer block which can further act as a stimuli responsive polymer. Typically, Figure 2 shows the SAXS/WAXS profiles of the 2nd generation dendronized block copolymers, in which the inert block is a low glass transition temperature (-27.1°C) poly(methoxy diethylene glycol methacrylate) (PMeDEG). The WAXS reflections suggested the liquid crystalline structures at the length scale 10^0~10^1 nm could vary among the columnar rectangular, tetragonal, hexagonal phases and the lamellar phase if both the generation of the dendronized block and the alkyl tail length were precisely controlled. No reflections at the accessible lower q region appear in the SAXS profile, possibly due to the overlap with the x-rays detector beamstop, settled at corresponding real space length scales

larger than 58 nm. Figure 3 gives gives TEM micrographs of the microstructure of some selected combinations of alkyl tails, dendronized polymers and spacer blocks. Each individual image illustrates the large length scale structures observed at low magnification, while each inset is a zoom up of the corresponding liquid crystalline structure observed at low length scale and high magnification within the segregated dendronized blocks (inset edge represents 55 nm). Clearly, the lipid columns or lamellae appear to orient normally to microphase segregated domain interfaces, irrespective of the liquid crystalline structure considered.

In summary, we have presented a new general approach to the hierarchical self-assembly of block copolymers (Figure 4) in which substituting the conventional linear supramolacular active block with dendronized polymers gives rise to increased topological complexities and morphologies not otherwise accessible with linear block copolymers.

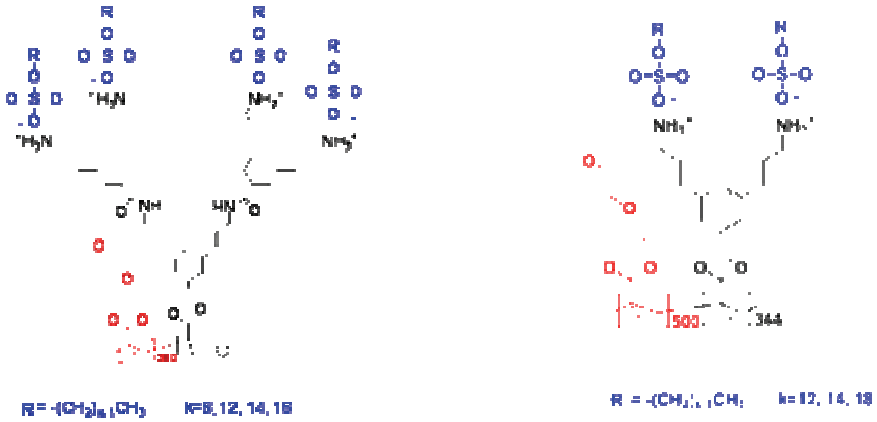

Figure 1. Chemical structures of the dendronized block copolymers complexed with sulfate alkyl tails.

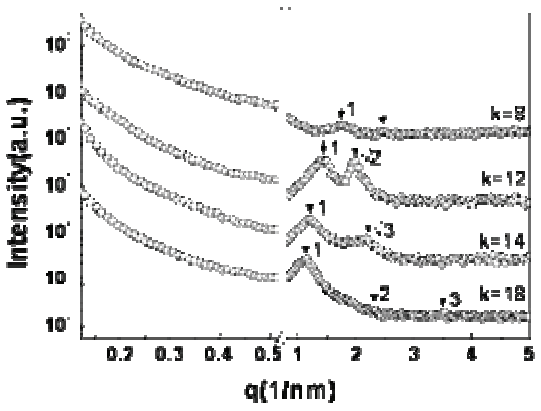

Figure 2. SWAXS profiles of the dendronized block copolymers complexed with sulfate alkyl tails: $PMeDEG_{380}PG2_{32}$-SO_4C_k complex.

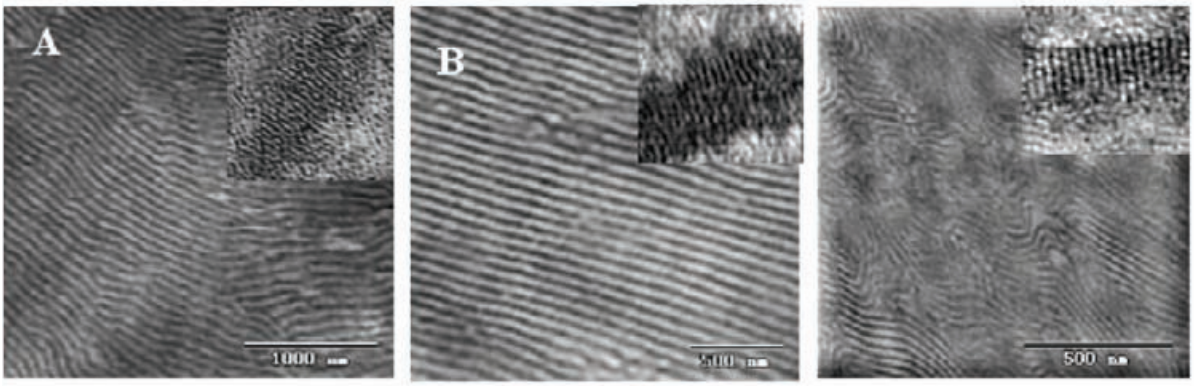

Figure 3. TEM images of dendronized block copolymers complexed with sulfate alkyl tails. a) Columnar tetragonal-within-lamellar structure, b) columnar hexagonal-within-lamellar structure, c), lamellar-within-lamellar structure.

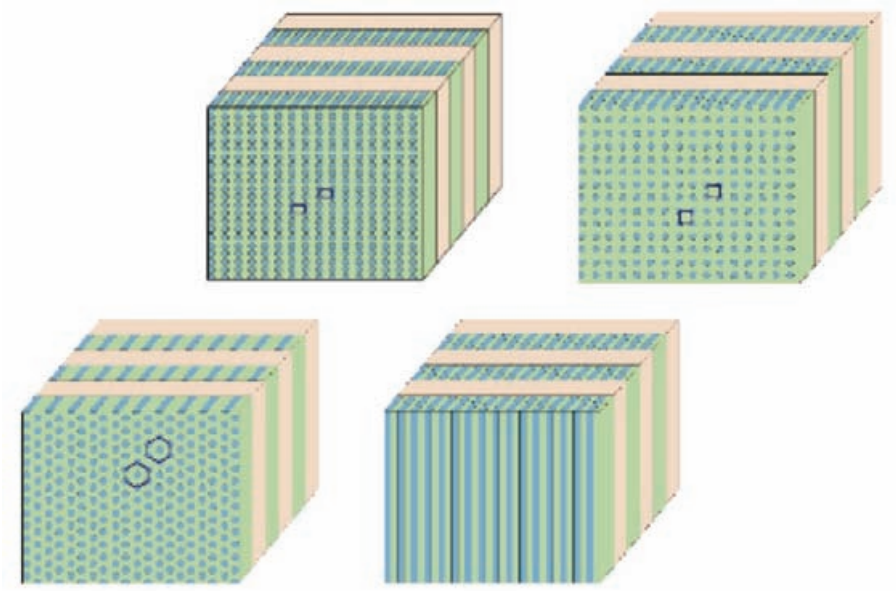

Figure 4. Schematic representation of hierarchical nanostructures obtained by self-assembly of sulfate alkyl tails:dendronized block copolymers complexes. Relative domains orientation of rectangular within-lamellar, tetragonal-within-lamellar, hexagonal-within-lamellar and lamellar-within-lamellar structures.

References:

M. R. Hammond, R. Mezzenga, Supramolecular routes towards liquid crystalline side-chain polymers. Soft Matter 4, 952-961 (2008).

O. Ikkala, G. ten Brink, Functional materials based on self-assembly of polymeric supramolecules. Science 295, 2407-2409 (2002).

CONFINED GROWTH OF IRON COBALT NANOCRYSTALS IN MESOPOROUS SILICA THIN FILMS: FeCo–SiO_2 NANOCOMPOSITES

L. Malfatti[1], S. Costacurta[1], A. Masili[2], A.Corrias[2], M. F. Casula[2], H. Amenitsch[3] and P. Innocenzi[1]

1.) Laboratorio di Scienza dei Materiali e Nanotecnologie, Dipartimento di Architettura e Pianificazione, Universita` di Sassari, CR-INSTM,Palazzo Pou Salid, Piazza Duomo 6, 07041 Alghero (Sassari), Italy
2.) Dipartimento di Scienze Chimiche and INSTM, Universita` di Cagliari, 09042 Cagliari, Italy
3.) Institute of Biophysics and Nanosystems Structure Research, Austrian Academy of Sciences, Schmiedlstraße 6, A-8042 Graz, Austria

Introduction

Bulk FeCo alloys are soft ferromagnets whose magnetic properties have been widely investigated owing to their technological importance; the major field of application of FeCo alloys is in the technology of transformer cores and electrical generators. To avoid agglomeration and coalescence between the iron–cobalt nanoparticles, they are usually incorporated into a coating, but an alternative approach lies in embedding the iron–cobalt nanoparticles in an insulating matrix, which acts as a dispersing medium. Sol–gel processing is very suitable for the preparation of such nanocomposites as it offers unique advantages in terms of compositional homogeneity, dispersion of the nanophase within the matrix and purity of the resulting material. We have obtained FeCo–SiO_2 nanocomposites using the mesopores of self-assembled mesoporous thin films as hosts and template for the growth of FeCo alloy nanoparticles. Mesoporous silica films show high resistance to thermal treatments even at high temperatures. In a previous work, we have observed that in block copolymer-templated mesoporous silica films the mesophase is maintained even at temperatures higher than 800 °C [1]. This property makes the mesoporous films an interesting host material for nanoparticles whose preparation requires high temperatures. Furthermore, mesoporous films fulfill the requirement of having good chemical stability to undergo an impregnation process, which is an intermediate step to the synthesis of several types of nanoparticles.
This synthetic approach represents a method for obtaining magnetic nanocomposites in the form of thin films, which is desirable for perspective integration in technological devices: tuning the magnetic properties of the nanocrystals can be accomplished by selecting the mesopore size of the host mesoporous matrix, which in turn can be achieved by using a suitable templating agent.

Results and discussion

We have prepared mesoporous silica films using two block-copolymers (Pluronic F68 and Pluronic F127) in order to obtain different types of porous phases in the samples after thermal treatment at 350 °C. Iron cobalt-mesoporous silica nanocomposites were prepared by impregnation of the silica mesoporous films with a precursor solution containing $Fe(NO_3)_3$ and $Co(NO_3)_2$, followed by heat treatment at 600 °C under a H_2 flow. Standard powder diffractometer was used to gather a first indication on the formation of FeCo nanocrystals by collecting patterns at wide angles (WA-XRD).
Figure 1 shows the WA-XRD patterns indicating that in both FeCo-F68 and FeCo-F127 nanocomposites a peak around 44° is present, corresponding to the most intense peak of *bcc* FeCo due to the (110) reflection. The lattice parameter determined from the 110 peak position is 0.286 nm, which is in good agreement with the lattice parameter for bulk $Fe_{70}Co_{30}$ alloy [2].

To determine the symmetry group of the mesostructured matrixes, a detailed characterization of the ordered porosity was performed by collecting two-dimensional GISAXS patterns. Silica films prepared with Pluronic F68 as the templating agent prior to impregnation and reduction gave GISAXS patterns presenting well-defined spots and no ring, indicating a high degree of order of the mesostructure within the film (Figure 2a). The patterns were assigned to a cubic symmetry mesostructure (body-centered cubic, space group *Im*-3*m*) with the (110) plane oriented perpendicular to the substrate (z direction), uniaxially distorted. GISAXS pattern of Figure 2b, referred to a film templated by Pluronic F68 that was impregnated with the Fe/Co solution and subsequently reduced at 600 °C, showed that no mesostructure symmetry change occurred upon impregnation. From this analysis, the cell parameters were estimated as $d_{110,x}$ = (14.1 ± 1.4) nm and $d_{110,z}$ = (7.1 ± 0.7) nm. The in-plane cell constant $d_{110,x}$ is substantially unaltered, whereas the out-of-plane cell constant $d_{110,z}$ is smaller in impregnated films treated at 600 °C. Films templated by Pluronic F127 have a two-dimensional hexagonal *p6mm* symmetry composed of ordered arrays of tubular micelles with hexagonal cross section [3] (Figure 2c and d). The presence of a distorted ring intersecting the spots indicates either that a wormlike region coexists with the ordered hexagonal mesophase within the film or that the hexagonal mesophase is globally not well-ordered.

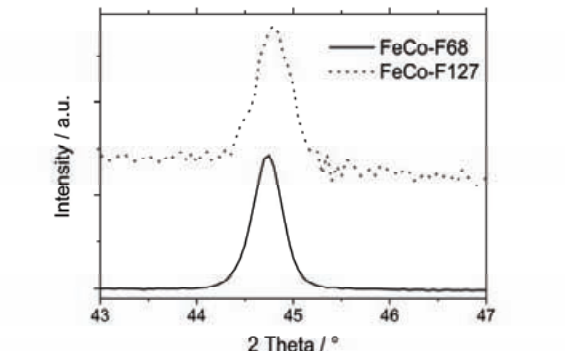

Figure 1. Selected angular regions XRD patterns of the FeCo-F68 (solid line) and the FeCo-F127 (dotted line) nanocomposites, indicating the presence of the FeCo alloy at high angles.

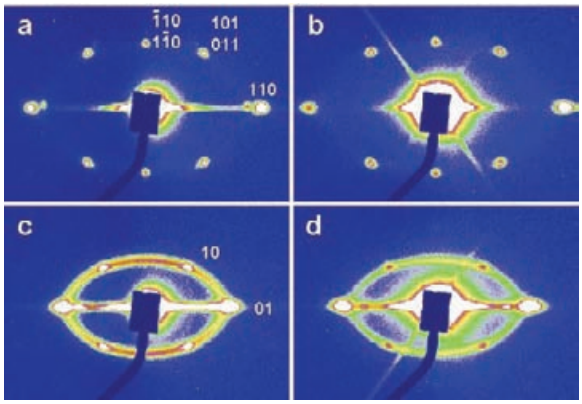

Figure 2. GISAXS patterns of F68-templated mesoporous silica films treated at 350 °C (a) and after impregnation and reduction at 600 °C (b). F127-templated mesoporous silica films treated at 350 °C (c) and after impregnation and reduction at 600 °C (d).

We have investigated by TEM the mesoporous silica films and the final nanocomposites obtained by the impregnation process and annealing at 600 °C. Figure 3a shows the ordered arrays of pores in the (100) projection plane (*Im*-3*m* cubic structure) of the mesoporous film templated by Pluronic F68. These analysis revealed that the pore-to-pore distance is different in the two orthogonal directions, which indicates the presence of a 2-fold symmetry axis, probably originating from the thermal contraction along the [110] direction of the *Im*-3*m* (z axis). Representative TEM image of the mesoporous film templated by Pluronic F127 (Figure 3b) show a short-range order, where the hexagonal packing extends only to the nearest neighbor mesopores. TEM bright field images of the FeCo-F68 and FeCo-F127 samples are shown in Figures 3c and d. Due to small nanocrystal size, the alloy nanoparticles are barely detectable as darker spots of the FeCo-F68 nanocomposite (Fig. 3c), whereas they are more evident in the FeCo-F127 sample (Fig. 3d) where larger nanocrystals can be imaged. The size distribution shows that the nanocrystal size is monodisperse in both samples and is centered around 4 and 6 nm in the FeCo-F68 and FeCo-F127 samples, respectively. No aggregated nanoparticles or nanoparticles outside the mesopores of the silica matrix are observed. Higher magnification micrographs indicate that nanocrystal growth took place inside the mesopores.

Silica mesoporous films were proved to be an effective matrix for the preparation of nanoparticles requiring high crystallization temperatures. The films maintain their porosity even after thermal treatment at 600 °C and show only a slight shrinkage after the impregnation process. As the mesopores represent a spatial confinement for the growth of the nanocrystals, the mesopore diameter constitutes an upper limit for the nanocrystal size, therefore nanocomposites with different FeCo sizes can be obtained by choosing the appropriate mesoporous host matrix. Our approach represents a method for obtaining monodisperse FeCo nanocrystals: for example, dissolution of the silica matrix from a FeCo–SiO_2 nanocomposite has been shown to be an effective way to fabricate FeCo graphitic nanoparticles to be used as magnetic resonance imaging (MRI) contrast agents.

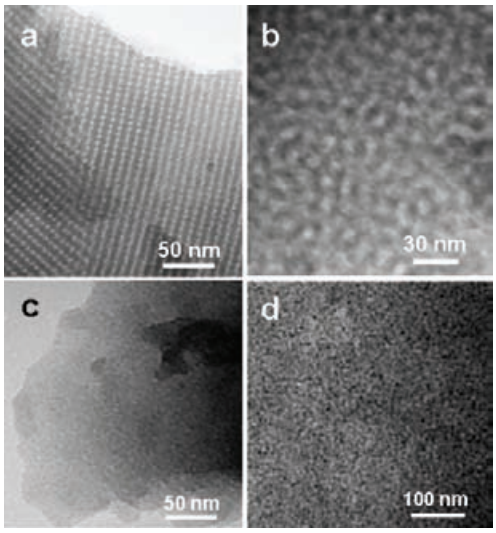

Figure 3. Bright-field TEM images of mesoporous silica films templated by F68 (a) and F127 (b) and representative images of the FeCo-F68 (c) and FeCo-F127 (d) nanocomposite

References:

[1] P. Falcaro, D. Grosso, H. Amenitsch, P. Innocenzi; J. Phys. Chem. B 108, 10942-10948 (2004).
[2] JCDD, International Centre for Diffraction Data, PDF Database, Card No. 48-1818.
[3] P. Innocenzi, P. Falcaro, D. Grosso, F. Babonneau; J. Phys. Chem. B 107, 4711-4717 (2003).

THERMAL FORMATION OF THIN NANOCOMPOSITE LAYERS – A TIME RESOLVED X-RAY SCATTERING STUDY

Thomas Rath[1,2], Kathrin Bohnemann[1], Heinz Amenitsch[3], Gregor Trimmel[1,2]

1.) Institute for Chemistry and Technology of Materials, Graz University of Technology, Stremayrgasse 16, 8010, Graz, Austria
2.) Christian Doppler Pilotlaboratory for Nanocomposite Solar Cells
3.) Institute of Biophysics and X-ray Structure Research, Austrian Academy of Sciences, Schmiedlstr. 6, A-8042 Graz, Austria

Nanoparticles and thin nanocrystalline films of semiconducting materials are discussed for numerous optoelectronic applications.[1] Especially metal oxide and metal sulfide layers are often used as active layers, buffer layers or interfacial layers in solar cells.[2,3] Therefore various fabrication methods for such films have been developed, like spray pyrolysis, chemical bath deposition or thermal conversion of precursor layers. Additional research is devoted to combinations of semiconductor nanoparticles with conjugated polymers, the so called nanocomposites, which are interesting materials for e.g. photoactive layers in solar cells or photodetectors.[4,5]

In our work we have prepared nanocrystalline thin films of ZnS or $CuInS_2$ as well as nanocomposite layers of these materials in combination with conjugated polymers. By applying a solution containing metal salts and sulfur source (and a polymer) on ITO (indium tin oxide) or silicon substrates, thin precursor layers were obtained which were thermally converted to a thin layer of nanocrystalline metal sulfide or of metal sulfide/polymer nanocomposite, respectively. This thermal formation process was simultaneously studied by time-resolved grazing-incidence small and wide angle X-ray scattering (GISAXS and GIWAXS) to obtain parameters like internal surface area, correlation lengths of the nanostructure but also the crystal phase of the inorganic metal sulfide layers. Figure 1 shows representative GISAXS and GIWAXS results obtained for a $CuInS_2$/polymer system on ITO at different times during the thermal conversion step. At lower temperature (below 140 °C) reflexes of metal-thiourea complexes can be observed and from about 160 °C mainly the broad (112)-reflex of nanocrystalline $CuInS_2$ is present.

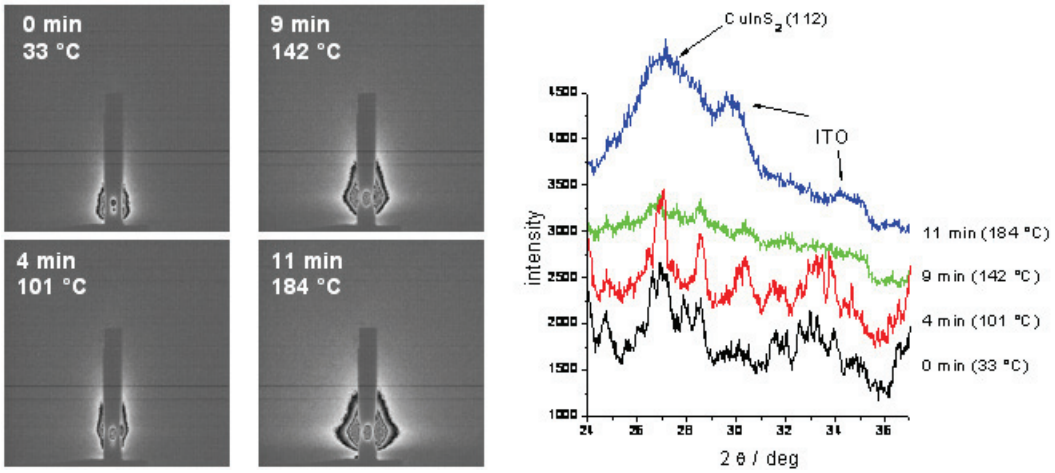

Figure 1. Results of GISAXS measurements (left) and WAXS measurements (right) of a polymer / CuInS2 nanocomposite layer at different temperatures

References:

[1] I. Matsui, J. Chem. Eng. Jap. 2005, 38, 535
[2] A. P. van Hal, M. M. Wienk, J. M. Kroon, W. J. H. Verhees, L. H. Slooff, W. J. H. van Gennip, P. Jonkheijm, R. A. Janssen, Adv. Mater. 2003, 15, 118
[3] B. Asenjo, A. M. Chaparro, M. T. Gutierrez, J. Herrero, J. Klaer, Sol. Energy Mater. Sol. Cells 2008, 92, 302
[4] W. U. Huynh, J. J. Dittmer, A. P. Alivisatos, Science 2002, 295, 2425
[5] S. A. McDonald, G. Konstantatos, S. Zhang, P. W. Cyr, E. J. D. Klem, L. Levina, E. H. Sargent, Nature Mater. 2005, 4, 138

PERIODIC MESOPOROUS CARBON THIN FILMS BY SOFT-TEMPLATING

J. Schuster[1], R. Köhn[1], A. Keilbach[1], A. Zürner[1], H. Amenitsch[2] and T. Bein[1]

1.) Department of Chemistry and Biochemistry and Center for NanoScience (CeNS) University of Munich, Butenandtstraße 5-13 (E), 81377 Munich, Germany
2.) Institute of Biophysics and Nanosystems Research, Austrian Academy of Sciences Schmiedlstraße 6, 8042 Graz, Austria

2D-hexagonal (plane group, p6mm) mesoporous carbon thin films were obtained through organic-organic evaporation-induced self-assembly (EISA) of a preformed oligomeric resol precursor and the triblock copolymer template pluronic P123 [1]. The carbon films were prepared on silicon wafers by spin-coating a mixture of precursor and surfactant in ethanol. EISA is followed by the formation of a condensed-wall material through thermopolymerization of the precursor oligomers, resulting in mesostructured phenolic resin thin films. Subsequent decomposition of the surfactant and carbonization were achieved through thermal treatment in inert gas atmosphere. The films are crack-free with tunable homogenous thicknesses, and show either 2D-hexagonal or lamellar mesostructure.

Synchrotron GISAXS experiments were carried out to identify the highly-ordered 2D hexagonal mesostructure as averaged structural information of the whole film, and to specify the unit cell parameters in terms of distortion during the thermal treatments. The resulting unit cells of a 2D-hexagonal structure before and after carbonization are shown in Figure 1.
They were calculated from the patterns depicted in Figure 2 which show diffraction spots that can be attributed to a 2D hexagonal lattice of cylinders with the cylinders oriented parallel to the substrate. A 500 nm thick film (A and B) showed intense patterns with several higher order reflections. All the reflections lie on a reciprocal lattice of a slightly distorted 2D-hexagonal structure and could be indexed according to corresponding lattice planes. The shrinkage in the carbonization process is shown in patterns C and D of a hexagonally mesostructured film. The reflections move to higher diffraction angles parallel to the vertical axis of the pattern which is equivalent with shrinkage along the substrate normal.
In summary we could reveal a highly ordered mesostructure, determine the structural parameters and follow the structural distortion along the substrate normal during a high temperature treatment.

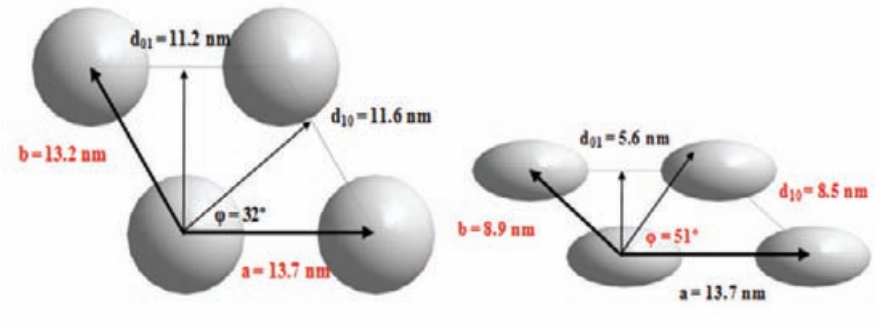

Figure 1: Unit cell parameters from of GISAXS data for the hexagonal spin-coated film before (left), and after carbonization (right), applying shrinkage of d_{01} by 50 % and a constant parameter a. The calculated values are marked in red.

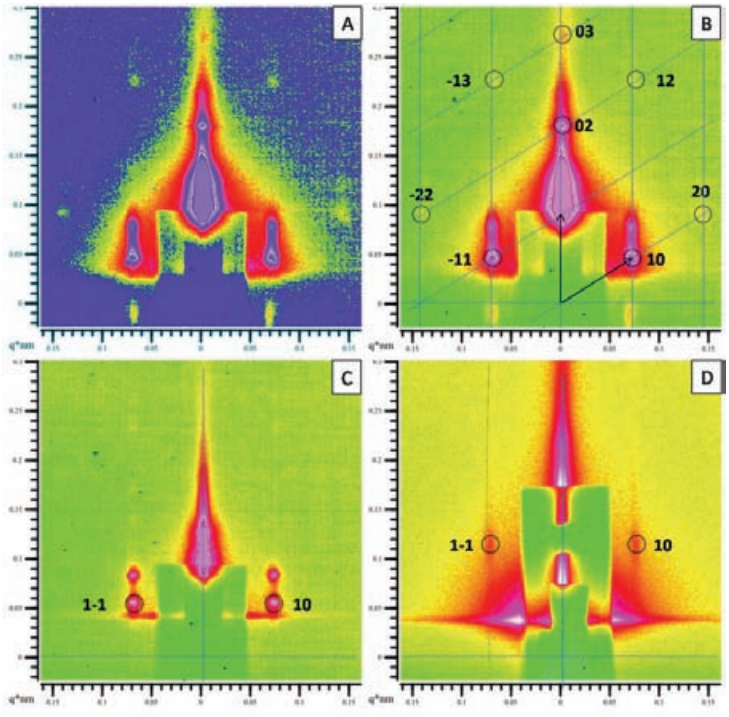

Figure 2: 2D-GISAXS patterns: A) Contrast enhanced image of a mesostructured film after thermopolymerization at 100 °C where the higher order reflections can be observed easily B) The same diffraction pattern with a linear intensity scaling visualizing the reciprocal lattice of the 2D-hexagonal structure (plane group, p6mm), the peaks are indexed in a 2D-hexagonal unit cell. C) Pattern of an only 200 nm thick film before and D) after carbonization at 400 °C. The indexing according to a 2D-hexagonal unit cell was retained, although it was distorted during template removal and carbonization. The most intense reflections are doubled due to the grazing incidence geometry, the first peak is resulting from the X-rays scattered at the lattice planes and the second on top is a specular reflection of the first one.

References:

[1] J. Schuster, R. Köhn, A. Keilbach, M. Döblinger, H. Amenitsch and T. Bein; Periodic Mesoporous Carbon Thin Films by Soft-Templating; Chem. Mater.; submitted

SMECTIC ORDERING IN 8CB AND 12CB LIQUID CRYSTALS

A. Zidanšek[1,2,3], H. Amenitsch[4], G. Cordoyiannis[5,1], D. Jesenek[3], S. Kralj[3,1], Z. Kutnjak[1,2], G. Lahajnar[1,2]

1.) Jozef Stefan Institute, Jamova 39, 1000 Ljubljana, Slovenia
2.) Jozef Stefan International Postgraduate School, Jamova 39, 1000 Ljubljana, Slovenia
3.) Faculty of Natural Sciences and Mathematics, University if Maribor, Koroška 160,2000 Maribor, Slovenia
4.) Institute of Biophysics and Nanosystems Research, Austrian Academy of Sciences, Schmiedlstr. 6, A-8012 Graz, Austria
5.) National Centre for Scientific Research "Demokritos", 153 10 Aghia Paraskevi, Greece

12CB and 8CB liquid crystals confined to CPG pores represent an interesting system, which reflects the interplay between elastic, surface interaction forces and finite-size effects. Randomly curved and interconnected pores introduce some kind of randomness into the system. For this reason one often considers such systems as a testing ground for the statistical physics of disorder [1, 2].

Temperature dependence of the small angle X-ray scattering smectic peak was measured in smectic phase of the 12CB and 8CB liquid crystals confined to CPG glasses of various pore diameters. The results confirmed our hypothesis that confinement to CPG pores has qualitatively different effect on 8CB versus 12CB liquid crystal.

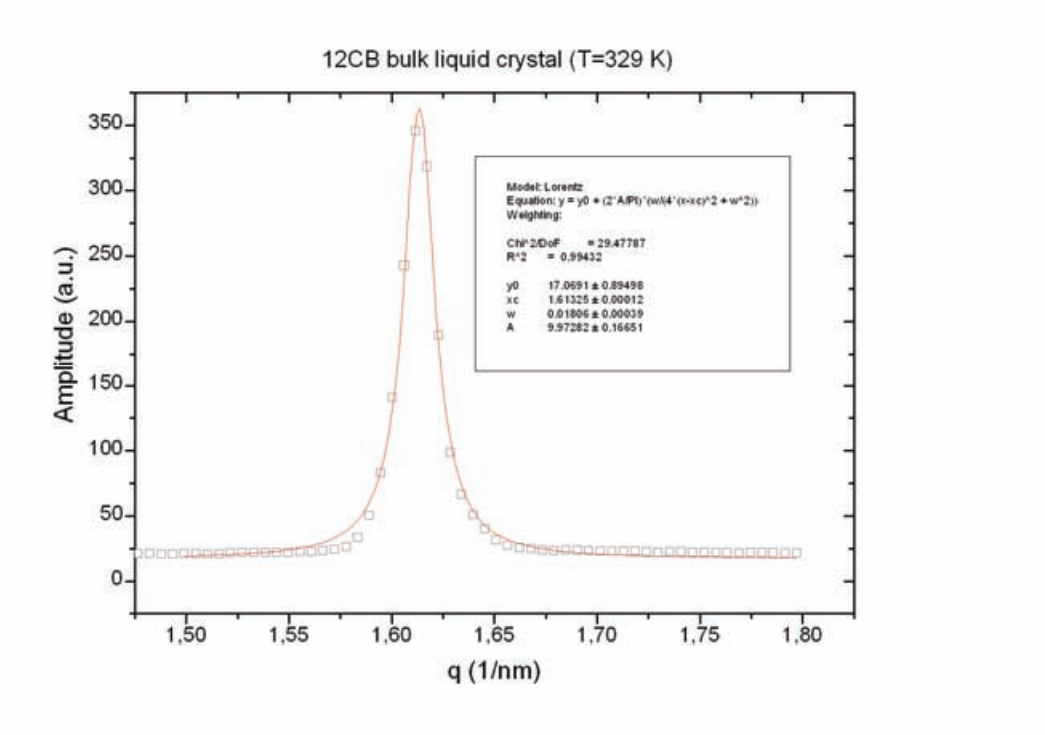

Figure 1. Example of the first order smectic peak in 12CB, which is fitted to a Lorentzian line at 329 K in the smectic phase. The sample was cooled down from the isotropic phase.

In this experiment we focused on the influence of different types of surface treatment of CPG glasses on the temperature dependence of smectic ordering, for CPG diameter in the range between 15nm and 127nm. The 8CB liquid crystal exhibits at high temperatures the isotropic (I) phase, crossing the nematic (N) phase, until strong smectic A (SmA) ordering is established at low temperatures. On the contrary, in 12CB the nematic phase is absent and the transition is directly from the isotropic into the smectic A phase.

Some typical results of the first order smectic peak measured with small angle X-ray scattering are shown in Figures 1 and 2.

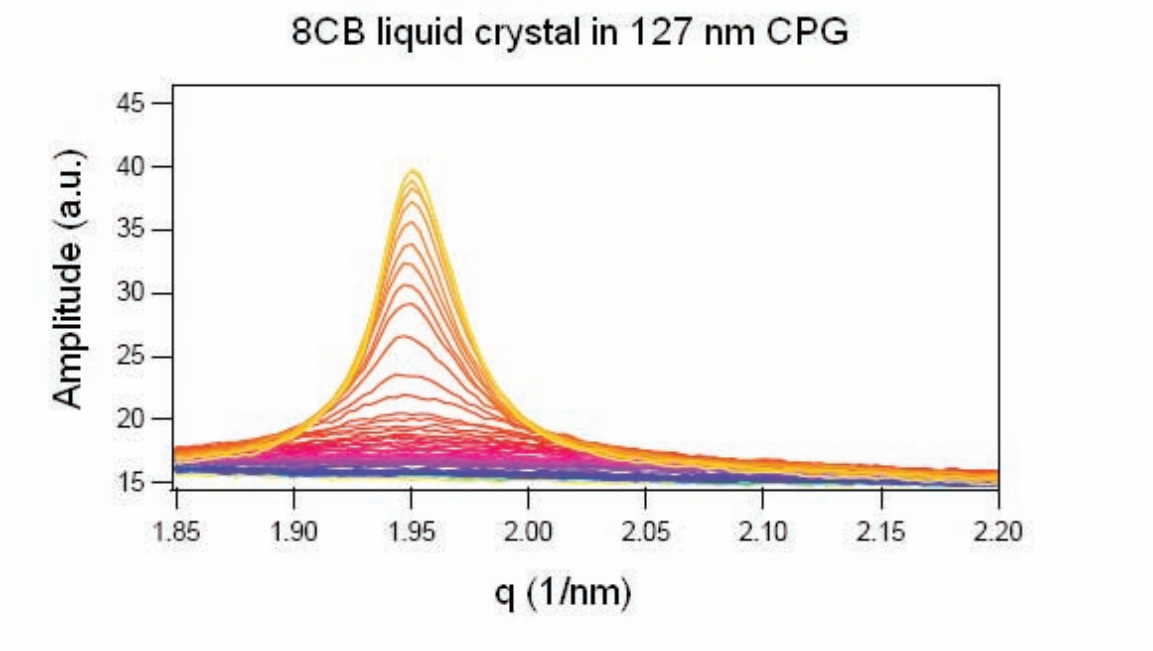

Figure 2. Example of the first order smectic peaks in 8CB liquid crystal confined to CPG with average pore diameter of 127 nm. The lines are shown for cooling from 323 K (bottom) until 300 K (top) at 0.3 K interval.

Results of this experiment can be explained in terms of the Landau-Ginzburg-de Gennes type phenomenological model. A more comprehensive review of these results has been published in Physical Review E [3]. We have also presented a poster at the 10th European Conference on Liquid Crystals [4].

References:

[1] Kancler A, Lahajnar G, Kralj S, Zidansek A, Amenitsch H, Bernstorff S; Smectic ordering of 8CB liquid crystal confined to a controlled-pore glass; MOLECULAR CRYSTALS AND LIQUID CRYSTALS 439: 1899-1908 (2005)

[2] Zidansek A, Kralj S, Repnik R, Lahajnar G, Rappolt M, Amenitsch H, Bernstorff S; Smectic ordering of octylcyanobiphenyl confined to control porous glasses; JOURNAL OF PHYSICS-CONDENSED MATTER 12: A431-A436 (2000)

[3] George Cordoyiannis, Aleksander Zidanšek, Gojmir Lahajnar, Zdravko Kutnjak, Heinz Amenitsch, George Nounesis, and Samo Kralj; Influence of the Controlled-Pore Glass Confinement on the Layer Spacing of Smectic A Liquid Crystals; PRE 79: 051703 (2009)

[4] George Cordoyiannis, Aleksander Zidanšek, Gojmir Lahajnar, Zdravko Kutnjak, Heinz Amenitsch, Dalija Jesenek, George Nounesis, and Samo Kralj; Influence of the Controlled-Pore Glass Confinement on the Layer Spacing of Smectic-A Liquid Crystals; 10th European Conference on Liquid Crystals / Colmar – France, April 19-24 (2009)

Publications

Publications in Journals and Reviewed Proceedings 2008

N. Baccile, C.V. Teixeira, H. Amenitsch, F. Villain, M. Lindén and F. Babonneau
Time-resolved in situ Raman and small-angle X-ray diffraction experiments: from silica precursor hydrolysis to development of mesoscopic order in SBA-3 surfactant- templated silica
Chemistry of Materials, 20 (3), 1161-1172, 2008

P.-L. Bardonnet, V. Faivre, P. Boullanger, J.-C. Piffaretti, F. Falson
Pre-formulation of liposomes against Helicobacter pylori: characterisation and interaction with the bacteria
European Journal of Pharmaceutics and Biopharmaceutics, 69 (3), 908-922, 2008

F. Bekkara-Aounallah, R. Gref, M. Othman, L.H, Reddy, B. Pili, V. Allain, C. Bourgaux, H. Hillaireau, S. Lepêtre-Mouelhi, D. Desmaële, J. Nicolas, N. Chafi, P. Couvreur
Novel PEGylated nanoassemblies made of self-assembled Squalenoyl nucleoside analogues
Adv. Funct. Mater. 18, 3715-3725 (2008)

G. Caracciolo, D. Pozzi, R. Caminiti, C. Marchini, M. Montani, A. Amici and H. Amenitsch
Enhanced transfection efficiency of multicomponent lipoplexes in the regime of optimal membrane charge density
Phys. Chem. B 112, 11298-11304 (2008)

G. Caracciolo, D. Pozzi, R. Caminiti, C. Marianecci, S. Moglioni, M.,Carafa and H. Amenitsch
Effect of hydration on the structure of solid-supported Niosomal membranes investigated by in situ energy dispersive X-ray diffraction
Chemical Physics Letters 462 (4-6), pp. 307-312 (2008)

G. Caracciolo, D. Pozzi, R. Caminiti, C. Marchini, M. Montani and H. Amenitsch
Effect of pH on the structure of lipoplexes
Journal of Applied Physics 104 (1), art. no. 014701 (2008)

C. Chemin, C. Bourgaux, J.-M. Péan, G. Pabst, P. Wüthrich, P. Couvreur and M. Ollivon
Consequences of ions and pH on the supramolecular organization of sphingomyelin and sphingomyelin/cholesterol bilayers
Chemistry and Physics of Lipids, Volume 153, Issue 2, June 2008, Pages 119-129

S. Costacurta, L. Malfatti, P. Innocenzi, H. Amenitsch, A. Masili, A. Corrias, M.F. Casula
Confined growth of iron cobalt nanocrystals in mesoporous silica thin films: FeCo-SiO2 nanocomposites
Microporous and Mesoporous Materials 115 (3), pp. 338-344 (2008)

P. Couvreur, L.H. Reddy, S. Mangenot, J.H. Poupaert, D. Desmaele, S. Lepetre Mouelhi, B. Pili, C. Bourgaux, H. Amenitsch and M. Ollivon
Discovery of new hexagonal supramolecular nanostructures formed by squalenoylation of an anticancer nucleoside analogue
Small 4(2), 247-253 (2008)

I.D. Desnica-Frankovic, Kresimir Furić, U. Desnica, P. Dubcek, M. Buljan, S. Bernstorff
Complementary application of Raman scattering and GISAXS in characterization of embedded semiconductor QDs
Superlattices and Microstructures 44, 385-394 (2008)

U.V. Desnica, K. Salamon, M. Buljan, P. Dubcek, N. Radic, I.D. Desnica-Frankovic, Z. Siketic, I. Bogdanovic-Radovic, M. Ivanda, S. Bernstorff
Formation of Ge-nanocrystals in SiO2 matrix by magnetron sputtering and post-deposition thermal treatment
Superlattices and Microstructures 44, 323-330 (2008)

A. W. Dong, C. Pascual-Izarra, Y.-D. Dong, S. J. Pas, A.J. Hill, B. J. Boyd, C. J. Drummond
Positron annihilation lifetime spectroscopy (PALS) and small angle x-ray scattering (SAXS) of self-assembled amphiphiles
Proceedings of SPIE, 2008, 6800 (Device and process technologies for microelectronics, MEMS photonics and nanotechnology IV), 680001C/1-68001C/6

Yao-Da Dong, Aurelia W Dong, Ian Larson, Michael Rappolt, Heinz Amenitsch, Tracey Hanley and Ben J. Boyd
Impurities in commercial phytantriol significantly alter its lyotropic liquid-crystalline phase behavior
Langmuir: the ACS journal of surfaces and colloids 24(13), 6998-7003 (2008)

P. Dubček, B. Pivac, I. Capan, S. Bernstorff, R. Mu and B. Vlahovic
Evolution of Nanoparticles in Gold-Implanted Glass
Vacuum 82, 130-133, (2008)

P. Falcaro, S. Costacurta, L. Malfatti, T. Kidchob, M. Casula, M. Piccinini, A. Marcelli, B. Marmiroli, H. Amenitsch, P. Schiavuta, P. Innocenzi
Fabrication of Mesoporous Functionalized Arrays by Integrating Deep X-Ray Lithography with Dip-Pen Writing
Advanced Materials 20 (10), pp. 1864-1869 (2008)

R. A. Farrell, N. Petkov, H. Amenitsch, J. D. Holmes and M. A. Morris
Thin and Continuous Films with Controlled Bi- and Tri-Modal Porosities by Embedment of Zeolite Nanoparticles in a Mesoporous Matrix
Journal of Materials Chemistry 18 (19), pp. 2213-2220 (2008)

R.A. Farrell, N. Petkov, K. Cherkaoui, H. Amenitsch, J.D. Holmes, P.K. Hurley, M.A. Morris
Facile and controlled synthesis of ultra-thin low dielectric constant meso/microporous silica films
Chem. Phys. Chem. 9 (11), pp. 1524-1527 (2008)

B. Gehl, J. I. Flege, V. Aleksandrovic, T. Schmidt, A. Kornowski, S. Bernstorff, J. Falta, H. Weller, M. Bäumer
Plasma modification of CoPt3 nanoparticle arrays: A route to catalytic coatings of surfaces
J. Vac. Sci. Technol. A 26 (4), pp. 908-912, Jul/Aug 2008

B. Gehl, A. Frömsdorf, V. Aleksandrovic, T. Schmidt, A. Pretorius, J.-I. Flege, S. Bernstorff, A. Rosenauer, J. Falta, H. Weller, M. Bäumer
Structural and chemical effects of plasma treatment on close-packed colloidal nanoparticle layers
Advanced Functional Materials 18 (16), pp. 2398-2410 (2008)

D. Gracin, K.Juraic, A. Gajovic, P. Dubcek, C. Devilee, H.J. Muffler, W.J. Soppe, S. Bernstorff
The structural ordering of thin silicon films at the amorphous to nano-crystalline phase transition by GISAXS and Raman spectroscopy
Renewable Energy 33 (2008) 326–330

A. Gupta, P. Rajput, S. Bernstorff, H. Amenitsch
Low-Dimensionality Effects in the Melting of a Langmuir-Blodgett Multilayer
Langmuir, Vol. 24 (15), pp. 7793-7796 (2008)

A. Hickel, S. Danner-Pongratz, H. Amenitsch, G. Degovics, M. Rappolt, K. Lohner and G. Pabst
Influence of antimicrobial peptides on the formation of nonlamellar lipid mesophases
Biochimica et Biophysica Acta - Biomembranes 1778 (10), pp. 2325-2333 (2008)

A. Hodzic, M. Rappolt, H. Amenitsch, P. Laggner and G. Pabst,
Differential modulation of membrane structure and fluctuations by plant sterols and cholesterol
Biophs. J. 94 (10), 3935-3944 (2008)

A. Hodzic, P. Zoumpoulakis, T. Mavromoustakos, M. Rappolt, P. Laggner, and G. Pabst
The role of membrane hydrocarbon chain composition in interactions withantihypertensive drugs
Biophys. J., Suppl. 94, 345A (2008)

S. Ibrahimkutty, M. Rappolt, B. Sartori, H. Amenitsch and P. Laggner
Novel in situ setup to study the formation of nanoparticles in the gas phase by small angle x-ray scattering
Rev. Sci. Instrum. 79 (4), art. no. 043905 (1-5) (2008)

P. Innocenzi, T. Kidchob, L. Malfatti, S. Costacurta, M. Takahashi, M. Piccinini, A. Marcelli
In-situ study of sol–gel processing by time-resolved infrared spectroscopy
Journal of Sol-Gel Science and Technology, 48, 253-259, 2008

P. Innocenzi, S. Costacurta, T. Kidchob, L. Malfatti, P. Falcaro, G. Soler-Illia
Mesoporous thin films: properties and applications
book chapter in "Sol-Gel Methods for Materials Processing" (Springer, 2008, XII, 508 p., Hardcover ISBN: 978-1-4020-8521-5)

C. Li, A.D. Schluter, A. Zhang, R. Mezzenga
A New Level of Hierarchical Structure Control by Use of Supramolecular Self-assembled Dendronized Block Copolymers
Adv. Mater. 20, 4530 (2008)

M. Lindén, F. Babonneau, H. Amenitsch, N. Baccile, A. Riley, S. Tolbert
On the mechanism of formation of SBA-1 and SBA-3 as studied by in situ synchrotron XRD
Studies in Surface Science and Catalysis 174 (Suppl. part A), pp. 103-108 (2008)

L. Malfatti, T. Kidchob, D. Aiello, R. Aiello, F. Testa, P. Innocenzi
Aggregation States of Rhodamine 6G in Mesostructured Silica Films
J. Phys. Chem. C 112, pp. 16225-16230, 6 pages (2008)

T. Mares, M. Daniel, S. Perutkova, A. Perne, G. Dolinar, A. Iglic, M. Rappolt, and I. Kralj
Role of Phospholipid Asymmetry in the Stability of Inverted Hexagonal Mesoscopic Phases
J. Phys. Chem. B 112, 16575–16584 (2008)

M. Mazaj, S. Costacurta, N. Zabukovec Logar, G. Mali, N. Novak Tušar, P. Innocenzi, *L. Malfatti, F. Thibault-Starzyk, H. Amenitsch, V. Kaucic, G.J.A.A. Soler-Illia*
Mesoporous aluminophosphate thin films with cubic pore arrangement
Langmuir 24 (12), pp. 6220-6225 (2008)

M. G. Ortore, R. Sinibaldi, P. Heyse, S. Paulussen, S. Bernstorff, B. Sels, P. Mariani, F. Rustichelli and F. Spinozzi
Grazing-incidence small-angle X-Ray scattering from alkaline phosphatase immobilized in atmospheric plasmapolymer coatings
Applied Surface Science 254, Issue 17, 30 June 2008, Pages 5557-5563

P. Piseri, T. Mazza, G. Bongiorno, M. Devetta, M. Coreno, P. Milani
CESyRa: A versatile setup for core-level absorption experiments on free metallic clusters using synchrotron radiation
J. Electron Spectrosc. 166-167, pp. 28 -37 (2008)

B. Pivac, P. Dubcek, I. Capan, H. Zorc, S. Bernstorff, S. Duguay, A. Slaoui
Structural analysis of annealed amorphous SiO/SiO2 superlattice
Thin Solid Films 516 (2008) 6796-6799

B. Pivac, P. Dubček, I. Capan, N. Radić, S. Bernstorff
GISAXS study of Si nanoclusters in SiO/SiO2 layers
Vacuum. 82, 189-192 (2008)

B. Pivac, P. Dubček, I. Capan, H. Zorc, S. Bernstorff, S. Duguay, A. Slaoui
Structural analysis of annealed amorphous SiO/SiO2 superlattice
Thin Solid Films. 516, 6796-6799 (2008)

R. Prassl, M. Pregetter, H. Amenitsch, M. Kriechbaum, R. Schwarzenbacher, J.M. Chapman and P. Laggner
Low Density Lipoproteins as Circulating Fast Temperature Sensors
PLoS ONE, 3 (12), e4079, Dec 2008

M. Rappolt and G. Pabst
Flexibility and struture of fluid bilyer interfaces. In: Structure and Dynamics of Membranous Interfaces
K. Nag (ed.), John Wiley & Sons, Inc., Hoboken (NJ), pp. 45-81 (2008)

M. Rappolt, A. Hodzic, B. Sartori, M. Ollivon, and P. Laggner
Conformational and hydrational properties during the L(beta)- to L(alpha)- and L(alpha)- to H(II)-phase transition in phosphatidylethanolamine
Chem. Phys. Lipids 154 (1), pp. 46-55 (2008)

D. Setman, E. Schafler, E. Korznikova, M.J. Zehetbauer
The presence and nature of vacancy type defects in SPD nanometals
Mater. Sci. Eng.A 493, 116-122 (2008)

E. Sevcsik, G. Pabst, W. Richter, S. Danner, H. Amenitsch and K. Lohner
Interaction of LL-37 with model membrane systems of different complexity: Influence of the lipid matrix
Biophysical Journal 94(12), 4688-4699 (2008)

A. Turkovic
SAXS characterization of mesoporous thin films: a solar energy point of view
Chapter 11 in: "Solar Energy: Research Technology and Applications", Editor: William L. Olofsson and V.I. Bengtsson, 2008 Nova Science Publishers, Inc., ISBN 978-1-60456-739-7

A. Turković, M. Pavlović, P. Dubček and S. Bernstorff
SAXS/WAXD/DSC study of Zn2+-ion conducting polymer electrolyte
Acta Chimica Slovenica 55 (4), pp. 822-827 (2008)

D. Vrsaljko, I. Šmit, V. Kovacević
Effect of calcium carbonate particle size and surface pretreatment on polyurethane composite. Part II: Phase behavior
Materials Research Innovations, Volume 12, Number 2, June 2008, pp. 72-77(6)

Anan Yaghmur, Peter Laggner, Mats Almgren, Michael Rappolt
Self-Assembly in Monoelaidin Aqueous Dispersions: Direct Vesicles to Cubosomes Transition
PLoS ONE, www.plosone.org, 1 November 2008, Volume 3, Issue 11, e3747, 10 pages

Anan Yaghmur, Peter Laggner, Barbara Sartori, Michael Rappolt
Calcium Triggered Lα-H2 Phase Transition Monitored by Combined Rapid Mixing and Time-Resolved Synchrotron SAXS
PLoS ONE, www.plosone.org, April 2008, Volume 3, Issue 4, e2072, 11 pages

Publications during January to June 2009

P. Angerer, H. Simunkova, E. Schafler, M. B. Kerber, J. Wosik, G. E. Nauer
Structure and texture of electrochemically prepared nickel layers with co-deposited zirconia nanoparticles
Surf. Coat. Tech. 203, 1438-1443 (2009)

J. Baldrian, M. Steinhart, H. Amenitsch, S. Bernstorff
Disorder-order-crystalline state transitions of PEO-b-PPO-b-PEO copolymers and their blends: SAXS/WAXS/DSC study
Journal of Macromolecular Science, Part B, Volume 48 (Issue 1), pp. 174-184 (January 2009)

M. Buljan, I. Bogdanovic-Radovic, M. Karlušic, U. V. Desnica, G. Drazic, N. Radic, P. Dubcek, K. Salamon, S. Bernstorff and V. Holý
Formation of long-range ordered quantum dots arrays in amorphous matrix by ion beam irradiation
Applied Physics Letters 95, 063104-1 - 063104-3 (2009) and
Virtual Journal of Nanoscale Science & Technology, issue of August 24, 2009

M. Buljan, U. V. Desnica, M. Ivanda, N. Radić, and P. Dubček, G. Dražić, K. Salamon, S. Bernstorff, V. Holý
Formation of three-dimensional quantum-dot superlattices in amorphous systems: Experiments and Monte Carlo simulations
Physical Review B 79, 035310 (2009) and
Virtual Journal of Nanoscale Science & Technology, Volume 19, Issue 4 (2009)

M. Buljan, U. V. Desnica, G. Dražić, M. Ivanda, N. Radić, P. Dubček, K. Salamon, S. Bernstorff and V. Holý
The influence of deposition temperature on the correlation of Ge quantum dot positions in amorphous silica matrix
Nanotechnology 20 (8) 085612 (6 pages) (03/2009)

C. Chemin, J.M. Péan, C. Bourgaux, G. Pabst, P. Wüthrich, P. Couvreur, and M. Ollivon
Supramolecular organization of S12363-liposomes prepared with two different remote loading processes
Biochimica et biophysica acta 1788(5), 926-935, 2009 May

G. Cordoyiannis, A. Zidanšek, G. Lahajnar, Z. Kutnjak, H. Amenitsch, G. Nounesis, and S. Kralj
Influence of the Controlled-Pore Glass Confinement on the Layer Spacing of Smectic A Liquid Crystals
Phys. Rev. E 79, 051703 (2009)

P. Falcaro, L. Malfatti, T. Kidchob, G. Giannini, A. Falqui, M.F. Casula, H. Amenitsch, B. Marmiroli, G. Grenci, P. Innocenzi
Hierarchical Porous Silica Films with Ultralow Refractive Index
Chem. Mater. 21-10, pp. 2055-7 (2009)

D. Gracin, B. Etlinger, K. Juraić, A. Gajović, P. Dubček and S. Bernstorff
DC conductivity of amorphous-nano-crystalline silicon thin films
Vacuum 84 (2009) 243-246

D. Grozdanić, R. Slunjski, B. Rakvin, P. Dubček, B. Pivac, N. Radić, S. Bernstorff
Structural analysis of amorphous Si films prepared by magnetron sputtering
Vacuum 84 (2009) 126–129

A. Keilbach, M. Döblinger, R. Köhn, H. Amenitsch, T. Bein
Periodic Mesoporous Organosilica in Confined Environments
CHEM-EUR J, Vol. 15 - 27, pp. 6645 (2009)

M.B. Kerber, E. Schafler, A.K. Wieczorek, G. Ribarik, S. Bernstorff, T. Ungar, M.J. Zehetbauer
Synchrotron X-ray line-profile analysis experiments for the in-situ microstructural characterisation of SPD nanometals during tensile deformation
Int. J. Mater. Res. (formerly Z. Metallk.) 100 (2009) 770-774 (5 Pages)

T. Lebold, L. A. Mühlstein, J. Blechinger, M. Riederer, H. Amenitsch, Ralf Köhn, K. Peneva, K. Müllen, J. Michaelis, C. Bräuchle, T. Bein
Tuning Single-Molecule Dynamics in Functionalized Mesoporous Silica
Chem. Eur. J., 15, 1661-1672, (2009)

C. Marchini, M. Montani, A. Amici, H. Amenitsch, C. Marianecci, D. Pozzi and G. Caracciolo
Structural stability and increase in size rationalize the efficiency of lipoplexes in serum
Langmuir 25, 3013-3021 (2009)

B. Marmiroli, G. Grenci, F. Cacho-Nerin, B. Sartori, E. Ferrari, P. Laggner, L. Businaro, H. Amenitsch
Free jet micromixer to study fast chemical reactions by small angle X-ray scattering,
Lab on a Chip, Vol. 9 - 14, pp. 2063-2069 (7 pages) (2009)

L. Malfatti, S. Costacurta, T. Kidchob, P. Innocenzi, M. Casula, H. Amenitsch, D. Dattilo, M. Maggini
Mesostructured self-assembled silica films with reversible thermo-photochromic properties
Microporous and Mesoporous Materials 120 (2009) 375–380

B. Pivac, P. Dubcek, I. Capan, I. Zulim, T. Betti, H. Zorc, and S. Bernstorff
Nano Si Superlattices for the Next Generation Solar Cells
J. Nanosci. Nanotechnol. 9, 3853–3857 (2009)

K. Salamon, O. Milat, M. Buljan, U.V. Desnica, N. Radić, P. Dubček and S. Bernstorff
Grazing incidence X-ray study of Ge-nanoparticle formation in (Ge:SiO2)/SiO2 multilayers
Thin Solid Films 517 (6), pp. 1899-1903 (2009)

C Sinturel, M Vayer, R Erre, H Amenitsch
Thermal induced mobility of self-assembled platelets of polyethylene-block poly(ethylene oxide) in liquid precursors of unsaturated polyester thermoset
Journal: EUR POLYM J, Vol. 45 - 9, pp. 2505-8 (2009)
International Conferences and Workshops in 2008

International Conferences and Workshops in 2008

H. Amenitsch
Small angle x-ray scattering: NanoMaterials and proteins in solution
Advanced School on "Synchrotron and Free Electron Laser Sources and their Multidisciplinary Applications", Trieste, Italy, 07 - 25 April 2008 (invited lecture)

H. Amenitsch
The Austrian SAXS beamline at ELETTRA - What can biologists learn from small angle X-ray scattering?
1st Tübingen-Elettra Meeting, 6.–8.10.2008, Trieste, Italy (lecture)

H. Amenitsch
SAXS and its applications to the life sciences
XVI Elettra Users Meeting, Trieste, Italy, 26.11.2008 (invited lecture)

H. Amenitsch
An der Grenze der Bio/Nano-Welten:Forschung an der Österreichischen Kleinwinkelstreustrahlführung bei ELETTRA
Institutsseminar an der Technische Chemie Graz, Austria, 10.06.08 (lecture)

H. Amenitsch
From advanced experiments to nanofabrication at the IBN outstation Elettra
ESG-Nano-Impulsveranstaltung "European Large Scale Facilities Go Nano", Vienna, Austria, 23.06.08 (lecture)

Amenitsch, S. Bernstorff, and M. Rappolt
Small angle scattering set-ups and data analysis
Advanced School on "Synchrotron and Free Electron Laser Sources and their Multidisciplinary Applications", Trieste, Italy, 07 - 25 April 2008 (tutorial)

H. Amenitsch, D. Cojoc, B. Marmiroli, B. Sartori, M. Rappolt, P. Laggner, E. Ferrari, V. Garbin, S. Santucci, G. Grenci, M. Burghammer, C. Riekel
In situ manipulation with laser teezer in X- rays experiments: new possibilities in micro-diffraction experiments
ÖPG Tagung 2008, Leoben, Aaustria, 22. – 26.09.08 (poster)

H. Amenitsch, D. Cojoc, C. Riekel
Optical tweezers for manipulating biopolymers in solution and perspectives
International Conference on Nanotechnology and Applications, Crete, Greece, 29.09. – 03.10.08 (lecture)

S. Bernstorff
Grazing Incidence Small Angle Scattering (GISAXS) in Material Sciences
Advanced School on "Synchrotron and Free Electron Laser Sources and their Multidisciplinary Applications", Trieste, Italy, 07 - 25 April 2008 (invited lecture)

S. Bernstorff
Nanomaterials as seen by Small Angle Scattering
Satellite Workshop WS2 of EPDIC 11: "Application of powder diffraction in nanomaterials", Warsaw 18 Sept, 2008 (invited talk)

S. Bernstorff
Nanostructured Materials as seen by Small Angle Scattering
Satellite Workshop of EMRS Fall 2008: "Current trends in nanostructured polymer and sol-gel thin films", Warsaw 16-17 Sept, 2008 (oral contribution)

Boulgaropoulos B., Laggner P., Pabst G.
Effect of ceramide on structure and fluctuations in ternary lipid model-systems
Microfluidics for X-ray Nanoanalytics Symposium, Graz, Austria, 13. -14.02.08 (poster)

Boulgaropoulos B., Laggner P., Pabst G.
Effect of sphingomyelinase on sphingomyelin containing lipid model membranes
Jahrestagung der Österreichischen Gesellschaft für Biochemie und Molekularbiologie, Graz, Austria, 22. – 24.09.08 (poster)

Boulgaropoulos B., Laggner P., Pabst G.
Effect of Sphingomyelinase on Sphingomyelin containing Lipid Model Membranes
6th European Federation for the Science and Technology of Lipids Congress, Athen, Greece, 07.09. – 10.06.08 (poster)

Klaus Brandenburg
Development of effective antimicrobial peptides for the fight against bacterial sepsis
Seminar talk at the Forschungszentrum Borstel, 22 October 2008

Klaus Brandenburg
Therapy of infectious diseases with special regard to bacterial sepsis
FIT (Forum Innovative Therapien), Hamburg-Blankenese, 30-31 October 2008 (talk)

M. Buljan, U. V. Desnica, G. Dražić, M. Ivanda, N. Radić, P. Dubček, K. Salamon, S. Bernstorff and V. Holy
Vertically correlated Ge quantum dots in amorphous silica matrix: Structural characterization and growth simulation
XTOP 2008, 9th Biennial Conference on High Resolution X-Ray Diffraction and Imaging, Linz (Austria), 15-19 September 2008 (oral presentation)

M. Buljan
Ge quantum dots in amorphous silica matrix: Determination of defects in crystal structure by using of Debye equation
Charles University, Prague, Czech Republic, November 2008 (seminar talk)

M. Buljan
Growth and characterization of Carbon nanoclusters in amorphous matrix
Rossendorf, Germany, December 2008 (seminar talk)

M. Buljan
Svojstva poluvodičkih nanočestica u amorfnoj SiO2 matrici
Institut Ruđer Bosković, Croatia, October 2008 (seminar talk)

Cacho-Nerin F., Schmid F., Holzapfel G.A., Laggner P., Amenitsch H.
The microstructure of the adventitia explains its macroscopic mechanical behavior
8th World Congress on Computational Mechanics, Venice, Italy, 30.06. – 04.07.08 (talk)

Cacho-Nerin F., Schmid F., Sartori B., Laggner P., Amenitsch H
Simultaneous macro- and nanoscopic mechanical characterization of soft biological materials under large deformations
ÖPG Tagung 2008, Leoben, Austria, 22. – 26.09.08 (poster)

C. Camerani
Industrial applications at MaxLab
Synchrotron Summer School, 26 May - 2 June, 2008, Lund, Sweden (invited lecture)

G. Caracciolo, D. Pozzi, R. Caminiti, C. Marchini, M. Montani, A. Amici and H. Amenitsch
Lipoplex-Cell Interaction: On the Mechanism of DNA Release
XCIV Congresso Nazionale Società Italiana di Fisica, Genova, 22–27 Settembre 2008 (oral)

G. Caracciolo, D. Pozzi, R. Caminiti, C. Marchini, M. Montani, A. Amici, H. Amenitsch
Improved Transfection Efficiency of Multicomponent Lipoplexes
X Annual Linz Winter Workshop, Linz (Austria), 15-19 Febbraio 2008 (poster)

U.V. Desnica, M. Buljan, K. Salamon, Dubcek, M. Ivanda, N. Radic, Z. Siketic, I. Bogdanovic-Radovic, I.D. Desnica-Frankovic, S. Bernstorff
Formation of germanium nanocrystals in SiO2 matrix using RT magnetron sputtering
EMRS Fall Meeting 2008, Warsaw, Poland, 15-19 September 2008 (oral)

Y. D. Dong, H. Amenitsch, M. Rappolt, S. Rizwan, S. Hook, T. Rades, B. J. Boyd
Equilibrium and Non-equilibrium Structure of Liquid Crystalline Nanoparticles
Particles 2008, Orlando, USA, 10-13th May 2008

A. W. Dong, C. Pascual-Izarra, Y.-D. Dong, S. J. Pas, A.J. Hill, B. J. Boyd, C. J. Drummond
Positron annihilation lifetime spectroscopy (PALS) and small angle x-ray scattering (SAXS) of self-assembled amphiphiles
26th Australian Colloid and Surface Science Student Conference, Warrnambool, Australia, 4-8th February, 2008

P. Dubček, B. Pivac, I. Capan, N. Radić, H. Zorc, S. Bernstorff
Growth of Ge nanostructures with different methods
ICTF14 & RSD2008, University of Ghent, Ghent, Belgia, Novembre 2008

P. Dubček, B. Pivac, I. Capan, N. Radić, H. Zorc, S. Bernstorff
Si based structures for advanced solar cells
15. Medjunarodni sastanak Vakuumska znanost i tehnika, Varazdin, Croatia, 04. 06. 2008 (talk)

Paolo Falcaro
Fabrication of X-Ray Patternable Mesostructured Silica Films
XVI Elettra Users Meeting, invited talk of the Fonda-Fasella Award winner, Trieste, Italy, 25.11.2008

J.I. Flege, B. Gehl, Th.Schmidt, V. Aleksandrovic, A. Froemsdorf, A. Kornowski, A. Pretorius, S. Bernstorff, A. Rosenauer, H. Weller, M. Baeumer, and J. Falta
Structural and chemical properties of self-assembled close-packed nanoparticle films under harsh conditions
Materials Research Society Fall Meeting, Boston, MA (USA), December 2–4, 2008 (Oral)

D. Gracin, B. Etlinger, K. Juraić, A. Gajović, P. Dubček, S. Bernstorff
DC conductivity of amorphous-nano-crystalline silicon thin films
12th joint vacuum conference (JVC-12), 10th European Vacuum Conference (EVC-10), and 7th Annual Meeting of the German Vacuum Society (AMDVG-7), Balaton, Hungary, 22.-26.09.2008 (poster)

D. Gracin, A. Gajović, M. Ceh, K. Juraić, D. Meljanac, P. Dubček, S. Bernstorff
Structural analysis of thin amorphous- nano-crystalline thin films by HRTEM, GISAXS and Raman spectroscopy
EUCMOS 2008 XXXIX European Congress on Molecular Spectroscopy (2008) (oral)

D. Gracin, K. Juraić, A. Gajović, P. Dubček, S. Bernstorff, M. Čeh
The structure of amorphous-nano-crystalline Si thin films by Raman spectroscopy, HRTEM, GISAXS
ICTF 14 & RSD, 2008 (oral)

D. Grozdanić, R. Slunjski, B. Rakvin, B. Pivac, P. Dubček, N. Radić, S. Bernstorff
Structural analysis of amorphous Si films prepared by magnetron sputtering
12th joint vacuum conference (JVC-12), 10th European Vacuum Conference (EVC-10), and 7th Annual Meeting of the German Vacuum Society (AMDVG-7), Balaton, Hungary, 22.-26.09.2008 (poster)

R. Hildebrand, Th. Schmidt, A. Zargham, M. Speckmann, C. Kruse, D. Hommel, and J. Falta
XRR investigations of II-VI and III-nitride based DBR structures, multilayers, and superlattices
DPG-Fruehjahrstagung2008, Berlin (Germany), February 25–29, 2008 (Oral)

A. Hodzic, P. Zoumpoulakis, T. Mavromoustakos, M. Rappolt, P. Laggner, G. Pabst
The role of membrane hydrocarbon chain composition in interactions with antihypertensive drugs
52nd Annual Meeting, Biophysical Society & IUPAB Meeting, Long Beach, USA, 02. - 06.02.08 (poster)

S. Ibrahimkutty, M. Rappolt, P. Laggner, and H. Amenitsch
Gas phase analysis of mesostructured Si aerosol particles using small angle X-ray scattering
Microfluidics for X-ray Nanoanalytics Symposium, Graz, Auastria, 13. -14.02.08 (poster)

S. Ibrahimkutty, M. Rappolt, P. Laggner, and H. Amenitsch
Gas phase analysis of mesostructured Si aerosol particles using small angle X-ray scattering
ÖPG Tagung 2008, Leoben, Austria, 22. – 26.09.08 (poster)

P. Innocenzi
Fabrication of Mesoporous Functionalized Arrays by Integrating Deep X-ray Lithography With Dip-pen Writing
6th International Mesotructured Materials Symposium, Namur, Belgium, September 8-11, 2008

A. Keilbach, R. Köhn, T. Bein;
Synthesis of Periodic Mesoporous Organosilicas within Anodic Alumina Pores
4th FEZA Conference, Paris, France, 02.-06.09.2008

R. Köhn, A. Keilbach, A. Zürner, B. Platschek, M. Döblinger, T. Bein
Silica Mesostructure Formation and Phase Transformation in the Confinded Space of Anodic Alumina Membranes
4th FEZA Conference, Paris, France, 02.-06.09.2008

P. Laggner
All you wanted to know about SAXS - but did not dare asking
Seminar am Atominstitut (Prof. Streli), Wien, Austria, 23.01.08 (lecture)

P. Laggner, H. Amenitsch, M. Rappolt, B. Sartori, D. Cojoc, C. Riekel
Microbeam x-ray diffraction on single phospholipid liposomes fixed by optical tweezers
52nd Annual Meeting, Biophysical Society& IUPAB Meeting, Long Beach, US 02. - 06.02.08 (poster)

P. Laggner
What you always wanted to know about SAXS - but did not dare asking. Bridging the gap to synchrotrons
1st Joint Austrian & Slovenian Polymer Meeting ASPM 2008 and the 9th Austrian Polymer Meeting, Graz, Austria, 26. - 28.03.08 (lecture)

P. Laggner
Power or convenience? A comparison of Synchrotron vs. laboratory SAXS for nano-analytics
14th Rolduc Polymer Meeting: From commodity plastics to speciality polymers?, Kerkrade, Netherlands 18. - 21.05.08 (lecture)

P. Laggner, H. Amenitsch, P. Herrnegger, M. Kriechbaum
New developments in laboratory X-ray nanoanalytics bridging the gap to synchrotrons
14th Rolduc Polymer Meeting: From commodity plastics to speciality polymers?, Kerkrade, Netherlands, 18. - 21.05.08 (poster)

Laggner P., Herrnegger P., Kriechbaum M.
Development and validation of quantitative methods using SAXS, SWAXS and GISAXS
IWPCPS-10: 10th International Workshop on Physical Characterization of Pharmaceutical Solids, Bamberg, Germany, 08. - 13.06.08 (lecture)

Laggner P., Herrnegger P., H. Amenitsch, Kriechbaum M.
Rapid structure analysis of thin lipid-protein films by home-laboratory GISAXS and X-ray reflectometry
ECIS 2008: 22nd Conference of the European Colloid and Interface Society, Cracow, Poland, 31.08. - 05.09.08 (lecture)

Laggner P., H. Amenitsch, Herrnegger P., Kriechbaum M.
New developments in laboratory X-ray nanoanalytics. Bridging the gap to synchrotrons
ECIS 2008: 22nd Conference of the European Colloid and Interface Society, Cracow, Poland, 31.08. - 05.09.08 (poster)

P. Laggner
Everything you wanted to know about SAXS, but did not dare asking. Overview on modern X-ray techniques
IV International Summer School “Supramolecular Systems in Chemistry and Biology”, Tuapse, Russia, 28.09. – 02.10.08 (lecture)

P. Laggner
Michel Ollivon and the DSC- SWAXS nanophaser: from prototype to industrial realization
Michel Ollivon’s Memorial Symposium 2008, UMR CNRS Paris, France, 02. – 03.10.08 (invited lecture)

P. Laggner
Nanoparticles and porous Solids: New developments in X-Ray nanoanalytics
Porotec Workshop, Bad Soden, Germany, 18. – 19.11.08 (lecture)

P. Laggner
Pulver und Partikel: SAXS
Bundesanstalt für Materialforschung und Prüfung (BAM), Berlin, Germany, 20.11.08 (lecture)

P. Laggner
New Developments in X-ray nanostructure analytics bridging the gap to synchrotrons
CSIRO Workshop 2008, Clayton, Australia, 25.11.08 (lecture)

P. Laggner
Visualisation of Self-Assembled Nanosystems by Old and New X-ray Techniques
RusNanoTech2008, Moskau, Russia, 03. – 05.12.08 (lecture)

M. Lončarić, J. Sancho-Paramon, M. Pavlović, H. Zorc, P. Dubček, A. Turković, S. Bernstorff, G. Jakopic, A. Haase
Optical and Structural Characterization of Silver Island Films on Glass Substrates
12th Joint Vacuum Conference (JVC-12), 10th European Vacuum Conference (EVC-10) and 7th Annual Meeting of the German Vacuum Society (AMDVG-7), Balatonalmadi, Lake Balaton, Hungary, 22.-26.09.2008 (poster)

Marmiroli B., Grenci G., Businaro L., Rappolt M., Sartori B., Cojoc D., Ferrari E., Gosparini A., Laggner P., Amenitsch H.
Microfluidics for SAXS experiments
Microfluidics for X-ray Nanoanalytics Symposium, Graz, Austria, 13. -14.02.08 (poster)

Marmiroli B., Grenci G., Amenitsch H., Sartori B., Gosparini A., Laggner P., Businaro L
Jet micromixer for studying ultrafast chemical reactions by small angle X-ray scattering
Microfluidics for X-ray Nanoanalytics Symposium, Graz, Austria, 13. -14.02.08 (lecture)

Marmiroli B., Grenci G., Amenitsch H., Sartori B., Cacho-Nerin F., Laggner P., De Angelis F., Businaro L.
Fabrication and engineering of a high aspect ratio jet micromixer for ultrafast chemical reaction studies
MNE 2008, Athens, Grecia, 15. – 18.09.08 (poster)

Marmiroli B., Grenci G., Businaro L., Rappolt M., Sartori B., , Cojoc D., Ferrari E., Cacho-Nerin F., Laggner P., Amenitsch H.
Microfluidics for small angle X-Ray scattering
ÖPG Tagung 2008, Leoben, Austria, 22. – 26.09.08 (poster)

G. Pabst
GAP - A tool for the global analysis of diffraction data from lamellar phases
Microfluidics for X-ray Nanoanalytics Symposium, Graz, Austria, 13. -14.02.08 (poster)

G. Pabst
Effect of ceramide on physical properties of membranes
Liquid Crystal Seminar at the Raman Research Institute, Bangalore, IN 04.12.08 (lecture)

G. Pabst
Lateral ordering of lipids by membrane interactions
3rd Christmas Biophysics Workshop, Donja Stubica, HR 15. – 16.12.08 (lecture)

M. Pavlović, M. Loncarić, J. Sancho-Parramon, H. Zorc, A. Turković, P. Dubcek and S. Bernstorff
GISAXS study of silver islands deposited on glass substrate
Croat-Slovenian Vacuum meeting, Varazdin, Croatia, 2.-6.6.2008

B. Pili, C. Bourgaux, S. Lepêtre-Mouelhi, P.Couvreur and M. Ollivon
Gemcitabine-squalene prodrug promotes the formation of a bicontinuous cubic phase in DPPC
6th World Meeting On Pharmaceutics, Biopharmaceutics and Pharmaceutical Technology; Barcelona, Spain, 7th to 10th April 2008 (poster)

B. Pivac, I. Capan, P. Dubček, N. Radić, S. Bernstorff
Nano Si superlattice for advanced solar cells
E-MRS 2008 Spring Meeting, Strasbourg, France, 26-30.05.2008 (talk)

B. Pivac, P. Dubček, I. Capan, R. Slunjski, N. Radić, H. Zorc, S. Bernstorff
Nano Si layers for solar cell application
12th joint vacuum conference (JVC-12), 10th European Vacuum Conference (EVC-10), and 7th Annual Meeting of the German Vacuum Society (AMDVG-7), Balaton, Hungary, 22.-26.09.2008 (poster)

P. Pivette, V. Faivre, G. Daste, S. Lesieur, M. Ollivon
Physical and thermal characterisation of lipidic excipients, application to lipidic microgranules
6th world meeting on pharmaceutics, biopharmaceutics and pharmaceutical technology, Barcelona, 7-10 April 2008

D. Pozzi, G. Caracciolo, R. Caminiti, C. Marchini, M. Montani, A. Amici, H. Amenitsch
On the Mechanism of DNA Release from Lipoplexes
X Annual Linz Winter Workshop, Linz (Austria), 15-19 Febbraio 2008 (poster)

S. di Stasio, A. Iazzetta, A. Onischuk, A. Baklanov and H. Amenitsch
Effect of Crystal Shrinking for Aerosol Zinc Nanoparticles subjected to Oxidation: in-situ SAXS vs. ex-situ XRD, TEM, ADB
European Aerosol conference, Helexpo Thessaloniki, Greece, 24-29.8.2008 (poster)

N. Radic, P. Dubcek, M. Ristic, S. Music, A.Tonejc, S. Bernstorff
Surface characterization of carbon-tungsten alloys prepared by reactive sputtering
E-MRS 2008 Spring Meeting, Strasbourg, France, May 25 - 29, 2008

N. Radic, P. Dubcek, M. Jercinovic, M. Ristic, S. Music, A. Tonejc, and S. Bernstorff
Surface Layer Morphology of Tungsten-Carbon Thin Films
Proceedings of ICTF14 & RSD2008, Ghent, 2008

M. Rappolt
Biologically relevant lipid/water mesophases as "seen" by X-rays
Centre for Drug Research, University of Helsinki, Finland, 21.-23.01.08 (lecture)

M. Rappolt
Tuning curvature and stability of monoolein bilayers by amphiphilic designer peptides
Centre for Drug Research, University of Helsinki, Finland, 21.-23.01.08 (lecture)

Michael Rappolt
The power of SAXS: exploration of the magic world of biomaterials
Campus 02: Triest Excursion, Italy, 01.-02.02.08 (lecture)

H. Amenitsch, S. Bernstorff, M. Rappolt
Tutorial in SAXS data analysis
Advanced School on Synchrotron and Free Electron Laser Sources and their Multidisciplinary Applications, Trieste, IT 08. – 11.04.08 (tutorial)

M. Rappolt
Membranes and SAXS
Workshop "Glycolipids, Structures, Function and Interactions" organized by Klaus Brandenburg (Forschungszentrum Borstel) at the University of Hamburg, Germany, 12./13.06.08 (lecture)

M. Rappolt
How and what can you "see" with X-rays
Institute of Biophysics, University of Ljubljana, Slowenia, 20.11.08 (lecture)

K. Salamon, O. Milat, M. Buljan, U.V. Desnica, N. Radić, P. Dubček, S. Bernstorff
X-ray investigation of Ge-nanocrystals formation in SiO2 matrix in multilayered films
XTOP 2008, 9th Biennial Conference on High Resolution X-Ray Diffraction and Imaging, Linz (Austria), 15-19 September 2008 (poster)

Erhard Schafler, M. Kerber, F. Spieckermann, H. Wilhelm, M. Zehetbauer
Investigations of Dislocations in Non-Metallic Materials
Int. Honorary Symp. Tamas Ungar, Budapest, Hungary, May 2008 (invited)

E. Schafler
X-ray Line Profile Analysis for the characterization in nanostructured materials
XXI Congress and General Assembly of the International Union of Crystallography, Osaka, Japan, August 2008 (invited)

Th. Schmidt, M. Speckmann, R. Hildebrand, S. Bernstorff and J. Falta
Nanoscale Ge islands on faceted Si(113) studied by grazing-incidence small-angle x-ray scattering
Materials Research Society Fall Meeting 2008, Boston, MA (USA), December 2–4, 2008 (poster)

J. Schuster, A. Keilbach, R. Köhn, T. Bein
Soft-Templating Method for Mesoporous Carbon Thin Films
4th FEZA Conference, Paris, France, 02.-06.09.2008

J. Schuster, A. Keilbach, M. Döblinger, R. Köhn, T. Bein
Ordered Mesoporous Carbon in Confined Environments through Soft-Templating: Thin Films and Tubular Hosts
CeNS Workshop, Venice, Italy, 29.09.-3.10.2008

Sevcsik E., Pabst G., Danner S., Richter W., Lohner K.
Interaction of the human antimicrobial peptide LL-37 with model membrane systems of different complexity - Influence of the lipid matrix
52nd Annual Meeting, Biophysical Society & IUPAB Meeting, Long Beach, US 02. - 06.02.08 (poster)

E. Sevcsik
Membrane interaction of the human antimicrobial peptide LL-37 – Influence of the lipid matrix
Seminar at the Dep. of Chemistry, Penn University, Philadelphia, USA 11.02.08 (lecture)

E. Sevcsik
Membrane interaction of the human antimicrobial peptide LL-37 – Influence of the lipid matrix
Seminar at the Dep. of Mol. Biophysics & Biochemistry, Yale University, New Haven, USA 13.02.08 (lecture)

A.Turkovic, M. Rakic, P. Dubcek, M. Lucic-Lavcevic, S.Bernstorff
SAXS/DSC/WAXD studij utjecaja brzine promjene temperature na nanopolimerni elektrolit
15. Medunanodui sastanak "Vakuumsha znanost i teknica", Varaždin, Croatia, 4.6.2008 (poster)

Turkovic et al
SAXS/DSC/WAXD study of polymer electrolyte for Zn rechargeable nanostructured galvanic cells
12th joint vacuum conference (JVC-12), 10th European Vacuum Conference (EVC-10), and 7th Annual Meeting of the German Vacuum Society (AMDVG-7), Balaton, Hungary, 22.-26.09.2008 (poster)

Yaghmur
Hexosomes and cubosomes
Centre of Drug Research, University of Helsinki, Finland, 21. – 23.01.08 (lecture)

Yaghmur
Colloid science basics for drug delivery systems
Centre of Drug Research, University of Helsinki, FI 21. – 23.01.08 (lecture)

A. Yaghmur, P. Laggner, S. Zhang, M. Rappolt
Self assembled nanostructures of biologically relevant lipid-designer short peptide surfactant systems
INNANO-Advances in Nanomedicine & Nanobiotechnology, Innsbruck, Austria, 09. – 11.04.08 (poster)

A. Yaghmur, P. Laggner, S. Zhang, M. Rappolt
Tuning curvature of lipidic nanostructures by designer short peptide surfactants
2nd Meeting on Pharmaceutical Engineering, Graz, Austria, 15. – 16.05.08 (poster)

A. Yaghmur, P. Laggner, S. Zhang, M. Rappolt
Modulation of lipidic nanostructures by designer short peptide surfactants
Helsinki Drug Research 2008 (HDR 2008), Helsinki, FI 09. – 11.06.08 (talk)

ELETTRA Highlights 2007-2008

P. Falcaro, S. Costacurta, L. Malfatti, T. Kidchob, M.F. Casula, M. Piccinini, A. Marcelli, B. Marmiroli, H. Amenitsch, M. Takahashi and P. Innocenzi
Fabrication of X-ray patternable mesostructured silica films
Elettra Research Highlight, pp. 64-65 (2008)

N. Baccile, C. V. Teixeira, H. Amenitsch, F. Villain, M. Lindén, F. Babonneau
Time-resolved in-situ small-angle X-ray diffraction experiments for a better understanding of the formation of surfactant-templated silica
Elettra Research Highlight, pp. 66-67 (2008)

SAXS training courses

The SAXS group participated in the Advanced School on "Synchrotron and Free Electron Laser Sources and their Multidisciplinary Applications", Trieste, Italy, 07 - 25 April 2008. They gave two lectures (S. Bernstorff, "Grazing Incidence Small Angle X-ray Scattering (GISAXS) in Material Sciences" and H. Amenitsch, "SAXS under extreme conditions: NanoMaterials and proteins in solutions"), and a half-day tutorial "Small angle scattering set-ups and data analysis" (H. Amenitsch, S. Bernstorff, and M. Rappolt)

Luciano Fonda and Paolo Maria Fasella Award

During the XVI ELETTRA Users' Meeting (Trieste, November 24-26, 2008) our user dr. Paolo Falcaro received the ELETTRA Award in Memory of Luciano Fonda and Paolo Maria Fasella, which is assigned each year to a young scientist for outstanding experiments performed with Elettra synchrotron light. Dr. Paolo Falcaro (Associazione CIVEN, Venezia Marghera, Italy) won this price for his studies concerning the "Fabrication of X-Ray Patternable Mesostructured Silica Films". The experiments were performed at the SAXS-beamline in close cooperation with the local research staff.

PhD Thesis 2008

Leandro R. S. Barbosa
Structural studies of relevant biological systems by small angle X-Ray Scattering
Instituto de Fisica da Universidade de São Paulo, São Paulo, Brasil

Maja Buljan
Properties of semiconductor nanoparticles in amorphous SiO2 matrix
University of Zagreb / Rudjer Boskovic Institue, Croatia

Y. D. (Charlie) Dong
PhD Thesis “Liquid crystalline particles for agricultural and drug delivery applications”
Monash University, Australia

Gábor Ribárik
Modeling of diffraction patterns based on microstructural properties
Eötvös Loránd University, Institute of Physics, Department of Materials Physics

Massimo Piccinini
In-Situ Study by Advanced Spectroscopic Techniques of Mesoporous Silica Films Obtained by Sol-Gel Processing
University of Roma Tor Vergata

Master Theses (Tesi di Laurea, Diplomarbeit) 2008

Sarka Perutkova
Nanomechanics of Inverted Hexagonal Phase in Biomembranes
Czech Technical University in Prague, Department of Mechanics, Biomechanics and Mechatronics

Authors Index

IBN
Institute of Biophysics and Nanosystems Research
Austrian Academy of Sciences
Schmiedlstraße 6, 8042 Graz, Austria
Tel.: +43 316 41 20-302
Fax: +43 316 41 20-390
ibn.office@oeaw.ac.at
www.ibn.oeaw.ac.at

ELETTRA
Sincrotrone Trieste
Strada Statale 14, km 163,5
34012 Basovizza (TS), Italy
Tel.: +39 040 375 8572
Fax: +39 040 93 809 02
E-mail: bernstorff@elettra.trieste.it
Web: www.elettra.trieste.it

Cover-pictures taken from Pinto et al., Boulgaropolous et al. and Garvey et al. (see pages 53, 69 and 78, respectively)